UNIVERSITY OF KWAZULU-NATAL

Index Modulation for Next Generation Radio Communications

Oso Oluwabukunmi Williams

2021

Index Modulation for Next Generation Radio Communications

Oso Oluwabukunmi Williams

217066985

Submitted in fulfilment of the academic requirements of

Master of Science in Engineering

Discipline of Electronic Engineering

School of Engineering, College of Agriculture, Engineering and Science

University of KwaZulu-Natal, Durban, South Africa

Supervisor: Dr. Narushan Pillay

Co-Supervisor: Prof. HongJun Xu

January 2021

CERTIFICATION

The research contained in this dissertation was completed by the candidate while based in the school of Engineering, Discipline of Electrical, Electronic and Computer Engineering, in the College of Agriculture, Engineering and Science, University of KwaZulu-Natal, Howard College, South Africa.

The contents of this work have not been submitted in any form to another university and, except where the work of others is acknowledged in the text, the results reported are due to investigations carried out by the candidate.

As the candidate's supervisor, I agree to the submission of this dissertation.

_____

Signed: Dr. Narushan Pillay

Date: 28th January, 2021

DECLARATION 1 - PLAGIARISM

I, Oso Oluwabukunmi Williams, declare that:

i the research reported in this dissertation, except where otherwise indicated, is my original research;

ii this dissertation has not been submitted for any degree or examination at any other university;

iii this dissertation does not contain other person's data, pictures, graphs or other information unless specifically acknowledged as being sourced from other persons;

iv this dissertation does not contain other persons' writing unless specifically acknowledged as being sourced from other researchers. Where other written sources have been quoted, then

a. their words have been re-written, but the general information attributed to them has been referenced,
b. where their exact words have been used, then their writing has been placed in italics, inside quotation marks and referenced;

v This dissertation does not contain texts, graphics or tables copied and pasted from the internet, unless specifically acknowledged, and the source being detailed in the thesis and the Reference section.

Signed:

_____

Oso Oluwabukunmi Williams

Date: 28th January, 2021

ACKNOWLEDGEMENTS

First and foremost, I want to thank God for his guidance and continued blessings throughout my research program.

I want to express my profound gratitude to my supervisor, Dr. Narushan Pillay, for giving me the privilege to serve under his tutelage for my research. His dynamism, vision, sincerity and motivation deeply inspired me. His insightful feedback pushed me to sharpen my thinking and brought my work to a higher level. Also, I would like to acknowledge my co-supervisor Prof. HongJun Xu in the role he played in the developmental stages of my research study.

I am incredibly grateful to my parents for their love, prayers, sympathetic ear and sacrifices towards my education. Also, I want to express my appreciation to my sisters for their support, constant encouragement, and valuable prayers.

Finally, my thanks go to all the people who have supported me to complete this research work directly or indirectly.

DEDICATION

This dissertation is dedicated to my parents' Pastor and Dr. Mrs Oso.

ABSTRACT

Man's insatiable desire for swift and more efficient internet service, a wide range of connectivity and increased data rate of transmission necessitated the need for further research to improve the efficiency of the existing systems. The development and evolution of the next-generation communication systems can be ascribed to the multiple-input multiple-output (MIMO) techniques implemented. The fundamental founding block of the MIMO systems is the spatial modulation (SM) which interestingly was able to attain high spectral efficiency as the receiver maintained significantly lower complexity. However, even with the feat achieved by the SM scheme, there was still a need improve on the performance of the SM scheme which meant an increase in the spectral efficiency was required, this prompted further research and a new scheme was introduced.

The quadrature SM (QSM) scheme was introduced to better the performance of the conventional SM. QSM retains all the good benefits the SM scheme offers, while still enhancing the spectral efficiency and improving overall throughput. However, the demand for increased reliability, i.e., improving the QSM scheme's error performance led to a new scheme being introduced.

Space-time QSM (ST-QSM) improves the QSM scheme's error performance by achieving second-order diversity gain for QSM. This scheme combines both the spatial dimension and diversity to the QSM scheme, bringing about a new and improved scheme.

In this dissertation, a scheme was introduced to fix the high computational complexity (CC) that affects MIMO systems transmitting at high data rates. Signal orthogonal projection (OP) was employed to decrease the CC of the space-time block coded spatial modulation (STBC-SM). The proposed scheme is called STBC-SM-OP and its results were investigated by comparing it with the STBC-SM with maximum likelihood detection (STBC-SM-ML). The proposed STBC-SM-OP scheme's error performance matched that of STBC-SM-ML tightly down to low BER whilst maintaining a low CC.

TABLE OF CONTENTS

LIST OF FIGURES

LIST OF TABLES

LIST OF ACRONYMS

ABEP……..…..Average Bit Error Probability
APM……..….....Amplitude/Phase Modulation
AQSM.....Adaptive Quadrature Spatial Modulation
ASM……..…….Adaptive Spatial Modulation
AWGN ……...Additive White Gaussian Noise
BER……..……..……Bit Error Rate
BPSK……...……...……Binary Phase Shift Keying
CC…….Computational Complexity
CSI……..……Channel State Information
ED…….....Euclidean-Distance
EDAS……..…….Euclidean Distance-Based Antenna Selection
FRFC……..……Frequency-Flat Rayleigh Fading channels
GSM……..……Generalized Spatial Modulation
i.i.d.……Independent and Identically Distributed
IAS….....Inter-Antenna Synchronization
ICI……..…….....Inter-Channel Interference
IEEE……Institute of Electrical and Electronic Engineers
MA-GSM…….Multiple Active Transmit Antenna for Generalized Spatial Modulation
MGF……..……Moment Generating Function
MIMO……Multiple-Input Multiple-Output
ML…….Maximum Likelihood
MRC……..……..Maximum Ratio Combining
MRRC……...……Maximum Ratio Receiver Combining
PEP…….Pairwise Error Probability
PSK……..……..Phase Shift Keying
QAM…….…….Quadrature Amplitude Modulation
QSM……Quadrature Spatial Modulation
RF……..……Radio Frequency
SA.....Single-Active
SER……...……..Symbol Error Rate
SM……..Spatial Modulation
SM-OD……Spatial Modulation with Optimal Detection
SMUX……..Spatial Multiplexing
SNR……...…….Signal-to-Noise Ratio
SSK……...…….Space Shift Keying

STC……..Space-Time Code

STBC……...……...Space-Time Block Code

STBC-SM…..……Space-Time Block Code Spatial Modulation

STBC-SM-ML…….Space-Time Block Code Spatial Modulation Using Maximum Likelihood

STBC-SM-OP…….....Space-Time Block Code Spatial Modulation Using Orthogonal Projection

ST-QSM…….……Space-Time Quadrature Spatial Modulation

SVD……Signal Vector-Based Detection

TAS…..……Transmit Antenna Selection

V-BLAST.....Vertical Bell Laboratories Layered Space-Time Architecture

WLAN.....Wireless Local Area Network

CHAPTER 1

1 Introduction

Wireless communication has come a long way in terms of development and technological advancements. It is one of the major sectors of the communication industry that is developing rapidly, given that it involves every aspect of human life. This feat achieved due to the increased interest in the field has led to a higher number of researchers focusing on wireless communication. The constant exigency for higher data rates and higher spectral efficiency led researchers to broaden the scope and keep improving the field. New systems in the form of the later releases of 5G and 6G are currently undergoing research, as they will increase link reliability and spectral efficiency of digital communication systems. These will be a total upgrade from the four previous generations of digital cellular technology [1, 2]. The new systems will require a larger number of antennas.

Signal transmission in wireless communication has several challenges ranging from susceptibility to noise, interference and distortion [3]. These led researchers to find a way to mitigate these shortcomings. The first scheme introduced to palliate the challenges aforementioned was the single-input single-output (SISO) scheme. The need for higher bandwidth, better performance, and improved quality of link reliability led to the upgrade of the SISO termed multiple-input multiple-output (MIMO) systems [4].

1.1 MIMO Systems

MIMO systems have exhibited many technological advancements in improving error performance and increasing throughput (spectral efficiency) in comparison to the existing SISO systems in digital communication systems [5]. MIMO systems utilize a wireless technology whereby multiple transmitters and receivers are employed, which transmits more data at a time. It uses the characteristic of radio waves known as multipath.

In MIMO systems, additional paths generated by utilizing multiple antennas can be used to an advantage. It facilitates extra sturdiness to the radio link, providing a better signal-to-noise ratio (SNR). The 3G/4G wireless system uses the MIMO systems principle to increase data rates and transmit high data rates by transferring several information streams in a parallel form. Also, multiple antennas lead to diversity, which in turn leads to increased reliability.

1.2 Techniques of MIMO systems

MIMO systems can be sub-divided based on their different forms of transmission techniques.

These include:

1.2.1 Spatial Multiplexing (SMUX)

This MIMO technique involves the transmission of several streams of information in parallel between the transmitter and the receiver, which leads to an increase in data rate [6]. SMUX utilizes the space dimension rather than frequency or time for multiplexing.
The maximum number of streams available depends on the number of transmit antennas present [3, 7]. SMUX makes transmission of message signals to multiple receivers possible.

1.2.2 Diversity

This technique provides receivers with multiples of the same signal, which leads to reduced signal degradation and effectively improves link reliability. More about diversity techniques is in the subsequent subsection:

a) Frequency diversity: This diversity technique allows the message to be transmitted at different frequencies. For the received message signals to be independently transmitted, the carrier frequency bands must have a more prominent data transfer capacity than the radio channel's coherent transmission capacity. These are dependent on the channel's multipath delay distribution [8]. One disadvantage of this technique is the receiver not being able to pick up all the message signals transmitted at once, so all the receivers being utilized would have to tune in to just a single frequency. It is not ideal to repeat the same message signal at multiple frequencies, as this causes interference/crosstalk. Instead, the signal is spread over a large bandwidth, so parts of the signal are conveyed by different frequency components.

b) Time diversity: This particular diversity technique allows information to be transmitted at different time slots [8]. It utilizes the wireless channel's different time paths to send the same message signal over multiple separate time slots.

c) Space diversity: This technique uses different antennas located at different positions to take advantage of the different radio paths in a typical environment.

The quality of the data received at the output strictly depends on the transmitted signal's fading components.

1.3 System Model for a MIMO System

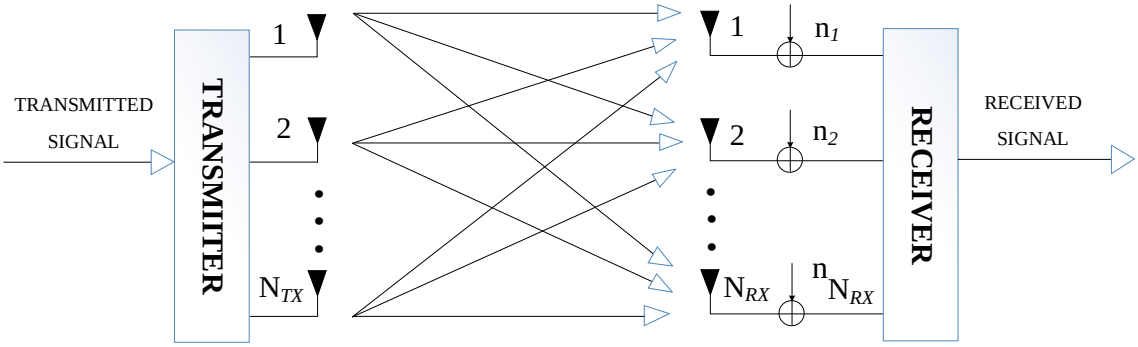

Figure 1-1. The system model of a MIMO system [9].

Figure 1-1 illustrates the MIMO system, which consists of N_{RX} receive antennas and N_{TX} transmit antennas with a fading channel $\boldsymbol{H}$ between the transmitter and the receiver.

The respective path of the channel $\boldsymbol{H}$ used for transmission with a constant channel gain can be represented as:

$$\boldsymbol{H} = [\boldsymbol{h}_1 \ \boldsymbol{h}_2 \ \dots \ \boldsymbol{h}_{N_{TX}}]. \tag{1-1}$$

The transmit antennas N_{TX} and the receive antennas N_{RX} can be put in a matrix format with a $N_{RX} \times N_{TX}$ dimension as shown:

$$\boldsymbol{H} = \begin{bmatrix} h_{1,1} & \cdots & h_{1,N_{TX}} \\ \vdots & \ddots & \vdots \\ h_{N_{RX},1} & \cdots & h_{N_{RX},N_{TX}} \end{bmatrix}, \tag{1-2}$$

where $h_{i,j}$ depicts the rows and columns of the channel $\boldsymbol{H}$, respectively, at a given time t, i.e. $i \in [1: N_{RX}]$ and $j \in [1: N_{TX}]$.

A transmit vector $\boldsymbol{r}$ of dimension $N_{TX} \times 1$, i.e. $\boldsymbol{r} = [r_1 \ r_2 \ r_3 \dots r_{N_{TX}}]^T$, which is to be sent over the wireless channel $\boldsymbol{H}$ contains a series of random message signals as depicted in Figure 1-1. These encounter additive noise known as additive white Gaussian noise (AWGN), $\boldsymbol{n}$ of dimension $N_{RX} \times 1$, i.e. $\boldsymbol{n} = [n_1 \ n_2 \ n_3 \dots n_{N_{RX}}]^T$ with Gaussian distribution $CN(0,1)$ and with independent and identically distributed (i.i.d.) entries. The transmission method through the channel $\boldsymbol{H}$ yields a receive signal vector $\boldsymbol{y}$, which is defined as:

$$\boldsymbol{y} = \sqrt{\rho}\boldsymbol{H}\boldsymbol{r} + \boldsymbol{n}, \tag{1-3}$$

where $\boldsymbol{H}$ and $\boldsymbol{n}$ are complex entry distributions in the form of $CN(0,1)$ and are assumed to be i.i.d. entries. ρ denotes the SNR at each receive antenna.

Wireless channels can be classified into large-scale fading and small-scale fading [10].

a) Large-scale fading depends on the distance involved. As the distance from the source of the transmitted signal increases, the signal-power reduces over a period of time t due to path loss attenuation and shadowing.
b) Small-scale fading occurs due to the channel's multiple paths, leading to distortion of the signal in amplitude, phase, and the angle of reception of the signal. Simply put, the multipath of the signal propagation causes it.

The MIMO systems' main significance is that the quality of error performance is greatly improved by increasing the diversity gain and the overall throughput with multiplexing. A MIMO system in a disjointed Rayleigh fading environment can provide a significant gain margin in channel capacity and a cogent increase in the system's spectral efficiency. Channel capacity can be described as the highest quantity of data that can be conveyed over a channel whilst the likelihood to detect error is kept to the barest minimum.

Despite MIMO systems having numerous advantages, the transmitter utilizes multiple radio frequency (RF) chains because of the concurrent transmission of data. Also, high power utilization leads to high cost considering all the antennas are ON simultaneously, which results in inter-channel interference (ICI) at the receiver.

The methods that can be utilized to reduce the MIMO systems' constraints will be examined and reviewed; examples of MIMO systems, including newly developed MIMO forms, will be presented in Section 1.4.

1.4 Forms of MIMO

SMUX is a futuristic scheme for wireless communication. It was developed to cater effectively to the need for the high demand for capacity in digital multimedia services. However, SMUX causes high ICI, which reduces the quality of error performance in the wireless link and this is caused by the coupling of space and time. The reduction in the quality of the error performance is the major limitation of SMUX. This limitation can be reduced by allowing sufficient spacing between transmit and receive antennas, although this might also lead to a reduced throughput [11, 12]. Several forms of innovative MIMO systems use SMUX; a significant example is the vertical-Bell Laboratories layered space-time architecture (V-BLAST) [13].

1.4.1 Vertical-Bell Laboratories Layered Space-Time Architecture (V-BLAST)

BLAST was introduced as a MIMO scheme in [14]. This optimistic wireless communication scheme led to the development of a more simplified version of BLAST, known as V-BLAST. By using the BLAST method in conjunction with the V-BLAST detection scheme, MIMO systems working in perfect conditions were able to achieve higher spectral efficiencies [13].

V-BLAST utilizes SMUX to enhance the spectral efficiency of the system by transmitting N_{TX} (total number of the available transmit antennas) signals at a single time instant and this results in

increased throughput. However, ICI and inter-antenna synchronization (IAS) exist in V-BLAST technology, since all transmissions occur at the same time [13]. For example, in a closely monitored enclosed area, spectral efficiency values of about 20 b/s/Hz can be obtained using the practical SNR range concept. The ICI at the receiver can be entirely avoided if N_{TX} symbols are compressed into a single symbol rather than different transmit antennas before transmission so that an algorithm that maps the single symbol to just one of the N_{TX} antennas can be used to retain the information.

1.4.2 The Alamouti Space-Time Block Coding System (STBC)

Alamouti STBC is a technique employed by wireless communication systems to mitigate wireless multipath fading channels' impairments. STBC exploits the independent fading nature of transmission paths between the source and the receiver, thereby, transmitting diverse versions of the information signals over multiple transmit antennas and multiple time slots. There is a high probability that some of the signals are less attenuated than others. The received message signals are combined at the receiver optimally; hence, the overall link reliability is improved.

The Alamouti STBC [15], is an example of an enhanced MIMO system with better quality. The use of spatial diversity is employed by the Alamouti STBC scheme to enhance the efficiency of the system by sending two symbols in the first-time slot such as r_1 and r_2. The negative conjugate of the second symbol sent in the first time slot, i.e. $(-r_2^*)$ together with the conjugate of the first symbol, i.e. (r_1^*) is transmitted during the second time slot such that the transmitted signal $\boldsymbol{R} = \begin{bmatrix} r_1 & r_2 \\ -r_2^* & r_1^* \end{bmatrix}$.

Since the system utilizes two-time slots to transmit the two symbols [15, 16], the data rate stays the same. Also, as a result of the replicated copies of data sent to the receiver over an independent path, there is a noticeable increase in the link's efficiency. As the constellation size increases, it is noticed that Alamouti STBC receiver's computational complexity (CC) also increases, making the physical application complicated and exorbitant [15]. Alamouti STBC does not need channel state information (CSI) or knowledge of channel co-efficient at the transmitter, making it very useful from a practical perspective.

1.4.3 Spatial Modulation (SM)

SM is an innovative MIMO transmission technique that was introduced by Mesleh *et al.* in [17]. It capitalizes upon the increased spectral efficiency achieved by V-BLAST. SM obliterates the major constraints of IAS and ICI encountered in conventional MIMO by utilizing numerous antennas in a novel manner and this is accomplished by using a dimension called the spatial dimension to transfer extra message bits. In comparison to the conventional MIMO systems, SM turns ON just one antenna at a certain time interval from an array of transmit antennas to propagate a symbol from a signal constellation during the symbol transmit interval. It should be taken into

account that the antennas that are not being utilized during the transmission transmit zero power. This is the reason why the innovative SM scheme successfully eradicates the ICI at the receiver, which in turn offers a substantial reduction in receiver complexity. The advantages of SM are:

a) IAS and ICI are completely obliterated.
b) It is cost-effective since only one RF chain will be used and this also results in higher energy efficiency.
c) It reduces complexity at the receiver.

Even with the listed advantages of SM, which makes it a very impressive scheme for use in wireless communication systems, there are still a few limitations.

a) Since SM uses only one active transmit antenna at a given time, it cannot exploit transmit diversity.
b) The number of transmit antennas must have a power of two.

SM is not a perfect system, but in comparison to V-BLAST, it has many advantages. There are other systems based on SM transmissions that have been proposed and presented to tackle the limitations.

1.4.3.1 Complexity Reduction Techniques for SM

Mesleh *et al.* in [17] proposed an SM detection scheme that utilizes maximum ratio combining (MRC) at the receiver. In this system, the transmission antenna index is first estimated and then its estimated result is further used to detect the modulated symbol. Jeganathan *et al.* in [19] researched further upon Mesleh's work and proved the MRC-based scheme to be sub-optimal. This made him propose the use of the maximum likelihood (ML) algorithm as a better alternative. The ML-based scheme explores the entire system to evaluate the transmit antenna and symbol simultaneously, which yields a greater error performance [19]. Although the system yields a better error performance, it causes an exceedingly high CC of the ML algorithm. In order to tackle the problem of this high CC linked with the ML-based SM detector, alternative detectors for SM have been suggested.

1.4.3.1.1 Sphere Decoding Detection (SD)

SD was proposed by Younis *et al.* in [20, 21] as an alternative to the ML-based SM detection system for low-complexity SM detection. In contrast to the conventional ML-based SM detector's working principle, this system avoids the complete search of the system; rather, it sieves through certain points of a specified radius. This simple process drastically reduces receiver complexity [20-22]. The detectors, receiver centric (Rx-SD) [20], transmitter centric (Tx-SD) [21] and combined-SD (C-SD) [21] all reduces receiver complexity whilst achieving error performances similar to that of the optimal SM detector.

Younis *et al*. proved that none of the SD detectors outperformed each other, but rather the optimal SD algorithm for the detection process was determined by the MIMO configuration in use. The detectors are employed for various functions, Rx-SD is utilized when N_{RX} is large; Tx-SD is employed when either or both N_{TX} and M are large and finally, C-SD is used when either N_{RX} or M is low.

1.4.3.1.2 Distance-Based Ordered Detection (DBD)

In [18], a solution was proffered to reduce the ML-based detection system's complexity while also preserving its performance. The authors came up with a DBD system for SM. In this system, the transmit antenna's symbols are individually computed and used to calculate the corresponding transmit symbol estimate. The estimated transmit symbols are then validated with the signal vector received. To jointly evaluate the final approximation of the active transmit antenna index and symbol being transmitted [18], the estimate with the nearest value is employed. In contrast to the ML-based detector scheme, which explores through the MN_{TX} points, the DBD scheme only searches through the N_{TX} points [18] and this reduces receiver complexity in comparison to the ML detection.

Hwang *et al.* in [22] presented a soft-output ML detector for SM systems (SM-SOMLD). As expected, it was discovered that the SM-SOMLD detector performed better than the hard-output ML detector under coded channel conditions. However, although it achieved a good error performance, its receiver complexity was still high. The need to remedy this problem led the authors of [18] to propose a low complexity soft-output DBD (SODBD) algorithm. SODBD was able to obtain an error performance result which was in close proximity to that of the ML whilst achieving a considerable decrease in CC [18].

1.4.3.1.3 Signal Vector-Based Detector (SVD)

SVD was presented in [23, 24] as a low-complexity and efficient algorithm, which maintained the high transmission rate of SM. It works based on the principle where the transmit antenna index estimate is acquired by looking for the least angle between the signal vector and the channel vector obtained [23, 24]. In other words, SVD calculates the transmit antenna index by choosing the channel gain vector that forms the smallest angle with the received signal vector. SVD determines the active transmit antenna index.

Although the complexity value of the SVD is lower than ML detection, the performance loss of SVD is enormous [24]. To counteract this deterioration in error performance, signal vector-based list detection, or list SVD, was introduced as an effective variation of SVD [25]. List SVD requires a two-step detection process: first, a list of the $'L'$ potential antennas, which form the $'L'$ with the least angles with the received signal, is created. Next, based on the list of candidate antenna indices, transmit symbol detection is performed [25]. For a limited list size, the list SVD's error

performance does not vary much to that of optimal ML algorithm. In contrast to the conventional SVD, the list SVD's improved error performance brings about an increase in complexity [25].

To rectify the limitations of the SM scheme, several adjustments have been made. In the subsequent section, several schemes have been summarized. These schemes focus on the receiver complexity of SM, the spectral efficiency of SM or the transmit diversity of SM. Such schemes can then be categorized into open-loop SM or closed-loop SM based on their architecture. The open-loop design refers to a system in which the information at the receiver does not influence the transmitter. On the other hand, the closed-loop design uses a feedback system that utilizes the CSI at the transmitter.

1.4.3.2 Open-loop Design for SM

This is a MIMO system based on SM where the transmitter does not receive any feedback. The following schemes fall under the open-loop system design.

1.4.3.2.1 SM-Orthogonal Frequency Division Multiplexing (SM-OFDM)

SM-OFDM is an impressive and efficient multi-antenna SM scheme in combination with OFDM [26, 27]. SM-OFDM improves the spectral efficiency of SM, while at the same time minimizing the effects of the frequency-selective fading by decomposing the channel into parallel frequency flat-fading sub-channels [26, 27]. This makes it possible for the bandwidth available to be efficiently employed and a reliable high-speed transmission is achieved.

For SM-OFDM, each sub-channel is mapped to a transmit antenna and it allows that only one transmit antenna can convey information at any time on a particular sub-channel [26, 27]. Consequently, SM-OFDM can completely avoid the limitations of both ICI and IAS at the receiver of the transmitter. Finally, [18] demonstrates that when the SM-OFDM is operated using a soft-output ML detection, it yields a better bit error rate (BER) performance compared to that of the traditional SM with ML detection. Therefore, it can be concluded that SM-OFDM is a feasible and spectrally efficient MIMO scheme that can significantly increase the BER performance of SM.

1.4.3.2.2 Fractional Bit Encoded Spatial Modulation (FBE-SM)

There are certain cases where it is not quite possible to implement SM due to space constraints imposed by compact mobile devices. This is because of SM's limitation that states that the number of transmit antennas present must be a power of two at any period in time. In [28], Serafimovski *et al.* proposed a way to overcome this restriction known as FBE-SM.

FBE-SM applies the principle of modulus conversion to obtain a fractional bit rate. In the FBE-SM method, only a fraction of bits, or a non-integer number of bits can be mapped to a constellation point in the spatial region. This gives enough room for the antenna index to be

encoded with a non-integer number of bits, while still allowing the encoding mechanism in the signal domain to remain unchanged [28].

FBE-SM was developed to be a versatile MIMO scheme that allows the transmitter to use an arbitrary number of antennas. FBE-SM utilizes the theory of modulus conversion for the sake of a framework that is better suited for compact wireless devices. However, a major restriction of this approach is that it is susceptible to performance degradation due to the effects of error propagation [28]. Hence, just like in the SM system, FBE-SM does not take advantage of the potential to transmit diversity gain.

1.4.3.2.3 Space-Time Block Coded Spatial Modulation (STBC-SM)

A novel MIMO transmission scheme was proposed by Basar *et al*. in [16] called STBC-SM, which uses amplitude/phase modulation (APM) technique and the spatial domain to relay information. STBC-SM takes the advantages and employs the principles of Alamouti STBC and SM while successfully eliminating their disadvantages. STBC-SM has substantially higher efficiency over the conventional SM. Furthermore, ICI at the receiver is eliminated as a result of the orthogonality of the Alamouti STBC. STBC-SM has demonstrated itself to be a suitable scheme for high-rate, low-complexity wireless communications.

1.4.3.2.4 Space Shift Keying Modulation (SSK)

SSK modulation is a special case under the SM transmission scheme. Unlike the conventional APM techniques, SSK modulation uses only spatial domain, i.e., the transmit antenna indices as the only means of relaying information [29]. SSK has all the advantages of SM mentioned above and has further reduced CC at the receiver since SSK does not employ any APM schemes to convey information. When high data rates are transmitted, SSK requires a high number of transmit antennas, hence posing impracticality for mobile stations. Like the SSK, the Bi-SSK modulation [30] uses only space domains for transmitting the information. Nevertheless, unlike SSK, to hold information at once, the Bi-SSK uses two sets of antenna indices connected with real and imaginary numbers, respectively. In addition to doubling the SSK transmission rate, it enjoys the same benefits as SSK.

1.4.3.2.5 Generalized Spatial Modulation (GSM)

The GSM scheme was proposed in [31] to improve upon the conventional SM. The mode of the GSM scheme's functionality is to transmit information bits by using a combination of active transmit antennas, which is considered a spatial constellation point and triggered simultaneously to transmit the same information. This thereby allows the GSM scheme to eliminate the ICI at the receiver. When this scheme is implemented, the number of transmit antenna being utilized will be reduced considerably. Also, higher spectral efficiency will be achieved whilst using a high

modulation order. This GSM scheme produced a close BER performance when it was compared to the conventional SM as there was not so much difference in their performance [31].

1.4.3.2.6 Multiple Active Transmit Antenna scheme for Generalized Spatial Modulation (MA-GSM)

The MA-GSM [32, 33] is a multi-antenna scheme proposed as a modification of the GSM scheme. The GSM scheme activates multiple transmit antennas at each time instant which transmits the same information bits [31] by applying the principle of SM. The major difference between the GSM scheme and the MA-GSM scheme is that in the MA-GSM scheme, the transmit antenna does not carry the same information bit rather each antenna carries a different information symbol. The MA-GSM scheme is similar to the GSM scheme as it lowers the SM scheme's limitation considerably, which requires the number of transmit antennas to have the power of two. MA-GSM also utilizes rotation angles, which brings about a reduction of the error probability of detecting overlapping antenna indices from different antenna sets. This yields a higher diversity gain, and hence, it is shown in [32, 33], that the MA-GSM scheme surpassed GSM and SM for various spectral efficiencies. Although the MA-GSM scheme has a lot of advantages over other schemes, the BER performance is reduced as the number of transmit antennas is increased.

1.4.3.2.7 Quadrature Spatial Modulation (QSM)

Mesleh *et al*., who proposed the pioneer SM scheme, to improve upon the SM scheme, proposed a new scheme that improves the performance and efficiency of the conventional SM called the QSM [34]. The SM and QSM schemes are quite similar, but the key difference is in the way their spatial constellations are processed before transmission occurs. The QSM scheme employs an extra spatial dimension referred to as the quadrature dimension. It decomposes the data symbols down into its real (in-phase) and imaginary components (quadrature). These carrier components are orthogonal, so QSM maintains the avoidance of ICI at the receiver. For this scheme to transmit simultaneously, the transmit antennas have to be contemporized. QSM has more advantages over the conventional SM, which are:

a) Better error performance than SM.
b) Increased spectral efficiency of SM by $\log_2 \mathrm{N}_{TX}$ bits that occur by decomposing the symbols before transmission.

Despite the advantages of the QSM scheme, it has been proven that both the QSM and SM schemes have the same receiver complexity [34, 35].

1.4.3.2.8 Space-Time Quadrature Spatial Modulation (ST-QSM)

ST-QSM is a form of MIMO transmission technique that was proposed in [36]. To achieve a second-order diversity gain for the QSM scheme, the ST-QSM scheme was introduced by integrating it with the Alamouti STBC or ABBA STBC. The transmit antennas in this scheme are

split into groups of two and along with the two complex modulated symbols, the antenna indices contained in these groups convey information bits.

Using the QSM scheme's working principle, the two APM complex symbols are extended into their real and imaginary parts and then transmitted independently via their respective active antennas.

ST-QSM is designed to work with 4, 6 and 8 antennas. These antennas are then further divided into two groups which would consist of two to four antennas. The ST-QSM scheme's transmission occurs in two-time slots. For the transmission in the first time slot, the real part of the first symbol and imaginary part of the second symbol is conveyed with the first group's antenna indices. Also, the real part of the second symbol and imaginary part of the first symbol is independently transmitted via the second group's antenna indices. Judging based on the number of available transmit antennas in the signal vectors of each of the groups, either Alamouti STBC or ABBA STBC transmission principle is employed to obtain an improved diversity gain.

It is shown that at similar spectral efficiency values, the ST-QSM scheme yields a greater error performance than the QSM scheme [36].

1.4.3.3 Closed-Loop Design for SM

A key drawback of the SM scheme is that full advantage of the transmit diversity is not effectively exploited. Therefore, a few closed-loop architectures have been researched. These schemes are primarily based on precoding transmission, antenna selection and adaptive modulation.

1.4.3.3.1 Adaptive Spatial Modulation (ASM)

A closed-loop SM system was proposed in [37] with the purpose of enhancing the error performance of SM schemes without increasing the average data rate. ASM uses a low-complexity modulation order selection criterion (MOSC), which uses the CSI at the receiver to choose a candidate with the optimum modulation for transmission. The chosen modulation order is then employed for the next channel use by the transmitter. For several data rates, ASM significantly improves error performance relative to SM in uncorrelated Rayleigh fading channels. Since ASM scheme's major objective is principally to enhance the error performance of SM, another scheme was proposed in [38] called the adaptive M-ary quadrature amplitude SM (A-QASM). The A-QASM scheme applies the principle of constant power adaptive modulation to SM to optimize the average data throughput of the system while maintaining an average target BER. One important factor that is needed in these adaptive schemes to determine the state of a channel is the equivalent received SNR. There are two methods of characterizing the equivalent received SNR for the A-QASM scheme: first-order statistics SNR and average statistics SNR [38]. When simulated, the results derived are shown to be similar to the closed-form performance bounds [38]. Moreover, the simulation results show that the equivalent receiver SNR methods

closely results in the same error performance and average data throughput for the A-QASM scheme [38].

Yang *et al.* in [39] proposed a scheme that integrates adaptive modulation and transmit-mode switching (TMS) techniques to enhance the BER performance. This scheme is called the optimal hybrid-SM (OH-SM). This scheme was proven to have a high CC. This, however, motivated the research of a scheme that will have a lower CC. This newer scheme was presented in the form of a sub-optimal scheme known as concatenated SM (C-SM). Both OH-SM and C-SM have shown significant spectral efficiency gains over conventional SM [17], especially in correlated channel conditions [39] for the same spectral efficiencies. Then OH-SM shows a greater error performance than both C-SM and ASM.

Further research on reducing the high CC led the authors of [40, 41] to introduce the Euclidean distance-based antenna selection for SM (EDAS-SM). This SM scheme produced a better error performance at a reduced CC [40]. Still, keen on reducing the CC further, Wang *et al.*, in [42], exploited rotational symmetry of the constellation to reduce the CC.

Another closed-loop MIMO scheme known as single transmit antenna selection with modulation (ST-ASM) was presented in [43-45]. The scheme has the advantages of SM, such as utilizing a single transmit antenna, using only one RF chain, IAS not needed at the transmitter and no ICI is achieved at the receiver. However, unlike the SM, the scheme achieves a full-diversity order.

1.4.3.3.2 Transmit Antenna Selection for SM (TAS)

The implementation of TAS for MIMO systems has been crucial in recent times. It has been verified that using TAS is less pricey, gives more room for gain capacity and reduces hardware complexity [46].

The TAS scheme was proposed in [40] for SM to mitigate the limitation of SM's error performance based on the active transmit antenna and its subsequent propagation channels only. In the first scheme, low-complexity EDAS (LC-EDAS) approach divides the set of transmit antennas into subsets with transmit antennas and then picks the optimum antenna subset for the transmission interval. The optimum antenna subset is the one which maximizes the minimum euclidean distance (ED) among all possible transmit vectors [40]. The optimum antenna subset is then employed and the active transmit antenna is selected from this subset for the transmission interval. The second scheme, the capacity-optimized antenna selection (COAS), obtains the optimum transmit antenna subset by selecting the transmit antenna, which has the largest channel gain amplitude [40]. SM systems employing LC-EDAS and COAS have shown to outperform SM systems with no TAS [40].

Furthermore, [40] demonstrates that SM-COAS outperforms SM-LCEDAS. Contrary to this claim, Pillay *et al.* in [41] demonstrated that SM-LC-EDAS was capable of outperforming SM-COAS, once correcting an error in the formulation of the LC-EDAS scheme [40]. Furthermore,

Pillay *et al*. in [41] modified the LC-EDAS scheme for SM [40], which results in a significant reduction in the CC of the scheme.

1.4.3.3.3 Adaptive Quadrature Spatial Modulation (AQSM)

A hybrid closed-loop architecture for QSM was proposed in [47] referred to as AQSM. It uses transmission candidate modes based on modulation order selection and optimal TAS. The candidates are selected to satisfy predefined spectral efficiency targets. It also uses optimal antenna selection which results in high CC.

1.4.3.3.4 Euclidean-Distance optimized Antenna Selection for QSM (EDAS-QSM)

In [48], EDAS was applied to QSM to achieve optimum error performance. A subset of transmit antennas that maximize the minimum ED between all transmit vectors are selected. Monte Carlo simulations showed that EDAS-QSM produced a good error performance. However, the CC in implementing EDAS-QSM is high. The real-world application of this scheme is impractical as a result of its high complexity. Therefore, it is important to lower the complexity of the EDAS-QSM without altering the system's performance.

1.4.3.3.5 Reduced-Complexity Euclidean-Distance optimized Antenna Selection for QSM (RCEDAS-QSM)

EDAS suffers from a practical limitation as a result of high CC despite producing optimum error performance. In this regard, [40, 41] proposed a low complexity EDAS-SM computational algorithm which decreased the complexity and also maintained the error performance of the original EDAS scheme. An algorithm for the efficient computation of EDAS-QSM was investigated and is called RCEDAS-QSM.

In the EDAS-QSM scheme, the ED between each symbol was calculated for all possible combinations while for the RCEDAS-QSM scheme, the need for redundant calculations is eliminated by the repetition of channel gain vector combinations. In doing so, all calculations in RCEDAS-QSM are distinct. By eliminating all the repetitive calculations, RCEDAS-QSM remains optimal but now has a much lower CC.

1.4.3.3.6 Orthogonal Projection

It is a well-known fact that high data transmission rates are essential in modern communication systems to provide efficient multimedia services. In [19], Jeganathan *et al.* proposed the use of the maximum likelihood (ML) algorithm. Although the ML detection method is described as the optimum detection, it is also impractical due to the high complexity imposed when there is an increase in the number of transmit antennas and at high modulation order. Other detectors such as zero-forcing (ZF), minimum mean squared error (MMSE) and ordered successive interference cancellation (OSIC) were introduced to mitigate the problem of the high CC, but they all

performed poorly when compared to the ML detector. However, in [69], a detection algorithm based on OP and *M*-algorithm was proposed. In this detection method, the MIMO channel is first estimated by the receiver; after that, the layers are then rearranged in relation to the SNR values measured. The OP with *M*-algorithm is then used to evaluate the candidate vectors. Unlike the ML detection, the OP detection can achieve optimal performance without a complete search of the channel and still derive a result close to the ML detector. Also, there was a 0.66 percent decrease in the CC compared to the ML detector.

In [73], the channel estimation for multi-panel millimeter wave MIMO (mmWave) was done. The OP method was implemented along with a least square evaluation. The numerical results generated showed that channel estimation based on the multi-panel OP performed better than the conventional algorithm based on compressive sensing and the joint multi-panel channel estimation.

Also, in [74], OP is employed reduce sea clutter which makes radar target difficult. This is done by fabricating a clutter subspace by the data vectors received by the range cells of the cell under test (CUT). The sea clutter is reduced by directing the received signal from the CUT to the orthogonal subspace of the clutter. Using a newly designed detector called cell averaging constant false alarm rate (CFAR) along with the OP, shows that the generated theoretical performance of the suppressed clutter was improved when OP was implemented. It was noticed that the CFAR detector implemented with OP generated similar results with singular value decomposition but the CC of the OP is more reduced. It was also noticed that it is easy to implement OP with CFAR when compared to other existing schemes.

1.5 Research Motivation and Contributions

As the next generation of wireless communication systems is being introduced and taking over from the previous generation, higher data speed transfer, increased spectral efficiency, and link reliability is required to surpass the existing systems. In this regard, there has been increased research in the telecommunication industry on multiple-input multiple-output systems to satisfy the requirements for the next generation communication systems. The SM scheme was, therefore introduced by Mesleh *et al.* in [49]. The SM scheme employs an innovative multiple-input multiple-output transmission technique that utilizes antenna indices to convey information implicitly, enhancing spectral efficiency. When the SM scheme is compared to V-BLAST architecture [13], the SM exhibits many desirable features, which includes IAS due to the single-active (SA) transmit antenna [49], the complete avoidance of ICI at the receiver, less power consumed as only just a single RF chain is needed [19] and higher BER performance [19].

Since the introduction of the SM scheme, researchers have implemented it in several systems to yield better error performances. A new scheme (STBC) was introduced by Alamouti *et al.* in [57]. The STBC scheme is a two-branched transmit diversity scheme for MIMO systems in which two symbols are transmitted with two transmit antennas over two-time slots [57]. In comparison to MRC performance, it was shown that the STBC scheme suffered a 3 dB loss in performance as a result of simultaneous data transmission, which led to the transmit power not being at full capacity. Even with this drawback, researchers still prefer STBC as it has proven to provide transmit diversity gains compared to the STC scheme and other diversity MIMO schemes as it possesses a low decoding complexity and the implementation of this scheme is relatively straightforward [64]. In the last decade, several high rate STBC schemes have been introduced [49, 65-67] but the high rate of their ML decoding complexity relative to their constellation size renders the implementation challenging and exorbitant for future work.

However, for STBC-SM and other MIMO schemes, the level of CC at the receiver, especially for high data rate transmission represents a significant challenge to its practicality. Example, in [16] an ML detection scheme for STBC-SM was presented and in terms of metric calculations requires cM^2 (where cM represents the total number of antenna combinations and modulation order, respectively.) of such operations. This represents a high CC. Motivated by this, Basar *et al*. in [16] also presented a simplified ML detector which reduces the number of metric calculations to $2cM$; however, the complexity is still relatively high, especially as the symbol constellation size increases.

Over time it has been evident that for a data service to be considered efficient, it must effectively exhibit specific characteristics such as a wide range of data coverage, high rate of data transmission, e.t.c.

In a bid to achieve this high rate of data transmission, a challenge arose in the form of high CC at the receiver, which affects the practicality of most MIMO schemes as well as the STBC-SM schemes. However in [16], the STBC-SM-ML scheme was introduced by Basar *et al.* with the hope of mitigating this challenge; but, it was noticed that the larger the size of the symbol constellation got, the higher CC. Several detectors such as zero-forcing (ZF), minimum mean squared error (MMSE) and ordered successive interference cancellation (OSIC) have been introduced to try to fix the problem of the high CC, but they all yielded less error performance results relative to the ML detector. Therefore, it was imperative to introduce a scheme that would yield an error performance close to the ML detection while keeping a much lower CC than the existing detectors.

The authors of [69] employed the orthogonal projection (OP) of signals to lower the CC of a MIMO system. Likewise, in [70], the CC of the STBC-SM with labelling diversity was minimized

by employing OP. The results obtained in the two cases showed an error performance result in close proximity to ML and a lowered CC relative to that of the ML detectors.

It was discovered that the OP for spatially multiplexed MIMO transmission was similar to the STBC symbol's dual antenna transmission and the STBC-SM's antenna bits. As evident in the literature cited in the previous paragraph, the OP detector provides good performance at a low CC; this motivated us to investigate OP for STBC-SM to reduce the CC at the receiver.

1.6 Research Objectives

Based on the motivation drawn earlier, the objectives of this study are as follows:

1. The replication of the performance analysis of the existing SM schemes from the literature.
2. The replication of the performance analysis of the existing QSM schemes from the literature.
3. The replication of the performance analysis of the existing ST-QSM schemes from the literature.
4. The introduction of OP into the STBCSM scheme to reduce of the CC at the receiver along with the numerical results and discussions.
5. The presentation of the proposed reduced complexity near-ML detector based on OP.

1.7 Overview of the Dissertation structure

The dissertation is structured as follows:

Chapter 2 presents a detailed description for SM, together with the theoretical error performance analysis by employing a lower bound and asymptotic union bound approach in i.i.d. FRFC to simulate the Monte Carlo simulation results.

Chapter 3 provides the system model for QSM with the theoretical error performance analysis by employing a lower bound and asymptotic union bound approach in i.i.d. frequency-flat Rayleigh fading channels (FRFC) to simulate the Monte Carlo simulation results.

Chapter 4 presents the system model for ST-QSM with the theoretical error performance analysis using a lower bound and asymptotic union bound approach in i.i.d. FRFC channels to substantiate the result of the Monte Carlo simulations.

Chapter 5 introduces a reduced complexity detector based on the concept of OP for the STBC-SM. The receiver CC analysis was presented for the proposed STBC-SM-OP scheme and demonstrated the significance of the detector in comparison to the STBC-SM-ML detector

especially for high-order symbol constellation size, which is required in high data rate applications.

1.8 Notations used in the Dissertation

Bold italics symbols denote vectors/matrices, while regular letters represent scalar quantities. $[\cdot]^T$, $(\cdot)^H$, $|\cdot|$, $\|\cdot\|_F$ and $(\cdot)^*$ represents transpose, Hermitian, Euclidean norm, Frobenius norm and the complex conjugate, respectively. $\lfloor\cdot\rfloor_{2^{\mathbb{Z}^p}}$ denotes the largest integer less than or equal to the argument that is a positive integer ($\mathbb{Z}^p$) power of 2. $\boldsymbol{I}_v$ represents an identity matrix of order v. $Q(\cdot)$ represents the Gaussian Q-function, $\mathcal{D}(\cdot)$ is the constellation demodulator or slicing function $E\{\cdot\}$ is the expectation operator, $Re\{\cdot\}$ is the real part of a complex value, while $Imag\{\cdot\}$ is the imaginary part of a complex value. $\underset{w}{\text{argmin}}(\cdot)$ represents the minimum value of an argument with respect to w, while $\underset{w}{\text{argmax}}(\cdot)$ represents the maximum value of an argument with respect to w, $\binom{\cdot}{\cdot}$ represents the binomial coefficient and i represents a complex number.

CHAPTER 2

Spatial Modulation

2 Introduction

SM is a groundbreaking MIMO technique that utilizes multiple antennas in an innovative manner. This novel technique has improved upon the conventional MIMO system by reducing the hardware complexity, thus increasing practicality and energy efficiency [33].

SM employs an efficient approach to utilize the spatial dimension to convey additional information by dividing the input message bits into two groups; the first group selects a SA transmit antenna from an array of antennas present in the system, while the second group is mapped into an APM constellation symbol. Likewise, SM employs a single transmit antenna at every transmission interval; hence, this allows it to successfully eliminate the ICI and IAS limitations that are encountered in the conventional MIMO system [17, 19]. The modulated signal is conveyed via the selected active transmit antenna. During transmission, unlike how the V-BLAST scheme operates, where all antennas are ON and present for concurrent transmission, in SM, only one antenna is ON at each time instant, this leads to a reduction in the amount of power needed for transmission, and hence, just an RF chain is needed in the SM scheme [49, 50]. During transmission, the non-active antennas emit zero power.

2.1 System Model and Transmission of the SM Scheme

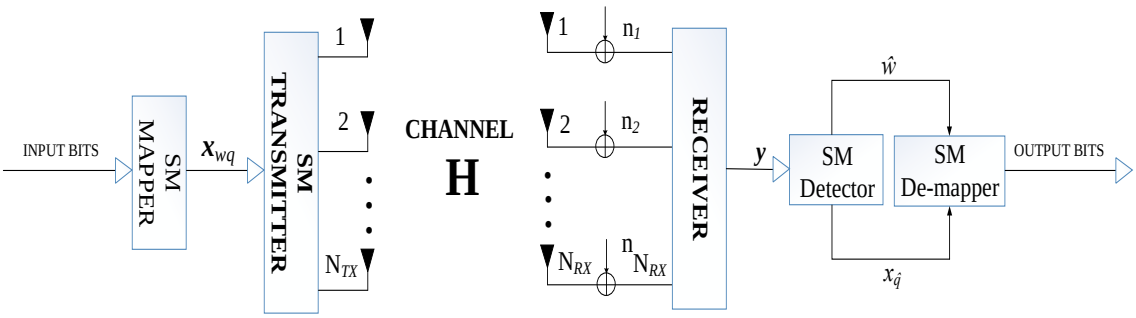

Figure 2-1. SM system model [9]

Figure 2-1 shows the working pattern of the SM scheme. It comprises of N_{TX} antennas and N_{RX} antennas which depict the transmit and receive antennas, respectively, in the MIMO wireless link. In SM, input bits are transmitted by employing the M-ary APM signal constellation, where the first $\log_2 N_{TX}$ bits activates one of the transmit antennas and a symbol from the M-ary APM signal constellation is selected by the remaining $\log_2 M$ bits. The spectral efficiency of the SM scheme is defined as $m = \log_2(MN_{TX})$ bits/s/Hz [5]. The output of the SM mapper, i.e., the transmit vector of the scheme can be expressed as:

$$\boldsymbol{x}_{wq} = \left[\underset{1^{st}\text{ position}}{0}\ 0\ \ldots\ \underset{w^{th}\ position}{x_q}\ \ldots\ \underset{N_{TX}^{th}\text{ position}}{0}\right]^T, \tag{2-1}$$

where x_q represents the q^{th} symbol in the M-ary APM signal constellation with $E\left[\left|x_q\right|^2\right] = 1$ in the w^{th} position, $w \in [1: \mathrm{N}_{TX}]$ and $q \in [1: M]$. Table 2-1 illustrates the pattern of mapping of the SM scheme employing Gray-coded 16-QAM constellation points.

Table 2-1: The mapping process for 4×4 Gray-coded 16-QAM SM transmission with spectral efficiency of 6 bits/s/Hz

Input Bits	**Antenna Index** (w)	**Symbol** (x_q)	**Transmission Vector** $(\boldsymbol{x}_{wq})$
0 0 0 0 0 0	[0 0] → 1	-3+3i	$[-3 + 3i\ 0\ 0\ 0]^T$
0 0 0 0 0 1	[0 0] →1	-3+1i	$[-3 + 1i\ 0\ 0\ 0]^T$
0 0 0 0 1 0	[0 0] → 1	-3-3i	$[-3 - 3i\ 0\ 0\ 0]^T$
0 0 0 0 1 1	[0 0] → 1	-3-1i	$[-3 - 1i\ 0\ 0\ 0]^T$
0 1 0 1 0 0	[0 1] → 2	-1+3i	$[0\ -1 + 3i\ 0\ 0]^T$
0 1 0 1 0 1	[0 1] → 2	-1+1i	$[0\ -1 + 1i\ 0\ 0]^T$
0 1 0 1 1 0	[0 1] → 2	-1-3i	$[0\ -1 - 3i\ 0\ 0]^T$
0 1 0 1 1 1	[0 1] → 2	-1-1i	$[0\ -1 - 1i\ 0\ 0]^T$
1 0 1 0 0 0	[1 0] → 3	3+3i	$[0\ 0\ 3 + 3i\ 0\ ]^T$
1 0 1 0 0 1	[1 0] → 3	3+1i	$[0\ 0\ 3 + 1i\ 0\ ]^T$
1 0 1 0 1 0	[1 0] → 3	3-3i	$[0\ 0\ 3 - 3i\ 0\ ]^T$
1 0 1 0 1 1	[1 0] → 3	3-1i	$[0\ 0\ 3 - 1i\ 0\ ]^T$
1 1 1 1 0 0	[1 1] → 4	1+3i	$[0\ 0\ 0\ 1 + 3i\ ]^T$

1 1 1 1 0 1	$[1\ 1] \rightarrow 4$	$1+1i$	$[0\ 0\ 0\ 1\ +\ 1i\ ]^T$
1 1 1 1 1 0	$[1\ 1] \rightarrow 4$	$1-3i$	$[0\ 0\ 0\ 1\ -\ 3i\ ]^T$
1 1 1 1 1 1	$[1\ 1] \rightarrow 4$	$1-1i$	$[0\ 0\ 0\ 1\ -\ 1i\ ]^T$

The modulated $\mathrm{N}_{TX} \times 1$ vector $\boldsymbol{x}_{wq}$ is transmitted via the selected transmit antenna in the w^{th} position over an $\mathrm{N}_{RX} \times \mathrm{N}_{TX}$ FRFC $\boldsymbol{H}$, which encounters AWGN $\boldsymbol{n} = [n_1\ n_1\ \cdots\ n_{\mathrm{N}_{RX}}]^T$ of dimension $\mathrm{N}_{RX} \times 1$. The elements of both $\boldsymbol{H}$ and $\boldsymbol{n}$ are assumed to be i.i.d. entries with $CN\ (0,1)$ distribution. The received signal, $\boldsymbol{y} = [y_1\ y_1\ \cdots\ y_{\mathrm{N}_{RX}}]^T$ is computed as:

$$\boldsymbol{y} = \sqrt{\rho}\boldsymbol{H}\boldsymbol{x}_{wq} + \boldsymbol{n}, \tag{2-2}$$

where ρ is the average SNR at each receive antenna.

Assuming symbol transmission from the w^{th} transmit antenna is used for transmission; the received signal can also be expressed as:

$$\boldsymbol{y} = \sqrt{\rho}\boldsymbol{h}_w x_q + \boldsymbol{n}, \tag{2-3}$$

where $\boldsymbol{h}_w$ connotes the w^{th} column of the channel matrix $\boldsymbol{H}$.

One important point to be taken into consideration in this scheme is that any transmit antenna $w \in [1{:}\ \mathrm{N}_{TX}]$, utilized at any time interval may not be the same at the next transmission time, as only one transmit antenna is ON at all-time intervals assuming the channel's full knowledge is known at the receiver. The ML rule is employed to optimally detect the transmit antenna index's estimate with the estimated modulated symbol at the receiver, which then demodulates the transmitted signal. This is further examined in the next sub-section.

2.2 SM Detection

Information is carried by the transmit antenna index and modulated symbol in the SM scheme; hence it is vitally important to estimate the active antenna index as well as the modulated symbol. The following sub-section outlines the optimal detection [19], sub-optimal detection [9], and low-complexity detection [49] that are important to the performance and analysis that follows.

2.2.1 Optimal Detection for Spatial Modulation

The ML detector follows the process of which the source input bits generated are transmitted and detected at the receiver by evaluating the transmit antenna and the modulated symbol by searching through the signal constellation of size M and the transmit antenna constellation points [19].

The estimates are then decoded by the SM de-mapper to recover the transmitted bits, using the SM mapping pattern, as shown in Table 2-1. The transmitted symbol and antenna indices are jointly detected by the ML technique. This is as demonstrated:

$$\left[\widehat{w}, x_{\hat{q}}\right] = \underset{w \in [1:N_{TX}], q \in [1:M]}{\operatorname{argmin}} \left[\sqrt{\rho}\left\|\boldsymbol{g}_{wq}\right\|_F^2 - 2Re\{\boldsymbol{y}^H \boldsymbol{g}_{wq}\}\right], \tag{2-4}$$

where $\boldsymbol{g}_{wq} = \boldsymbol{h}_w x_q$. $\widehat{w}$ and $x_{\hat{q}}$ represents the estimated transmit antenna index and the estimated transmitted symbol, respectively.

2.2.2 Sub-Optimal Detection for Spatial Modulation

The introduction of MRC as a detector at the receiver to determine the transmit antenna index was proposed by the authors of [17, 49]. The MRC algorithm has a perfect knowledge of the channel to estimate the transmit index correctly. Jeganathan *et al.* in [19], proved that the sub-optimal detector produces more accurate results in restricted channels. So, Jeganathan *et al.* in [19] proposed a revised version of the MRC algorithm. Employing (2-3), under conventional channel conditions, the revised detection principles to be followed are as follows [19],

Step 1: Each transmit antenna metric z_w for element w is calculated with,

$$z_w = \frac{\boldsymbol{h}_w^H \boldsymbol{y}}{\|\boldsymbol{h}_w\|_F}, \quad w \in [1: \mathrm{N}_{TX}]. \tag{2-5}$$

Step 2: The active transmit antenna index's $\widehat{w}$ estimation is calculated by,

$$\widehat{w} = \underset{w \in [1:N_{TX}]}{\operatorname{argmax}} |z_w|. \tag{2-6}$$

Step 3: Implement the principle of ML detection to deduce the estimate of the transmit symbol using,

$$x_{\hat{q}} = \underset{q \in [1:M]}{\operatorname{argmin}} \left[\sqrt{\rho}\left\|\boldsymbol{h}_{\widehat{w}} x_q\right\|_F^2 - 2Re\{\boldsymbol{h}_{\widehat{w}}^H \boldsymbol{y}\, x_q^*\}\right]. \tag{2-7}$$

Although this detector lowers the receiver complexity [9], it results in a loss in error performance compared to the ML-based optimal detector [19], thereby presenting a practical restriction. The authors of [18] proposed a low complexity scheme to reduce the receiver complexity while also achieving near-ML error performance.

2.2.3 Low-Complexity near-ML based Detector

Tang *et al.* in [18] proposed a low complexity near-ML SM detector scheme, which uses the principle of the DBD scheme. The method of detection is described in the subsequent subsections [18].

Step 1: Using (2-3) for each transmit antenna element w, the equalized symbol d_w in the antenna array is calculated with,

$$d_w = \frac{\boldsymbol{h}_w^H \boldsymbol{y}}{\|\boldsymbol{h}_w\|_F^2}, \quad w \in [1: \mathrm{N}_{TX}]. \tag{2-8}$$

Step 2: Each transmit antenna's transmit symbol is demodulated by,

$$\hat{x}_{qw} = \mathcal{D}(d_w), \tag{2-9}$$

where $\mathcal{D}(\cdot)$ depicts the constellation slicing function [49], [19], which produces the real and imaginary parts from the equalized symbol d_w.

Step 3: The symbol's final evaluation and active antenna index are selected by applying the ML detection's working principle.

$$\left[\widehat{w}, \hat{x}_{q_{\widehat{w}}}\right] = \underset{w \in [1:N_{T_X}]}{\operatorname{argmin}} \left[\sqrt{\rho}\left\|\boldsymbol{z}_{wq}\right\|_F^2 - 2Re\{\boldsymbol{y}^H \boldsymbol{z}_{wq}\}\right], \tag{2-10}$$

where $\boldsymbol{z}_{wq} = \boldsymbol{h}_w \hat{x}_{q_w}$. $\widehat{w}$ and $\hat{x}_{q_{\widehat{w}}}$ depicts the estimated antenna index and symbol, respectively.

2.3 Performance Analytical Bounds for Spatial Modulation

Mesleh *et al.* first introduced the performance analysis of the M-QAM SM with sub-optimal detection (M-QAM SM-OD) in FRFC in [17, 51] using the analytic union bounding technique [49]. This same technique was also employed in the derivation of the analytical framework for the binary phase-shift keying SM-OD (BPSK SM-OD) by Jeganathan *et al.* [29]. The method introduced in [9] used the same approach as in [17, 51], to derive the overall bit error probability (BEP) P_e, which can be lower bounded by:

$$P_e \geq 1 - (1 - P_a)(1 - P_d) = P_a + P_d - P_a P_d, \tag{2-11}$$

where P_a is the probability that the estimation of the transmit antenna index is incorrect given that APM symbol is correctly detected and P_d is the probability that the estimation of the transmit symbol is incorrect given that the antenna index is detected correctly.

In [9], the modulated symbol and antenna index are independently processed, and the optimal ML-based SM detector jointly detects the active transmit antenna index and transmit symbol, therefore, yields the best performance [17, 29, 51].

2.3.1 Analytical BER of Transmit Symbol Estimation

In [9], P_d is the probability that the estimation of the transmit symbol is wrong given that the antenna index is detected correctly. This means that P_d can be approximated as:

$$P_d \cong \frac{SER(\rho)}{m}, \tag{2-12}$$

where $m = \log_2 M$ and $SER(\rho)$ is the average symbol error rate of M-QAM with MRC over FRFC [52], and it is defined as:

$$SER(\rho) = \left(\frac{a}{c}\left[\frac{1}{2}\left(\frac{2}{b\rho+2}\right)^{\mathrm{N}_{RX}} - \frac{a}{2}\left(\frac{2}{b\rho+1}\right)^{\mathrm{N}_{RX}} + (1-a)\sum_{i=1}^{c-1}\left(\frac{B_i}{b\rho+S_i}\right)^{\mathrm{N}_{RX}} + \sum_{i=c}^{2c-1}\left(\frac{B_i}{b\rho+S_i}\right)^{\mathrm{N}_{RX}}\right]\right), \quad (2\text{-}13)$$

where $a = 1 - \frac{1}{\sqrt{M}}$, $b = \frac{3}{M-1}$, $B_i = 2\sin^2\theta$, $\theta = \frac{i\pi}{4c}$, $c > 10$, and c is the total number of summations.

2.3.2 Analysis of Transmit Antenna Index Estimation

If the evaluation transmit symbol is done correctly, the antenna index's bit error probability is obtained in a similar format to [9]. The antenna index is union bounded by:

$$P_a(k) \leq \frac{1}{\mathrm{N}_{TX} M \log_2(\mathrm{N}_{TX})} \sum_{q=1}^{M} \sum_{\widehat{w}=1}^{\mathrm{N}_{TX}} \sum_{w=1}^{\mathrm{N}_{TX}} N(w,\widehat{w})\, \mathrm{P}\left(\boldsymbol{x}_{wq} \to \boldsymbol{x}_{\widehat{w}q}\right), \quad (2\text{-}14)$$

where $\mathrm{P}\left(\boldsymbol{x}_{wq} \to \boldsymbol{x}_{\widehat{w}q}\right)$ is the pairwise error probability (PEP) of selecting the signal vector $\boldsymbol{x}_{\widehat{w}q}$, given that $\boldsymbol{x}_{wq}$ was transmitted. $N(w,\widehat{w})$ is the number of bit errors between the transmitted antenna index w and the estimated transmit antenna index $\widehat{w}$.

The closed-form of the conditional PEP of the channel matrix $\boldsymbol{H}$ is given in [9] as:

$$\mathrm{P}\left(\boldsymbol{x}_{wq} \to \boldsymbol{x}_{\widehat{w}q} | \boldsymbol{H}\right) = P\left(\left\|\boldsymbol{y} - \sqrt{\rho}\boldsymbol{h}_{\widehat{w}} x_q\right\|_F < \left\|\boldsymbol{y} - \sqrt{\rho}\boldsymbol{h}_w x_q\right\|_F\right) = Q(\sqrt{\gamma}), \quad (2\text{-}15)$$

where $\gamma = \frac{\rho}{2}\left\|\boldsymbol{h}_w x_q - \boldsymbol{h}_{\widehat{w}} x_q\right\|_F^2$ which can be simplified further:

$$\gamma = \frac{\rho}{2}\left|x_q\right|^2 \|\boldsymbol{h}_w - \boldsymbol{h}_{\widehat{w}}\|_F^2. \quad (2\text{-}16)$$

Using $Q(x) = \frac{1}{\pi}\int_0^{\pi/2} \exp\left(-\frac{s^2}{2\sin^2\theta}\right) d\theta$ as shown in [9], and solving for $P_\gamma = \int_0^\infty Q(\sqrt{\gamma})\, d\gamma$, the closed-form of (2-15) can be confirmed to be the same as (33) in [9]. This is computed using integration by parts, with the moment generating function (MGF) and the alternative form of Q-function, to get the average PEP over a joint distribution of the channel gain and this can be varied to be [9]:

$$\mathrm{P}\left(\boldsymbol{x}_{wq} \to \boldsymbol{x}_{\widehat{w}q}\right) = \mu^{\mathrm{N}_{RX}} \sum_{k=0}^{\mathrm{N}_{RX}-1} \binom{\mathrm{N}_{RX} - 1 + k}{k} [1-\mu]^k, \quad (2\text{-}17)$$

where $\mu = \frac{1}{2}\left(1 - \sqrt{\frac{\alpha}{\alpha+1}}\right)$ and $\alpha = \frac{\rho}{2}|x_q|^2$.

2.4 Computational Complexity Analysis at the Receiver

The complexity of the sub-optimal, optimal, and low-complexity near-ML SM detection schemes are computed in this section, employing complex addition and complex multiplication.

2.4.1 Sub-optimal Detection

This detection scheme involves the process of transmit antenna index evaluation combined with symbol estimation. Equations (2-5) and (2-6) set the rules for detecting antennas. The numerator in (2-5) requires N_{RX} complex multiplications and $(N_{RX} - 1)$ complex additions [49]. By taking a vector of length N_{RX} and multiplying it with its complex conjugate and then calculating the square root; then the Frobenius norm in the denominator of (2-5) is formulated. This yields N_{RX} complex multiplications and zero complex additions. Since (2-5) is evaluated for $j \in [1: N_{TX}]$, therefore, it requires a total of $2N_{TX}N_{RX} + N_{TX}(N_{RX} - 1)$ complex operations. The absolute value operation in (2-6) needs one complex multiplication and zero complex additions. Likewise, (2-6) is analyzed for $j \in [1: N_{TX}]$ and it will need N_{TX} complex operations [55].

The combination of the complexity contributions of both (2-5) and (2-6) results in the cumulative complexity for the antenna detection,

$$\delta_{ant} = 2N_{TX}N_{RX} + N_{TX}(N_{RX} - 1) + N_{TX} = 3N_{TX}N_{RX}. \quad (2\text{-}18)$$

To derive the complexity of the symbol estimation, (2-7) is analyzed. As seen in [19], where the first term is simplified by splitting $\left\|\boldsymbol{h}_{\widehat{w}}x_q\right\|_F^2 = \|\boldsymbol{h}_{\widehat{w}}\|_F^2\left|x_q\right|^2$. The complexity of $\|\boldsymbol{h}_{\widehat{w}}\|_F^2$ is not taken into consideration to avoid repetition since $\|\boldsymbol{h}_{\widehat{w}}\|_F$ has been previously calculated in (2-5) and the squaring of $\|\boldsymbol{h}_{\widehat{w}}\|_F$ is a non-complex operation. The evaluation of $\left|x_q\right|^2$ involves one complex multiplication and zero complex additions. This operation is done for $q \in [1: M]$ and therefore requires M complex operations. Note that the complexity of computing $\sqrt{\rho}\|\boldsymbol{h}_{\widehat{w}}\|_F^2\left|x_q\right|^2$ is not considered, since it requires the multiplication of non-complex quantities. In the second term of (2-7), $\boldsymbol{h}_{\widehat{w}}^H\, \boldsymbol{y}\, x_q^*$ is evaluated for $q \in [1: M]$ and therefore requires M complex multiplications and zero complex additions. Thus, the complexity of symbol detection can be expressed as,

$$\delta_{symbol} = 2M. \quad (2\text{-}19)$$

Therefore, the cumulative CC of sub-optimal SM detection is given by,

$$\delta_{sub-opt} = \delta_{ant} + \delta_{symbol} = 3N_{TX}N_{RX} + 2M. \quad (2\text{-}20)$$

2.4.2 Optimal SM detector

The ML-based detection approach shown in (2-4) is evaluated to obtain the complexity of SM-OD. As seen in [19], where the first term is made simple by splitting $\left\|\boldsymbol{h}_w x_q\right\|_F^2 = \|\boldsymbol{h}_w\|_F^2\left|x_q\right|^2$. The Frobenius norm operation $\|\boldsymbol{h}_w\|_F^2$ needs N_{RX} complex multiplications and zero complex additions. $\|\boldsymbol{h}_w\|_F^2$ is calculated for $j \in [1: N_{TX}]$ and therefore needs $N_{TX}N_{RX}$ complex multiplications and zero complex additions. The formulation of $\left|x_q\right|^2$ needs one complex

multiplication and zero complex additions. This operation is done for $q \in [1: M]$ and includes M complex multiplications and zero complex additions. Therefore, the first term of (2-10) has complexity [19],

$$\delta_{opt\_term1} = \mathrm{N}_{TX}\mathrm{N}_{RX} + M. \tag{2-21}$$

The second term's complexity in (2-10) depends on the calculation of $(\boldsymbol{y}^H \boldsymbol{h}_w)x_q$. The $\boldsymbol{y}^H \boldsymbol{h}_w$ operation is done for $j \in [1: \mathrm{N}_{TX}]$ and hereby requires $\mathrm{N}_{TX}\mathrm{N}_{RX}$ complex multiplications and $\mathrm{N}_{TX}(\mathrm{N}_{TX} - 1)$ complex additions. It can be proven that the multiplication of $\boldsymbol{y}^H \boldsymbol{h}_w$ by x_q needs $\mathrm{N}_{TX}M$ complex multiplications [19] and zero complex additions. Therefore, the second term's complexity is expressed as,

$$\delta_{opt\_term2} = \mathrm{N}_{TX}(2\mathrm{N}_{RX} + M - 1). \tag{2-22}$$

Hence, the total CC of SM-OD is given by,

$$\delta_{opt} = \delta_{opt\_term1} + \delta_{opt\_term2} = \mathrm{N}_{TX}(3\mathrm{N}_{RX} + M - 1) + M. \tag{2-23}$$

2.4.3 Computational Complexity of the Low-Complexity near-ML Detector

The initial step undertaken by the low-complexity near-ML Detector [18] is the computation of the equalized symbols from each transmit antenna element (2-8). The expression $\boldsymbol{h}_w^H \boldsymbol{y}$, requires N_{RX} complex multiplications and $(\mathrm{N}_{RX} - 1)$ complex additions for each transmit antenna element w. Also important to note that $\boldsymbol{y}^H$ is a $(1 \times \mathrm{N}_{RX})$ row vector and $\boldsymbol{h}_w$ is an $(\mathrm{N}_{RX} \times 1)$ column vector. $\|\boldsymbol{h}_w\|_F^2$ is the same as $\boldsymbol{h}_w^H \boldsymbol{h}_w$ and it requires N_{RX} complex multiplications and zero complex additions for each transmit antenna element w. The CC that is derived from the first step is,

$$\delta_{First\_step} = \mathrm{N}_{TX}(3\mathrm{N}_{RX} - 1) = 3\mathrm{N}_{RX}\mathrm{N}_{TX} - \mathrm{N}_{TX}. \tag{2-24}$$

The second step the detector undertakes is the demodulation of the estimated symbol of each transmit antenna element by employing the constellation demodulator/slicing function. Complex additions or multiplications are not required by the constellation demodulator/slicing function, and it also represents a one-to-one mapping [9], [19]. The second step does not impose any further CC. Hence, $\delta_{Second\_step} = 0$.

The third step undertaken by the low-complexity near-ML detector (2-10) is the application of the ML-decision rule [9] to derive a final estimation of both the transmit symbol and the transmit antenna index. The first term of (2-10), $\left\|\boldsymbol{z}_{wq}\right\|_F^2 = \left\|\boldsymbol{h}_w \hat{x}_{q_w}\right\|_F^2$ can be expressed as $\|\boldsymbol{h}_w\|_F^2 \left|\hat{x}_{q_w}\right|^2$. In the first step, the computation of $\|\boldsymbol{h}_w\|_F^2$ for $w \in [1: \mathrm{N}_{TX}]$ was executed; therefore, the results that were stored can be used. Hence, further N_{TX} complex multiplications are required for the computation of $\left\|\boldsymbol{z}_{wq}\right\|_F^2$ for $w \in [1: \mathrm{N}_{TX}]$ as a result of the computation of $\left|\hat{x}_{q_w}\right|^2$. Also computed

in the first step was $\boldsymbol{y}^H\boldsymbol{h}_w$ for $w \in [1{:}\,\mathrm{N}_{TX}]$ where the stored results can be used; so the complexity imposed by the second step of (2-10) $\boldsymbol{y}^H\boldsymbol{z}_{wq} = \boldsymbol{y}^H\boldsymbol{h}_w\hat{x}_{q_w}$, is as a result of $\boldsymbol{y}^H\boldsymbol{h}_w$ being multiplied by $\hat{x}_{q_w}$, and N_{TX} complex multiplications are required for $w \in [1{:}\,\mathrm{N}_{TX}]$.

Therefore, the CC imposed by the third step is expressed as,

$$\delta_{Third\_step} = 2\mathrm{N}_{TX}. \tag{2-25}$$

The CC imposed by the near-ML detector's low-complexity [18] is:

$$\delta_{low-complexity} = \delta_{First\_step} + \delta_{Second\_step} + \delta_{Third\_step} = (3\mathrm{N}_{RX} + 1)\mathrm{N}_{TX}. \tag{2-26}$$

2.4.4 Comparing Computational Complexities for SM Detectors

The CC formulated in Subsections 2.4.1, 2.4.2, and 2.4.3 are evaluated for 2×2, 2×4, 4×2 and 4×4 of different MIMO configurations with variable *M*-QAM constellation sizes; the results are tabulated in Table 2-2.

For the 2×2 4-QAM SM system, the optimal ML-based detector [19] is shown to impose 22 complex multiplications and additions, while the modified sub-optimal detector [9] and low-complexity near-ML detector [18] impose 20 and 14 complex operations, respectively. This represents a 9% and 30% reduction in receiver CC, respectively. However, the modified sub-optimal detector [9] achieves reduced receiver complexity at the expense of error performance compared to the optimal ML-based detector [19], as illustrated in the subsequent section. In contrast to the previous statement, the low-complexity near-ML detector [18] achieves an error performance result that is closely matched with the optimal ML-based detector [19], and it also yields a significant decrease in receiver complexity. Furthermore, since the CC of the low-complexity detector [18] is directly proportional to the constellation size, a significant reduction in complexity is achieved for $M > 16$, compared to the optimal ML-based detector [19].

In the 2×4 4-QAM SM system, the optimal ML-based detector [19] is shown to impose 34 complex multiplications and additions, while the modified sub-optimal detector [9] and low-complexity near-ML detector [18] impose 32 and 26 complex operations, respectively. This represents a 6% and 19% reduction in receiver CC.

Also, the 2×2 16-QAM SM system, the optimal ML-based detector [19], is shown to impose 58 complex multiplications and additions, while the modified sub-optimal detector [9] and low-complexity near-ML detector [18] impose 44 and 14 complex operations, respectively. This represents a 24% and 68% reduction in receiver CC.

The 2×4 16-QAM SM system, the optimal ML-based detector [19], is shown to impose 70 complex multiplications and additions, while the modified sub-optimal detector [9] and low-

complexity near-ML detector [18] impose 56 and 26 complex operations, respectively. This represents a 20% and 53% reduction in receiver CC.

For the 4×2 64-QAM SM system, the optimal ML-based detector [19] is shown to impose 340 complex multiplications and additions, while the modified sub-optimal detector [9] and low-complexity near-ML detector [18] impose 152 and 28 complex operations, respectively. This represents a 55% and 82% reduction in receiver CC.

Finally, in the 4×4 64-QAM SM system, the optimal ML-based detector [19] is shown to impose 364 complex multiplications and additions, while the modified sub-optimal detector [9] and low-complexity near-ML detector [18] impose 176 and 52 complex operations, respectively. This represents a 52% and 70% reduction in receiver CC.

Table 2-2: Comparison of computational complexities between SM detectors

Configuration	**Modified MRRC-based Sub-Optimal Detector -** (2-20)	**Optimal ML-based Detector -** (2-23)	**Low-Complexity near ML-based detector -** (2-26)
$\mathrm{N}_{TX} = 2, \mathrm{N}_{RX} = 2, M = 4$	20	22	14
$\mathrm{N}_{TX} = 2, \mathrm{N}_{RX} = 4, M = 4$	32	34	26
$\mathrm{N}_{TX} = 2, \mathrm{N}_{RX} = 2, M = 16$	44	58	14
$\mathrm{N}_{TX} = 2, \mathrm{N}_{RX} = 4, M = 16$	56	70	26
$\mathrm{N}_{TX} = 4, \mathrm{N}_{RX} = 2, M = 64$	152	340	28
$\mathrm{N}_{TX} = 4, \mathrm{N}_{RX} = 4, M = 64$	176	364	52

2.5 Simulation Results and Discussion

In this section, Monte Carlo simulation results for various SM configurations have been presented. For each configuration, the simulation results plot the average BER performance against the average SNR at each receive antenna. Furthermore, these results are compared to the analytical performance bounds detailed in (2-10) – (2-14).

Monte Carlo simulations are performed over i.i.d. Rayleigh frequency-flat fading channel with AWGN. Gray-coded M-QAM constellations have been utilized for all simulations. Additionally, it is assumed that the receiver has full knowledge of the channel. The Monte Carlo simulations

are depicted for spectral efficiencies of 4, 6, and 8 b/s/Hz. This ensures the consideration of a wide variety of hardware configurations for SM. The notation used to denote the $N_{TX} \times N_{RX}$ configuration of SM is M, N_{TX}, N_{RX}.

The result presented in Figure 2-4 is equipped with two transmit antennas coupled with four and two receive antennas, respectively, employing 4-QAM. The analytical result validates the Monte Carlo simulation results, as they closely match from low SNR to high SNR region. It was observed that, as the number of the receive antenna increases, the BER performance of the system improves as expected. At a BER of 10^{-5}, the 2×4 4-QAM SM system achieves a gain of approximately 11 dB over 2×2 4-QAM SM system.

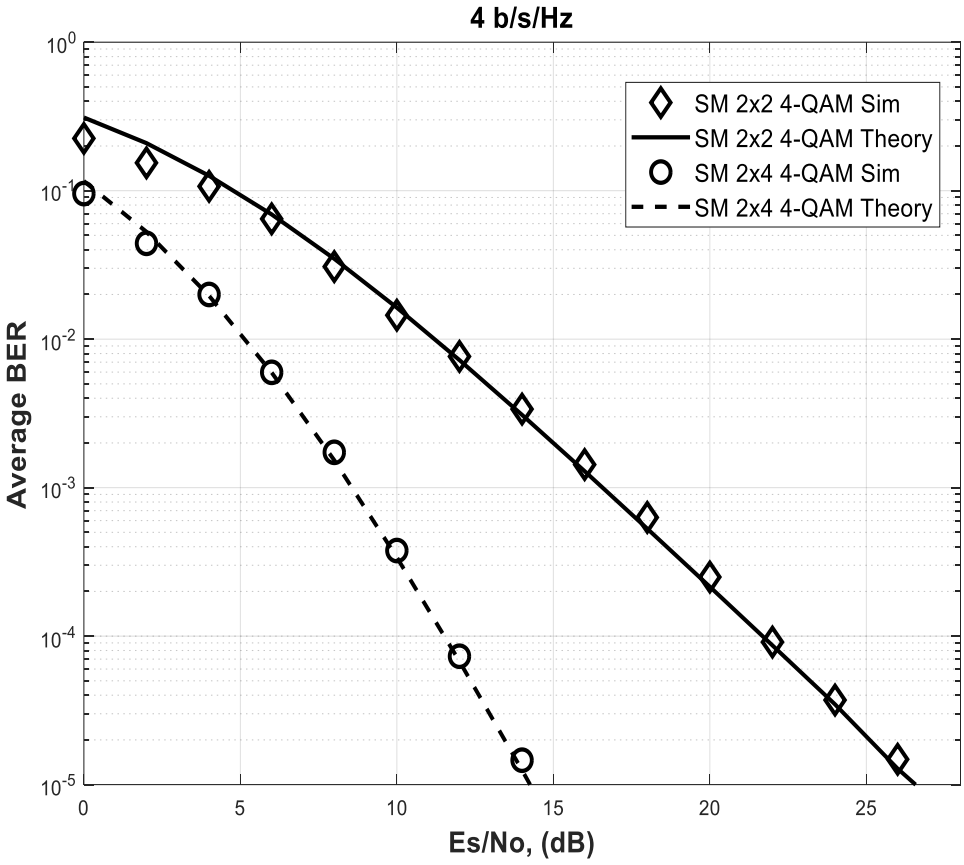

Figure 2-4. Validation of 4-QAM 2×2 and 2×4 SM theoretical analysis with the Monte Carlo simulation result.

The result presented in Figure 2-5, is equipped with two transmit antennas coupled with four and two receive antennas, respectively, employing 16-QAM. The theoretical result validates the Monte Carlo simulation results. At a BER of 10^{-5} the 2×4 16-QAM SM system achieves a gain of approximately 10 dB over the 2×2 16-QAM SM system.

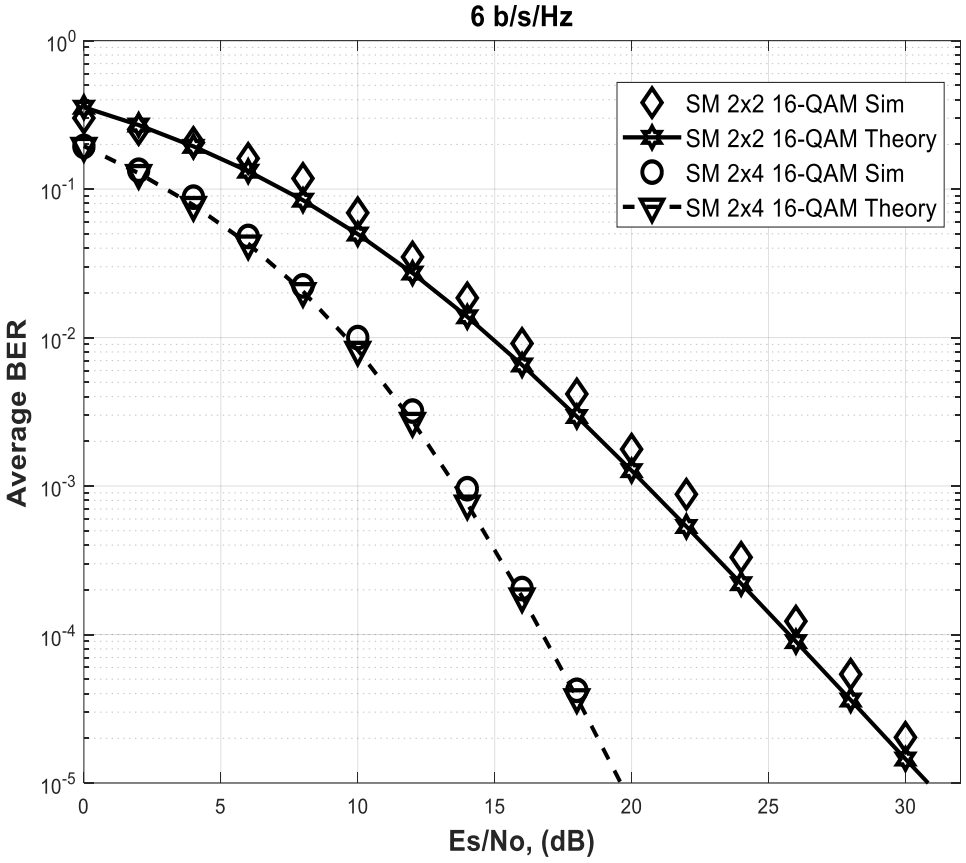

Figure 2-5. Validation of 16-QAM 2 × 2 and 2 × 4 SM theoretical analysis with the Monte Carlo simulation result.

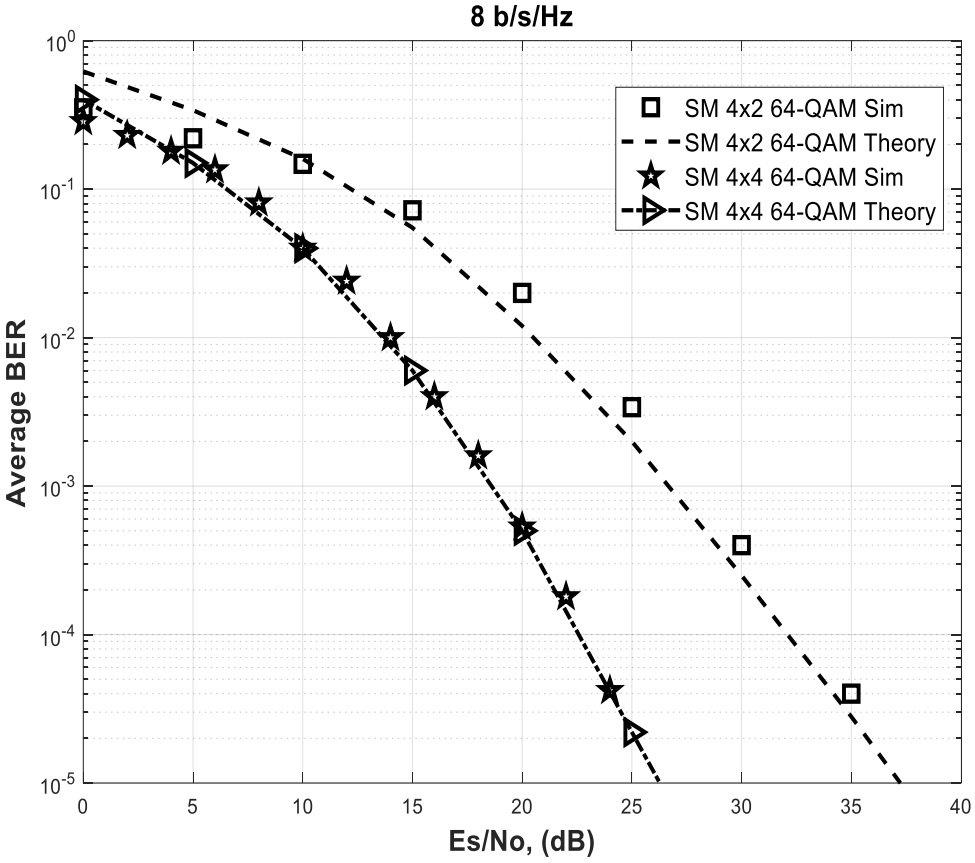

Figure 2-6. Validation of 64-QAM 4×2 and 4×4 SM theoretical analysis with the Monte Carlo simulation result.

In Figure 2-6, at a BER of 10^{-5} the 4×4 64-QAM SM system achieves a gain of approximately 10 dB over 4×2 64-QAM SM system, with the theoretical result validating the Monte Carlo simulation results from low SNR to high SNR region.

Chapter Summary

The system model of a conventional SM system with an optimal detector was presented in this chapter. Similarly, the average BER for M-QAM SM system with optimal detector over an i.i.d Rayleigh frequency-flat fading channel $\boldsymbol{H}$ was also presented. The formulated theoretical analysis validated the Monte Carlo simulation results. The performance analysis is shown to be relatively tight with the simulated BER of the SM system, as shown in Figures 2-4, 2-5, and 2-6, respectively.

CHAPTER 3

Quadrature Spatial Modulation

3 Introduction

The major limitation of the SM scheme is that its data rate only increases in logarithm base-two of the entire transmit antennas compared to other SMUX techniques. This led to a method with improved spectral efficiency of SM being introduced called QSM.

In wireless communication, high data rates are highly desirable, but an increase in data rates requires extra transmit antennas, which leads to increased cost. Consequently, the higher the number of transmit antennas utilized, the higher the CC. MIMO systems can attain high spectral efficiencies with good system robustness [7, 10]; this has attracted lots of researchers to the system over time resulting in the creative use of multiple transmitting antennas to achieve high spectral efficiency. While SM is viewed as a hugely advantageous MIMO system, there are still improvements to be made. Mesleh *et al.* introduced the QSM scheme [35, 53] as a creative means to improve upon the SM spectral efficiency. QSM adds an extra dimension to its spatial dimensional modulation, which splits the spatial dimension to the in-phase and quadrature dimensions to increase the system's overall spectral efficiency [54]. The constellation symbols are further broken down into their real and imaginary parts. At the same time, the first antenna transmits the real part of the constellation symbol, and the imaginary part is transmitted with the second antenna. Note, the antennas may be identical and is based on the mode of mapping employed.

In the QSM scheme, IAS and ICI are completely avoided, since the constellation symbols modulate their in-phase and quadrature parts to the cosine and sine carriers [53, 54].

3.1 System Model of Quadrature Spatial Modulation

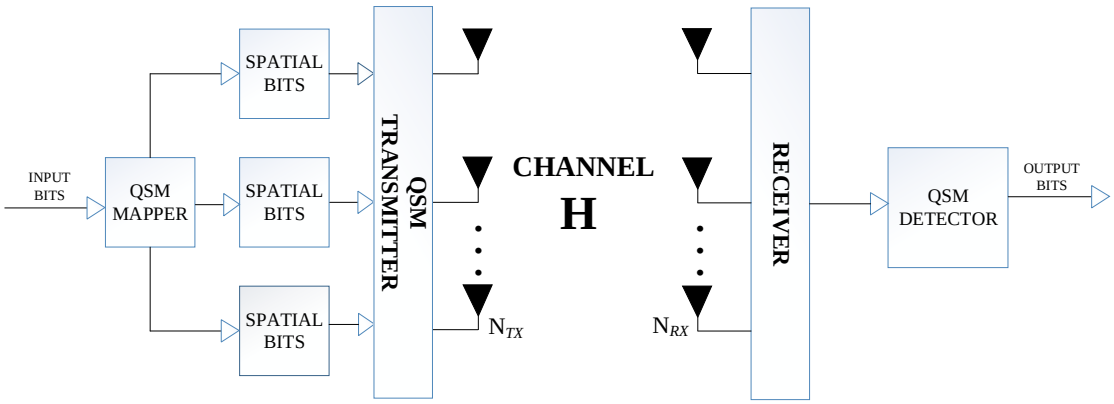

Figure 3-1. QSM System Model [48]

The QSM system's spectral efficiency is denoted by $m = \log_2(M\mathrm{N}_{TX}^2)$ [53, 54], where M is the modulation order of M-ary APM constellation signal and N_{TX} is the total number of transmit antennas. In the QSM scheme, the $\log_2 M$ bit modulates the M-QAM symbol r_q, $q \in [1: M]$. The real part of the symbol is transmitted by the active transmit antenna selected by the $\log_2 \mathrm{N}_{TX}$ bits. However, the extra $\log_2 \mathrm{N}_{TX}$ bits are utilized in choosing the second transmit antenna, which transmits the symbol's imaginary part. Consequently, a total of $2\log_2 \mathrm{N}_{TX}$ bits are needed to select the active antenna indices expected to transmit the constellation symbol at each given transmission instant.

Hence, the modulated symbol $r_q = r_{Re}^q + ir_{Imag}^q$ is decomposed further into its real and imaginary parts, while the real part of the modulated symbol r_{Re}^q is transmitted by one of the selected active transmit antenna index j_{Re}, the imaginary part of the modulated symbol ir_{Imag}^q is transmitted by the second transmit antenna index j_{Imag}. The QSM scheme utilizes transmit antennas which could be either one or two based on the mode of mapping employed, and it yields an improvement in its spectral efficiency compared to the conventional SM scheme.

Table 3-1: Table showing the constellation points used for Gray-coded 16-QAM

$\log_2 M$ bits	M-QAM Symbol
0 0 0 0	$r_q = -3 + 3i$
0 0 0 1	$r_q = -3 + 1i$
0 0 1 0	$r_q = -3 - 3i$
0 0 1 1	$r_q = -3 - 1i$
0 1 0 0	$r_q = -1 + 3i$
0 1 0 1	$r_q = -1 + 1i$
0 1 1 0	$r_q = -1 - 3i$
0 1 1 1	$r_q = -1 - 1i$
1 0 0 0	$r_q = 3 + 3i$
1 0 0 1	$r_q = 3 + 1i$

1 0 1 0	$r_q = 3 - 3i$
1 0 1 1	$r_q = 3 - 1i$
1 1 0 0	$r_q = 1 + 3i$
1 1 0 1	$r_q = 1 + 1i$
1 1 1 0	$r_q = 1 - 3i$
1 1 1 1	$r_q = 1 - 1i$

Table 3-1 shows the constellation points used to deduce the mapping technique shown in Table 3-2. Configurations for the 4-QAM and 16-QAM mapping patterns are illustrated in Table 3-2.

Table 3-2 shows the QSM system with varying spectral efficiencies as a result of their different N_{TX} and modulation order M. Taking the third row as an example, it is a 4×4 16-QAM QSM system with a generated spectral efficiency of 8 b/s/Hz.

The symbol r_q, is chosen by the first four bits, while the antenna index j_{Re} that is to convey the real part of the symbol r_{Re}^{q} is activated by the next two bits, and the remaining two bits activate the antenna index j_{Imag} that carries the imaginary part of the symbol ir_{Imag}^{q}.

The symbol r_q, being transmitted consists of both r_{Re}^{q} and r_{Imag}^{q} and is transmitted assuming a Rayleigh frequency-flat fading channel $\boldsymbol{H}$. $\boldsymbol{H}$ is a complex channel gain matrix of dimension $\mathrm{N}_{RX} \times \mathrm{N}_{TX}$, with i.i.d entries of $CN(0,1)$ distribution and encounters AWGN which is modelled as an $\mathrm{N}_{RX} \times 1$ complex vector $\boldsymbol{n}$ with i.i.d entries and $CN(0,1)$ distribution.

When the two antennas are identical, it should be noted that the antenna indices for selecting the antenna to transmit both the in-phase and the quadrature parts of the constellation symbol are the same when a single transmitting antenna is being employed, so that $r_q = r_{Re}^{q} + ir_{Imag}^{q}$. Therefore, the received signal vector obtained is:

$$\boldsymbol{y} = \sqrt{\rho}\boldsymbol{h}_{\ell} r_q + \boldsymbol{n}, \ell \in [1{:}\,\mathrm{N}_{TX}], \ell = j_{Re} = j_{Imag}, q \in [1{:}\,M], \tag{3-1}$$

where $\rho = \frac{E_s}{N_0}$ is the average SNR at each receive antenna, E_s is the average symbol energy for each symbol, N_0 is the single-sided power spectral density. Also, ℓ is the transmit antenna index, while $\boldsymbol{h}_{\ell}$ represents the ℓ^{th} column of $\boldsymbol{H}$.

Table 3-2: Example of the mapping process for the QSM system

Configuration	**Input Bits** $\log_2 M\mathrm{N}_{TX}^2$	**First** $\log_2 M$ **bits**	**Second** $\log_2 \mathrm{N}_{TX}$ **bits**	**Third** $\log_2 \mathrm{N}_{TX}$ **bits**
$M = 4$ $\mathrm{N}_{TX} = 2$	0 1 0 1	$\log_2 4 = 2$ bits [0 0] $r_q = -1 + i$ $r_{Re}^q = -1$ $r_{Imag}^q = +i$	$\log_2 2 = 1$ bit [0] $j_{Re} = 1$	$\log_2 2 = 1$ bit [1] $j_{Imag} = 2$
$M = 4$ $\mathrm{N}_{TX} = 4$	0 1 1 0 0 1	$\log_2 4 = 2$ bits [0 1] $r_q = -1 + i$ $r_{Re}^q = -1$ $r_{Imag}^q = +i$	$\log_2 4 = 2$ bits [1 0] $j_{Re} = 3$	$\log_2 4 = 2$ bits [0 1] $j_{Imag} = 2$
$M = 16$ $\mathrm{N}_{TX} = 4$	1 0 0 1 1 1 0 1	$\log_2 16 = 4$ bits [1 0 0 1] $r_q = +3 + i$ $r_{Re}^q = +3$ $r_{Imag}^q = +i$	$\log_2 4 = 2$ bits [1 1] $j_{Re} = 4$	$\log_2 4 = 2$ bits [0 1] $j_{Imag} = 2$

For the case of different antenna mappings, the t^{th} antenna is used to transmit the real and imaginary components of the symbol. Therefore, the received signal can be expressed as:

$$\boldsymbol{y} = \sqrt{\rho}\boldsymbol{h}_{j_{Re}} r_{Re}^q + \sqrt{\rho} i \boldsymbol{h}_{j_{Imag}} r_{Imag}^q + \boldsymbol{n}, \tag{3-2}$$

where $\boldsymbol{h}_{j_{Re}}$ and $\boldsymbol{h}_{j_{Imag}}$ represents the j_{Re}^{th} and j_{Imag}^{th} columns of $\boldsymbol{H}$.

In (3-2), $\boldsymbol{y}$ represents the received signal when two transmit antennas are used for transmission. In this way, the active transmit antenna that transmits both the real and imaginary components of the constellation symbol is selected by different antenna indices.

To recover the transmitted information, the modulated symbol and antenna index are estimated by the optimal detection of the received signal $\boldsymbol{y}$, provided the full knowledge of the channel is assumed to be known at the receiver.

3.1.1 Optimal Detection

In this subsection, the received signal is demodulated optimally by employing the ML detection, as the entire signal space of the M constellation points and all antenna index combinations are thoroughly searched. The joint estimation of $\hat{j}_{Re}, \hat{j}_{Imag}$ which are the antenna indices detected for both the real and imaginary components and $\hat{r}_{Re}^{q}, \hat{r}_{Imag}^{q}$ which indicate the detected data symbols for both the real and imaginary components are employed in retrieving the original message and is illustrated as:

$$\left[\hat{j}_{Re}, \hat{j}_{Imag}, \hat{r}_{Re}^{q}, \hat{r}_{Imag}^{q}\right] = \underset{j_{Re}, j_{Imag}, r_{Re}^{q}, r_{Imag}^{q}}{\operatorname{argmin}} \left(\left\| \boldsymbol{y} - \sqrt{\rho} \left(\boldsymbol{h}_{j_{Re}} r_{Re}^{q} + i \boldsymbol{h}_{j_{Imag}} r_{Imag}^{q} \right) \right\|_{F}^{2} \right). \quad (3\text{-}3)$$

However, if

$$\boldsymbol{g} = \sqrt{\rho} \left(\boldsymbol{h}_{j_{Re}} r_{Re}^{q} + i \boldsymbol{h}_{j_{Imag}} r_{Imag}^{q} \right), \quad (3\text{-}4)$$

expanding the Frobenius norm in Equation (3-3) will be simplified to derive:

$$\left[\hat{j}_{Re}, \hat{j}_{Imag}, \hat{r}_{Re}^{q}, \hat{r}_{Imag}^{q}\right] = \underset{j_{Re}, j_{Imag}, r_{Re}^{q}, r_{Imag}^{q}}{\operatorname{argmin}} \left\{ \|\boldsymbol{g}\|_{F}^{2} - 2Re\{\boldsymbol{y}^{H} \boldsymbol{g}\} \right\}, \quad (3\text{-}5)$$

where $Re\{\cdot\}$ is the real part of the complex value.

3.2 The Performance Analysis of M-QAM Quadrature Spatial Modulation using Asymptotic Tight Union Bound

In [53], a detailed theoretical error performance analysis for the M-QAM QSM system was computed.

Taking into account the signal received, $\boldsymbol{y}$ in Equation (3-2), we let $\widehat{\boldsymbol{g}} = \sqrt{\rho} \boldsymbol{h}_{\hat{j}_{Re}} \hat{r}_{Re}^{q} + \sqrt{\rho} i \boldsymbol{h}_{\hat{j}_{Imag}} \hat{r}_{Imag}^{q}$, while $\boldsymbol{g}$ is defined in Equation (3-4) then [53],

$$P_{r}(\boldsymbol{g} \to \widehat{\boldsymbol{g}} | \boldsymbol{H}) = Q\left(\sqrt{\zeta}\right), \quad (3\text{-}6)$$

where $P_{r}(\boldsymbol{g} \to \widehat{\boldsymbol{g}} | \boldsymbol{H})$ denotes the PEP conditioned on the channel matrix $\boldsymbol{H}$, $Q(\cdot)$ designates the Gaussian Q-function and ζ is a random variable given by:

$$\zeta = \|\boldsymbol{g} - \widehat{\boldsymbol{g}}\|_{F}^{2} = |\mathbf{A} + i\mathbf{B}|^{2}, \quad (3\text{-}7)$$

where: $\mathbf{A} = \sqrt{\rho} \left[Re\left(\boldsymbol{h}_{j_{Re}} r_{Re}^{q}\right) - Imag\left(\boldsymbol{h}_{j_{Imag}} r_{Imag}^{q}\right) - Re\left(\boldsymbol{h}_{\hat{j}_{Re}} \hat{r}_{Re}^{q}\right) + Imag\left(\boldsymbol{h}_{\hat{j}_{Imag}} \hat{r}_{Imag}^{q}\right) \right]$,

$$\mathbf{B} = \sqrt{\rho}\left[Imag\left(\boldsymbol{h}_{j_{Re}} r_{Re}^{q}\right) + Re\left(\boldsymbol{h}_{j_{Imag}} r_{Imag}^{q}\right) - Imag\left(\boldsymbol{h}_{\hat{j}_{Re}} \hat{r}_{Re}^{q}\right) - Re\left(\boldsymbol{h}_{\hat{j}_{Imag}} \hat{r}_{Imag}^{q}\right)\right].$$

In [53], ζ is given as a random variable which has the following mean conditions:

$$\bar{\zeta} = \begin{cases} \rho\left(\left|r_{Re}^{q}\right|^2 + \left|\hat{r}_{Re}^{q}\right|^2 + \left|r_{Imag}^{q}\right|^2 + \left|\hat{r}_{Imag}^{q}\right|^2\right) \text{ if } \boldsymbol{h}_{j_{Re}} \neq \boldsymbol{h}_{\hat{j}_{Re}}, \boldsymbol{h}_{j_{Imag}} \neq \boldsymbol{h}_{\hat{j}_{Imag}}, \\ \rho\left(\left|r_{Re}^{q} - \hat{r}_{Re}^{q}\right|^2 + \left|r_{Imag}^{q}\right|^2 + \left|\hat{r}_{Imag}^{q}\right|^2\right) \text{ if } \boldsymbol{h}_{j_{Re}} = \boldsymbol{h}_{\hat{j}_{Re}}, \boldsymbol{h}_{j_{Imag}} \neq \boldsymbol{h}_{\hat{j}_{Imag}}, \\ \rho\left(\left|r_{Re}^{q} - \hat{r}_{Re}^{q}\right|^2 + \left|r_{Imag}^{q} - \hat{r}_{Imag}^{q}\right|^2\right) \text{if } \boldsymbol{h}_{j_{Re}} = \boldsymbol{h}_{\hat{j}_{Re}}, \boldsymbol{h}_{j_{Imag}} = \boldsymbol{h}_{\hat{j}_{Imag}}, \\ \rho\left(\left|r_{Re}^{q}\right|^2 + \left|\hat{r}_{Re}^{q}\right|^2 + \left|r_{Imag}^{q} - \hat{r}_{Imag}^{q}\right|^2\right) \text{ if } \boldsymbol{h}_{j_{Re}} \neq \boldsymbol{h}_{\hat{j}_{Re}}, \boldsymbol{h}_{j_{Imag}} = \boldsymbol{h}_{\hat{j}_{Imag}}. \end{cases} \quad (3\text{-}8)$$

Therefore, the average PEP assuming just a single receive antenna ($\mathrm{N}_{RX} = 1$) is given as [53]:

$$\overline{\mathrm{P}}_e(\boldsymbol{g} \to \hat{\boldsymbol{g}}) = \frac{1}{2}\left(1 - \sqrt{\frac{\frac{\bar{\zeta}}{2}}{1+\bar{\zeta}/2}}\right), \quad (3\text{-}9)$$

where $\bar{\zeta}$ has been defined in (3-8).

Hence, to evaluate the ABEP of the QSM scheme, an asymptotic tight union bound shown in Equation (3-10) is employed and it is illustrated by [53]:

$$P_b \leq \frac{1}{m2^m} \sum_{n=1}^{2^m} \sum_{k=1}^{2^m} \frac{1}{m} \overline{\mathrm{P}}_e(\boldsymbol{g} \to \hat{\boldsymbol{g}}) e_{(n,k)}, \quad (3\text{-}10)$$

where m is the spectral efficiency of the QSM scheme, $\overline{\mathrm{P}}_e$ is the average PEP and $e_{(n,k)}$ is the number of bit errors associated with the corresponding PEP event. On the other hand, assuming N_{RX} receive antennas; the instantaneous PEP is given by [53]:

$$\mathrm{P}_e(\boldsymbol{g} \to \hat{\boldsymbol{g}}) = Q\left(\sqrt{\sum_{k=1}^{\mathrm{N}_{RX}} \zeta_k}\right). \quad (3\text{-}11)$$

The average PEP is written as [53]:

$$\overline{\mathrm{P}}_e(\boldsymbol{g} \to \hat{\boldsymbol{g}}) = \gamma_\lambda^{\mathrm{N}_{RX}} \sum_{k=0}^{\mathrm{N}_{RX}-1} \binom{\mathrm{N}_{RX} - 1 + k}{k} [1 - \gamma_\lambda]^k, \quad (3\text{-}12)$$

where γ_λ equals $\frac{1}{2}\left(1 - \sqrt{\frac{\frac{\bar{\zeta}}{2}}{1+\bar{\zeta}/2}}\right)$. The average PEP after taking the Taylor series of (3-12) and ignoring higher-order terms is given by the following asymptotic average PEP [53]:

$$\overline{\mathrm{P}}_e(\boldsymbol{g} \to \hat{\boldsymbol{g}}) \cong \frac{2^{\mathrm{N}_{RX}-1}\Gamma(\mathrm{N}_{RX}+0.5)}{\sqrt{\pi(\mathrm{N}_{RX})!}} \left(\frac{1}{\bar{\zeta}}\right)^{\mathrm{N}_{RX}}, \quad (3\text{-}13)$$

showing a diversity gain of N_{RX}.

The Monte Carlo simulation results were validated using the upper bound approach, with just a slight difference noticed at the lower SNR regions. When a lower bound approach is employed in the calculation of the performance analysis for *M*-QAM SM, there is a better validation of the

Monte Carlo simulation results in the low SNR as shown in [9], so this is the motivation that led to the derivation of the performance analysis for QSM system employing the lower bound approach of [9] to validate the Monte Carlo simulation results.

3.3 The Performance Analysis for M-QAM Quadrature Spatial Modulation using Lower-Bound

Just as shown in [9], a lower bound approach was employed in the theoretical analysis of the square *M*-QAM QSM method, which showed an improvement at the lower SNR. The theoretical analysis of the lower-bound QSM system is estimated as:

$$\mathrm{P}_e \geq 1 - \big((1 - P_a)(1 - P_b)\big) = P_a + P_b - P_a P_b, \tag{3-14}$$

where P_a represents the bit error probability of the antenna index provided the symbol is detected correctly and P_b is the bit error probability of the estimated symbol provided the antenna index is detected correctly.

3.3.1 Analytical Average BER of Symbol Estimation

Taking into account that the antenna index is correctly detected and the derived symbol estimation when using the square *M*-QAM, then P_b can be formulated in a similar way as in [9] and [52]:

$$P_b = \frac{1}{\log_2 M}\left(4A_l^M - \left(4A_l^M\right)^2\right), \tag{3-15}$$

where $A_l^M = \left(1 - \frac{1}{\sqrt{M}}\right) Q\left(\sqrt{\frac{3\rho}{2(M-1)}}\right)$. Since there are two transmit antennas active at the same time to transmit the real and imaginary component of the symbol, $\frac{\rho}{2}$ is used.

If the alternative Q-function is substituted into P_b and the trapezoidal rule is applied to $Q(x)$ and $Q^2(x)$ in MGF as seen in [52] for the MRC and the Rayleigh fading channel, the closed-form of P_b is shown in [9] and [52] as:

$$P_b(k) = \frac{1}{\log_2 M}\left(\frac{a}{c}\left[\frac{1}{2}\left(\frac{2}{b\rho+2}\right)^{\mathrm{N}_{RX}} - \frac{a}{2}\left(\frac{1}{b\rho+1}\right)^{\mathrm{N}_{RX}} + (1-a)\sum_{i=1}^{c-1}\left(\frac{2\sin^2\theta}{b\rho+2\sin^2\theta}\right)^{\mathrm{N}_{RX}} + \sum_{i=c}^{2c-1}\left(\frac{2\sin^2\theta}{b\rho+2\sin^2\theta}\right)^{\mathrm{N}_{RX}}\right]\right), \tag{3-16}$$

where $a = 1 - \frac{1}{\sqrt{M}}$, $b = \frac{3}{M-1}$, $\theta = \frac{i\pi}{4c}$ and c is the number of summations, where $c > 10$ results in the converging of the simulated and theoretical SER.

3.3.2 Analytical Average BER of Transmit Antenna Index Estimation

Also, employing the mode of computation as used in [9], and provided that the transmit symbol is estimated correctly, P_a is derived as the transmit antenna index bit error probability and can be estimated as:

$$P_a(k) \leq \frac{1}{N_{TX} \times M \times \log_2(\mathrm{N}_{TX})} \sum_{q=1}^{M} \sum_{n=1}^{\mathrm{N}_{TX}} \sum_{k=1}^{\mathrm{N}_{TX}} e_{(n,k)} \times \overline{\mathrm{P}}_e(\boldsymbol{g} \to \widehat{\boldsymbol{g}}), \tag{3-17}$$

where $e_{(n,k)}$ is the number of bit errors associated with the corresponding PEP event. To deduce the average PEP, we average (3-14) over joint probability distribution of the channel gain using MGF and alternative form of Q-function over a Rayleigh fading channel, which is given in [38]. Using integration by part, the closed-form can be expressed as [9],

$$\overline{\mathrm{P}}_e\,(\boldsymbol{g} \to \widehat{\boldsymbol{g}}) = \gamma_\lambda^{\mathrm{N}_{RX}} \sum_{k=0}^{\mathrm{N}_{RX}-1} \binom{\mathrm{N}_{RX} - 1 + k}{k} [1 - \gamma_\lambda]^k, \tag{3-18}$$

where $\gamma_\lambda = \frac{1}{2}\left(1 - \sqrt{\frac{\frac{\bar{\zeta}}{2}}{1+\bar{\zeta}/2}}\right)$ and $\bar{\zeta}$ is the mean random variable defined in (3-8).

Also, due to the decomposition of the constellation symbol into its real and imaginary parts with two different transmit antennas, respectively, the antenna error of transmitting the real part and the imaginary part of the symbol is considered independently such that, $P_a = 2P_a$, considering P_a^2 is negligible given that:

$$P_a = 1 - (1 - P_a)(1 - P_a) \cong 2P_a. \tag{3-19}$$

As the two transmit antennas are active at the same time, therefore, the substitution of (3-18) in (3-17) will be expressed as:

$$P_a(k) \leq \sum_{q=1}^{M} \sum_{n=1}^{\mathrm{N}_{TX}} \sum_{k=1}^{\mathrm{N}_{TX}} \frac{\gamma_\lambda^{\mathrm{N}_{RX}} \sum_{k=0}^{\mathrm{N}_{RX}-1} \binom{\mathrm{N}_{RX}-1+k}{k} [1-\gamma_\lambda]^k e_{(n,k)}}{\mathrm{N}_{TX} \times M \times \log_2(\mathrm{N}_{TX})}. \tag{3-20}$$

3.4 Simulated Results of the BER and the Computed Analytical BER of the Quadrature Spatial Modulation System

In this section, an asymptotic tight union bound and the lower bound approach was used in computing the analytical result of the conventional QSM system to substantiate the result of the Monte Carlo simulations. Also, the error performance of QSM has been compared to Monte Carlo simulations of SM. The notation $\mathrm{N}_{TX} \times \mathrm{N}_{RX}$ denotes the number of transmit antennas and the number of receive antennas, respectively.

As seen in Figure 3-2, the system has two transmit antennas and with two and four receive antennas, respectively, when employing 4-QAM, i.e., it is a 2×4 4-QAM and 2×2 4-QAM system. There was a noticeable improvement in the BER performances as the number of receive antenna N_{RX} increased. There was a gain of approximately 12 dB in the 2×4 4-QAM QSM system over the 2×2 4-QAM QSM system at a BER of 10^{-5}.

Employing a lower bound approach to obtain the analytical result, which substantiates the result of the Monte Carlo simulations from a region low SNR to high SNR region in comparison to the

asymptotic union bound approach, which has a wider range of values at the low SNR region. When using the configuration of $N_{RX} = 4$, the result that was obtained when the asymptotic union bound approach was employed had a variation of approximately 2 dB at the lower SNR as opposed to the 1.5 dB at the lower SNR obtained when the proposed lower bound approach was utilized.

Also, in Figure 3-2, using the configuration of $N_{RX} = 4$, the result that was obtained when the asymptotic union bound approach was employed had a variation of approximately 6 dB at the lower SNR as opposed to the 4 dB at the lower SNR obtained when the proposed lower bound approach was utilized, this is shown in Table 3-4.

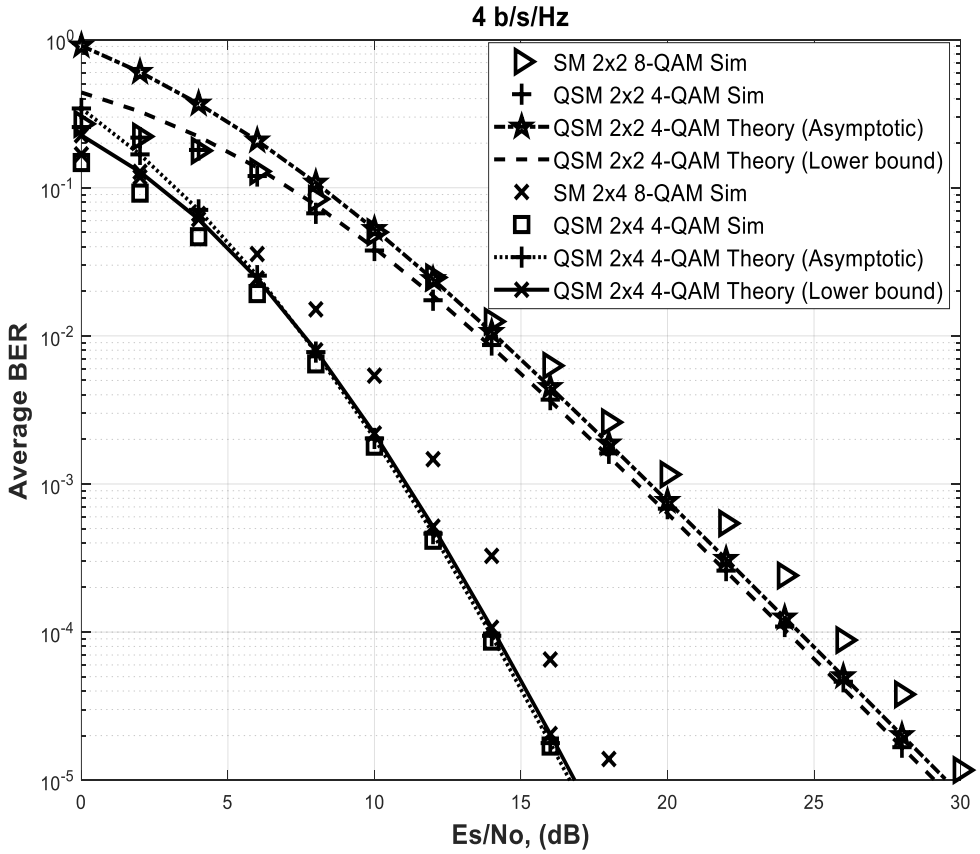

Figure 3-2. Validation of 8-QAM 2 × 2 SM and 4-QAM 2 × 2, 2 × 4 QSM theoretical analysis with the Monte Carlo simulation result.

As seen in Figure 3-3, it consists of two system configurations for the QSM scheme, i.e., the 4 × 4 4-QAM and 4 × 2 4-QAM system. When the configuration of $N_{RX} = 4$ is set, the result that was obtained when the asymptotic union bound approach was employed had a variation of approximately 4 dB at the low SNR region as opposed to the 1.8 dB when the proposed lower bound approach was utilized. There was a gain of approximately 13 dB in the 4 × 4 4-QAM QSM system over the 4× 2 4-QAM QSM system at a BER of 10^{-5}.

The 4×4 4-QAM QSM system is also compared with the SM system of the same spectral efficiency. There is a 3 dB gain over the SM at a set configuration of $N_{RX} = 4$. Also, using the same system settings with a set configuration of $N_{RX} = 2$, i.e., 4×2 4-QAM QSM and 4×2 16-QAM, the SM system was compared, and a gain of approximately 2 dB was achieved. Table 3-3 shows the various gain achieved under different configurations.

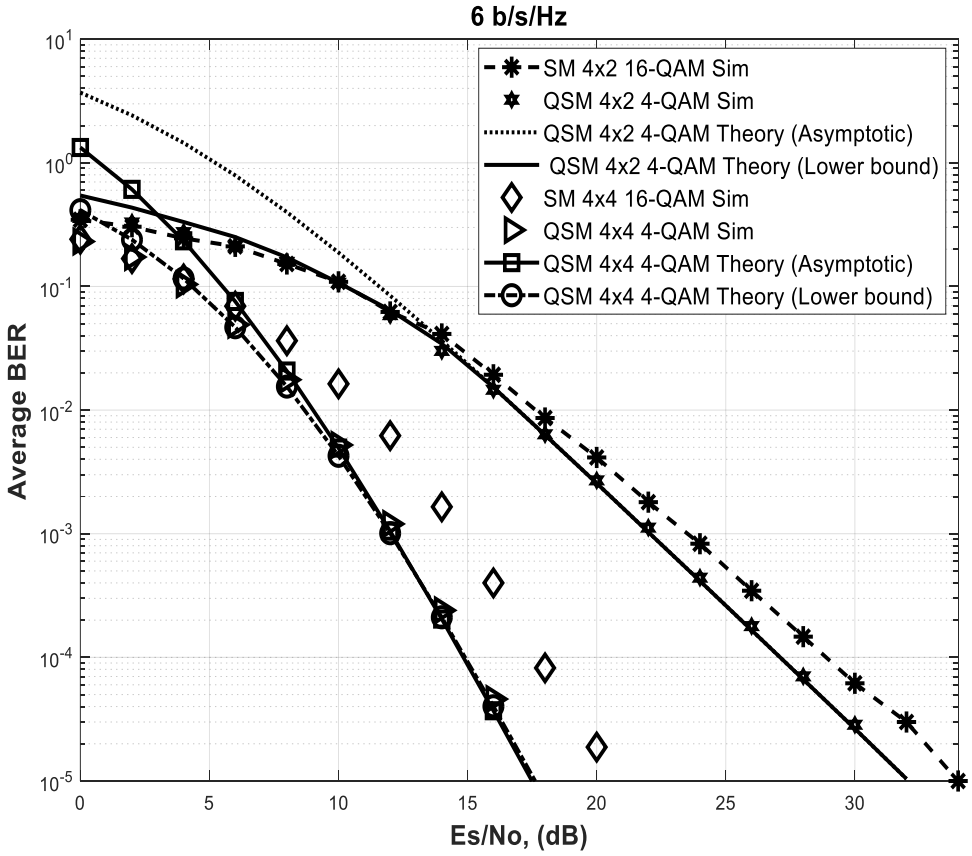

Figure 3-3. Validation of 16-QAM 4×2 SM and 4-QAM 4×2, 4×4 QSM theoretical analysis with the Monte Carlo simulation result.

In Figure 3-4, a QSM system with configuration 4×4 16-QAM and 4×2 16-QAM is shown. It was noticed that as the number of receive antenna N_{RX} increases, the analytical result, and the Monte Carlo simulation results are both tight at higher SNR regions. Consequently, there seems to be an improvement in the BER performance of the overall system as the number of the receive antenna N_{RX} increases. The 4×4 16-QAM QSM system achieves a gain of approximately 13 dB over the 4×2 16-QAM QSM system at a BER of 10^{-5}.

As seen in Figure 3-5, when the configuration of $N_{RX} = 4$ is set, the result that was obtained when the asymptotic union bound approach was employed had a variation of approximately 9 dB at the low SNR region as opposed to the 3.5 dB when the proposed lower bound approach was utilized, which proves a better validation of the Monte Carlo simulation result.

Likewise, when the configuration of $N_{RX} = 2$ is set, the lower bound approach has a variation of approximately 6 dB, as opposed to the asymptotic union bound approach, which has a variation of approximately 14 dB. Table 3-3 shows the various gain achieved under different configurations.

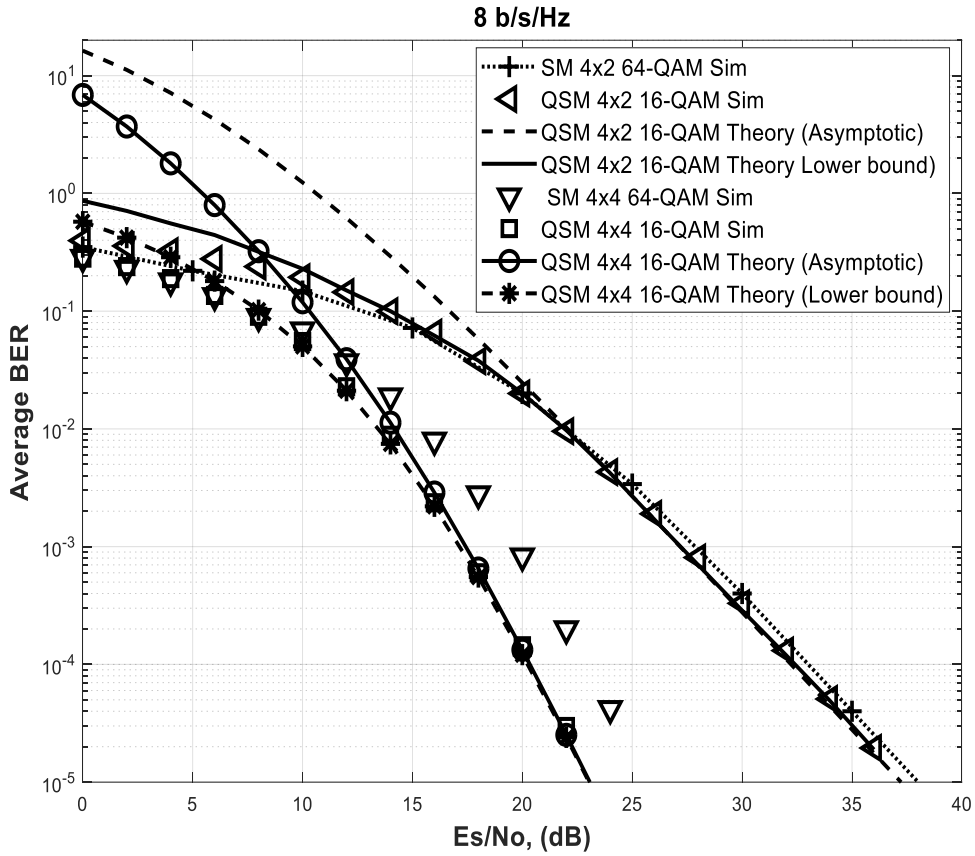

Figure 3-4. Validation of 64-QAM 4 × 2 SM and 16-QAM 4 × 2, 4 × 4 QSM theoretical analysis with the Monte Carlo simulation result.

The QSM system is compared to the SM system with the same spectral efficiency; the gain achieved under different configurations is tabulated in Table 3-3.

Table 3-3: SNR gain (dB) of QSM achieved over SM

Configuration	$\boldsymbol{M = 4, N_{TX} = 2}$	$\boldsymbol{M = 4, N_{TX} = 4}$	$\boldsymbol{M = 16, N_{TX} = 4}$
$N_{RX} = 2$	1.70	2	1.2
$N_{RX} = 4$	2	3.0	2.0

Table 3-4: SNR gain (dB) variation of lower bound approach achieved over asymptotic union bound

Configuration	**Lower Bound Approach $\mathbf{N_{RX} = 2}$**	**Upper Bound Approach $\mathbf{N_{RX} = 2}$**	**Lower Bound Approach $\mathbf{N_{RX} = 4}$**	**Upper Bound Approach $\mathbf{N_{RX} = 4}$**
4-QAM $N_{TX} = 2$	2	6	1.5	2
4-QAM $N_{TX} = 4$	4	10	1.8	4
16-QAM $N_{TX} = 4$	6	14	3.5	9

Chapter Summary

In order to deduce the average BER performance for the M-QAM QSM system, both the lower bound approach and the upper bound approach was employed in this chapter. Figures 3-2, 3-3, and 3-4 show the tightness between the analytical result and the simulated BER, thereby validating the analytical framework. The generated simulation results also show that QSM has a better error performance than the SM scheme.

Chapter 4

Space-Time Quadrature Spatial Modulation

4 Introduction

In wireless communication, there is always an upgrade being executed on existing systems to improve their performance. Just as the SM scheme was upgraded to the QSM scheme, which increased the schemes' overall throughput by adding an extra base-two logarithm to the available antennas, it was imperative to improve the performance of the QSM scheme. Hence, a new scheme was introduced by Basar *et al*. [56] to that effect, known as the ST-QSM scheme.

By merging both the STBC and QSM concepts, this scheme improves upon the QSM scheme thereby effectively capitalizing on the diversity gain at the transmitter, i.e., considerable use of less power in transmission while it still yields superior error performance than the QSM scheme.

The derivation of the ST-QSM's transmission matrix is extrapolated by implementing the Alamouti's STBC [57] or the ABBA STBC's [58] working principle on two distinct QSM transmission vectors at the same time the transmit diversity is obtained.

In the ST-QSM scheme, the technique employed in the QSM scheme is applied to two APM symbols which are then broken down into their real and imaginary components. The active antennas then independently transmit these decomposed components. The ST-QSM scheme can only be employed when there are transmit antennas ranging between four, six, and eight in number. The available antennas are then decomposed into two groups, comprising two or four antennas.

In the ST-QSM scheme, transmission occurs in two-time slots. For the transmission in the first time slot, the real part of the first symbol and imaginary part of the second symbol are conveyed with the antenna indices of the first group, while the real part of the second symbol and imaginary part of the first symbol are independently transmitted via the antenna indices of the second group, respectively. In the second time slot, Alamouti's STBC [57] or the ABBA STBC [58] is employed to obtain a diversity gain; either mode of transmission may be utilized on the transmitted vectors of each group based on the number of antennas available per group. The added diversity gain makes the ST-QSM yield greater error performance than both the SM and QSM schemes.

4.1 System Model of Space-Time Quadrature Spatial Modulation

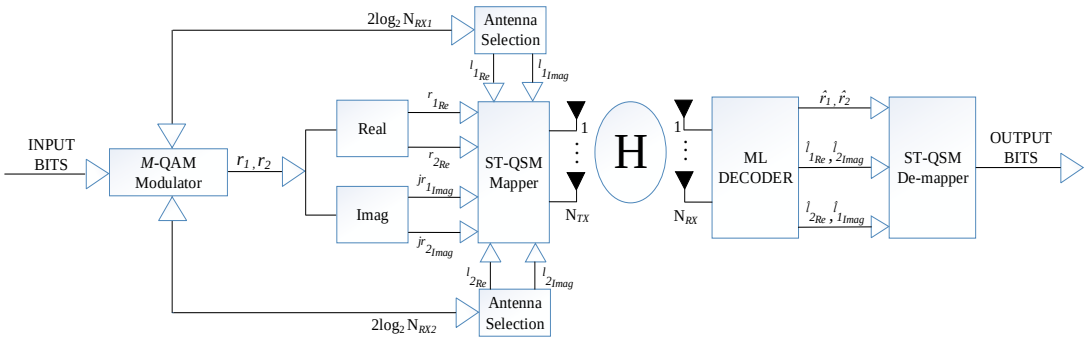

Figure 4-1. ST-QSM System Model [56]

Taking into account the working principle of both the SM and QSM schemes, where their antenna indices are treated as a whole unit, rather, the ST-QSM scheme splits its total transmit antennas into two groups, and then the antenna indices independently transmits the message bits in each group along with the two APM constellation symbols. The diversity gain is achieved by employing the transmission principle of Alamouti's STBC and ABBA STBC, which is then applied to the transmission vectors. Although the application of this transmission principle solely depends on the number of transmit antennas present in each group. The expression of the transmission matrix of the Alamouti's STBC is given as [56]:

$$\mathbf{Q}_{Alamouti} = \begin{bmatrix} r_{11} & r_{12} \\ -r_{12}^{*} & r_{11}^{*} \end{bmatrix}, \tag{4-1}$$

where r_{11} and r_{12} represents the M-ary symbols and $(\cdot)^{*}$ depicts the complex conjugate. The ABBA STBC is formed by the sequential alignment of two Alamouti matrices which is expressed as [56]:

$$\boldsymbol{Q}_{ABBA} = \begin{bmatrix} r_{11} & r_{12} & r_{13} & r_{14} \\ -r_{12}^{*} & r_{11}^{*} & -r_{14}^{*} & r_{13}^{*} \end{bmatrix}, \tag{4-2}$$

where r_{11}, r_{12}, represents the M-ary symbols as seen when the Alamouti concept was applied, while r_{13} and r_{14} are the two extra M-ary symbols added depicting the ABBA STBC concept.

The spectral efficiency of the ST-QSM system is denoted by $m = \log_2 M + \log_2 \mathrm{N}_{TX1} + \log_2 \mathrm{N}_{TX2}$ b/s/Hz [56], where M is the modulation order of the M-ary APM constellation signal, while N_{TX1} and N_{TX2} depicts the number of antennas in Group 1 and Group 2, respectively.

Examining an $\mathrm{N}_{TX} \times \mathrm{N}_{RX}$ MIMO configuration, where N_{TX} denotes the number of transmit antenna and N_{RX} is the number receive antenna, respectively. The N_{TX} antennas present are split into two groups, i.e., group 1 and group 2 and are denoted by N_{TX1} and N_{TX2}, respectively.

Two complex APM symbols are decomposed into their real and imaginary components, i.e. r_1 and r_2, where $r_1 = r_{1_{Re}} + jr_{1_{Imag}}$ and $r_2 = r_{2_{Re}} + jr_{2_{Imag}}$. For the transmission in the first time

slot, the real part of the first symbol $r_{1_{Re}}$ and imaginary part of the second symbol $jr_{2_{Imag}}$ are conveyed with the antenna indices of the first group, $l_{1_{Re}}$th and $l_{2_{Imag}}$th, where $l_{1_{Re}}, l_{2_{Imag}} \in \{1, 2, \dots, \mathrm{N}_{TX1}\}$ yields a transmission vector of $\boldsymbol{e}^1 \in \mathbb{Q}^{1\times \mathrm{N}_{TX1}}$. Similarly, the real part of the second symbol $r_{2_{Re}}$ and imaginary part of the first symbol $jr_{1_{Imag}}$ are independently transmitted via the antenna indices of the second group, $l_{2_{Re}}, l_{1_{Imag}} \in \{1, 2, \dots, \mathrm{N}_{TX2}\}$, respectively, which yields a transmission vector of $\boldsymbol{f}^1 \in \mathbb{Q}^{1\times \mathrm{N}_{TX2}}$.

Consequently, we achieve:

$$\mathbf{Q}_{\mathrm{N}_{TX1}} = \begin{bmatrix} \boldsymbol{e}^1 \\ \boldsymbol{e}^2 \end{bmatrix}, \mathbf{Q}_{\mathrm{N}_{TX2}} = \begin{bmatrix} \boldsymbol{f}^1 \\ \boldsymbol{f}^2 \end{bmatrix}. \tag{4-3}$$

Equation (4-3) shows the matrices $\mathbf{Q}_{\mathrm{N}_{TX1}} \in \mathbb{Q}^{2\times \mathrm{N}_{TX1}}$ and $\mathbf{Q}_{\mathrm{N}_{TX2}} \in \mathbb{Q}^{2\times \mathrm{N}_{TX2}}$ that collects the transmitted information bits in Group 1 and Group 2, respectively. Depending on the number of antennas available, the transmission vector in the second time slot, depicted by $\boldsymbol{e^2}$ and $\boldsymbol{f^2}$ are deduced employing (4-1) and (4-2).

Therefore the overall transmission matrix is expressed:

$$\mathbf{R} = \begin{bmatrix} e^1 & f^1 \\ f^2 & e^2 \end{bmatrix}. \tag{4-4}$$

Various design illustrations of the ST-QSM transmission matrix is further explained in the subsequent sub-sections.

4.2 ST-QSM Scheme for Four Transmit Antennas

To simplify and make the explanation of the ST-QSM with four transmit antennas easy, (4-1) is used to implement a structure for **R** of (4-4) with$\mathrm{N}_{TX} = 4$.

$$\mathbf{R} = \left[\begin{array}{cc|cc} r_{11} & r_{12} & r_{13} & r_{14} \\ -r_{12}^* & r_{11}^* & -r_{14}^* & r_{13}^* \end{array}\right], \tag{4-5}$$

where $r_{11}, r_{12} \in \left\{r_{1_{Re}}, jr_{2_{Imag}}, r_{1_{Re}} + jr_{2_{Imag}}, 0\right\}$ and $r_{13}, r_{14} \in \left\{r_{2_{Re}}, jr_{1_{Imag}}, r_{2_{Re}} + jr_{1_{Imag}}, 0\right\}$.

The diagrammatic expression of this scheme is represented in Figure 4-1.

Take, for instance, that $\{01110010\}$ is a message bit sequence of length $2m$, sent over a MIMO system with $\mathrm{N}_{TX} = 4$ and $M = 4$. In the ST-QSM scheme with four antennas, (4-1) is used to implement the structure for **R** of (4-4) with $\mathrm{N}_{TX} = 4$.

Recall that N_{TX} antennas are split into two groups, so $\mathrm{N}_{TX1} = \mathrm{N}_{TX2} = 2$, since $\mathrm{N}_{TX} = 4$.

The first $\log_2 M$ bits $\{0\ 1\}$ will be assigned the first 4-QAM symbol:

$(r_1 = -1 - j)$,

where $r_{1_{Re}} = -1$ and $jr_{1_{Imag}} = -j$.

The subsequent $\log_2(\mathrm{N}_{TX1}\mathrm{N}_{TX2})$ bits (1 1) triggers an antenna in both Group 1 and Group 2: $l_{1_{Re}} = 1$ and $l_{1_{Imag}} = 1$ to transmit: $r_{1_{Re}} = -1$ and $jr_{1_{Imag}} = -1$. Hence, the transmission of the symbol r_1 would yield: $\mathbf{r}_1 = [-1\ 0\ |{-j}\ 0]$.

Likewise, the remaining $\log_2 M$ bits (0 0) will be assigned to the second 4-QAM symbol:

$(r_2 = -1 + j)$,

where $r_{2_{Re}} = -1$ and $jr_{2_{Imag}} = j$.

while the last $\log_2(\mathrm{N}_{TX1}\mathrm{N}_{TX2})$ bits (1 0) triggers an antenna in both Group 1 and Group 2:

$l_{2_{Re}} = 1$ and $l_{2_{Imag}} = 2$ to be able to transmit: $r_{2_{Re}} = -1$ and $jr_{2_{Imag}} = j$. Hence, the transmission of the symbol r_2 would yield a transmission:

$\mathbf{r}_2 = [0\ j\ |{-1}\ 0]$.

Hence the overall transmission matrix **R** is formulated as:

$$\mathbf{R} = \left[\begin{array}{cc|cc} -1 & j & -1-j & 0 \\ 0 & -1+j & j & -1 \end{array}\right]. \tag{4-6}$$

4.3 ST-QSM Scheme for Eight Transmit Antennas

To simplify and make the explanation of the ST-QSM with eight transmit antennas easy, (4-2) is used to implement the structure for **R** of (4-4) with $\mathrm{N}_{TX} = 8$.

$$\mathbf{R} = \left[\begin{array}{cccc|cccc} r_{11} & r_{12} & r_{13} & r_{14} & r_{15} & r_{16} & r_{17} & r_{18} \\ -r_{16}^* & r_{15}^* & -r_{18}^* & r_{17}^* & -r_{12}^* & r_{11}^* & -r_{14}^* & r_{13}^* \end{array}\right], \tag{4-7}$$

where $r_{11}, r_{12}, r_{13}, r_{14} \in \left\{r_{1_{Re}}, jr_{2_{Imag}}, r_{1_{Re}} + jr_{2_{Imag}}, 0\right\}$. and $r_{15}, r_{16}, r_{17}, r_{18} \in \left\{r_{2_{Re}}, jr_{1_{Imag}}, r_{2_{Re}} + jr_{1_{Imag}}, 0\right\}$.

For the case of an ST-QSM scheme with modulation of 64-QAM, N_{TX} antennas are split into two groups, so $\mathrm{N}_{TX1} = \mathrm{N}_{TX2} = 4$, since $\mathrm{N}_{TX} = 8$. where $\mathrm{N}_{TX} = 8$

Let us consider the message bits received in the system are $r_1 = 5 + 3j$ and $r_2 = -7 + j$ complex symbols with active antenna indices of $l_{1_{Re}} = 1$, $l_{1_{Imag}} = 3$, $l_{2_{Re}} = 2$ and $l_{2_{Imag}} = 3$.

The transmission vectors of $\mathbf{r}_1 = [5\ 0\ 0\ 0\ |\ 0\ 0\ 3j\ 0]$ and $\mathbf{r}_2 = [0\ 0 - j\ 0\ |\ 0 - 7\ 0\ 0]$ where $\mathrm{N}_{TX1} = 4$ and $\mathrm{N}_{TX2} = 4$ are formulated when the components of $r_{1_{Re}}$, $jr_{1_{Imag}}$, $r_{2_{Re}}$ and $jr_{2_{Imag}}$ are sent via the active antenna indices of $l_{1_{Re}}$, $l_{1_{Imag}}$, $l_{2_{Re}}$ and $l_{2_{Imag}}$.

Hence, their superimposition, i.e. $\mathbf{r}_1$ and $\mathbf{r}_2$ would be formulated as:

$$[\mathbf{r}_1 + \mathbf{r}_2] = [5\ 0\ -j\ 0 \mid 0\ -7\ 3j\ 0], \tag{4-8}$$

where the first part with N_{TX1} antennas is equivalent to the vector of $\boldsymbol{e}^1 = [5\ 0 - j\ 0]$ and the other part with N_{TX2} antennas corresponds to the vector of $\boldsymbol{f}^1 = [0 - 7\ 3j\ 0]$.

Considering that $\mathrm{N}_{TX1} = \mathrm{N}_{TX2} = 4$, both $\mathbf{Q}_{\mathrm{N}_{TX1}}$ and $\mathbf{Q}_{\mathrm{N}_{TX2}}$ comply with the principle of the ABBA STBC matrix. Hence the transmission matrix **R** given in (4-4) is formulated as:

$$\mathbf{R} = \left[\begin{array}{cccc|cccc} 5 & 0 & -j & 0 & 0 & -7 & 3j & 0 \\ 7 & 0 & 0 & -3j & 0 & 5 & 0 & j \end{array}\right]. \tag{4-9}$$

Table 4-1: The mapping process for the ST-QSM system scheme with $\mathrm{N}_{TX} = 4$

Configuration	**Input Bits $\log_2 M + \log_2 \mathrm{N}_{TX1} + \log_2 \mathrm{N}_{TX2}$**	**First $\log_2 M$ bits**	**Second $\log_2 \mathrm{N}_{TX1}$ bits**	**Third $\log_2 \mathrm{N}_{TX2}$ bits**
First 4 bits				
$M = 4$ $\mathrm{N}_{TX} = 4$	0 1 0 1	$\log_2 M = 2$ bits [0 1] $r_1 = -1 - j$ $r_{1_{Re}} = -1$ $jr_{1_{Imag}} = -j$	$\log_2 2 = 1$ bit [0] $r_{1_{Re}} = -1$	$\log_2 2 = 1$ bit [1] $jr_{1_{Imag}} = -j$
	Second 4 bits			
	0 0 1 0	$\log_2 M = 2$ bits [0 0] $r_2 = -1 + j$ $r_{2_{Re}} = -1$ $jr_{2_{Imag}} = j$	$\log_2 2 = 1$ bit [1] $r_{2_{Re}} = -1$	$\log_2 2 = 1$ bit [0] $jr_{2_{Imag}} = j$

The received signal matrix **y** with dimension $2 \times \mathrm{N}_{RX}$ is defined as:

$$\mathbf{y} = \sqrt{\frac{\rho}{2}}\mathbf{R}\mathbf{H} + \mathbf{n}, \tag{4-10}$$

where ρ is the average SNR at each receive antenna. **R** is the transmission matrix with dimension $2 \times \mathrm{N}_{TX}$, **H** is an $\mathrm{N}_{TX} \times \mathrm{N}_{RX}$ complex Rayleigh frequency-flat fading channel vector and **n** is a $2 \times \mathrm{N}_{RX}$ AWGN vector. The entries of **H** and **n** are assumed to be i.i.d complex Gaussian RVs, both distributed as $CN(0, 1)$.

4.4 Optimal Detection

In this subsection, the received signal is demodulated optimally employing ML detection, as the entire signal space of the M constellation points and all antenna index combinations are thoroughly searched.

The receiver is believed to have perfect CSI (P-CSI). The ML detector examines all the possible outcomes of the active antenna indices for $l_{1_{Re}}$, $l_{1_{Imag}}$, $l_{2_{Re}}$ and $l_{2_{Imag}}$ in their respective APM constellation symbols r_1 and r_2 and antenna groups to jointly estimate the antenna indices $\hat{l}_{1_{Re}}$, $\hat{l}_{1_{Imag}}$, $\hat{l}_{2_{Re}}$ and $\hat{l}_{2_{Imag}}$ and also the data symbols $\hat{r}_1$ and $\hat{r}_2$:

$$\left[\hat{r}_1, \hat{r}_2, \hat{l}_{1_{Re}}, \hat{l}_{1_{Imag}}, \hat{l}_{2_{Re}}, \hat{l}_{2_{Imag}}\right] = \underset{r_1, r_2, l_{1_{Re}}, l_{1_{Imag}}, l_{2_{Re}}, l_{2_{Imag}}}{\operatorname{argmin}} \left\| \mathbf{y} - \sqrt{\frac{\rho}{2}} \mathbf{RH} \right\|_F^2. \quad (4\text{-}11)$$

4.5 The Performance Analysis of M-QAM Space-Time Quadrature Spatial Modulation

A union bounding technique was employed to investigate the error performance of the ST-QSM system in this section [56]. An ABEP involved in detecting $\widehat{\mathbf{R}}$ given **R is** transmitted as follow:

$$P_b \leq \frac{1}{2^{2m}} \sum_{\mathbf{R}} \sum_{\widehat{\mathbf{R}}} \frac{P(\mathbf{R} \to \widehat{\mathbf{R}}) e(\mathbf{R}, \widehat{\mathbf{R}})}{m}, \quad (4\text{-}12)$$

where m is the spectral efficiency of the ST-QSM scheme, $P(\mathbf{R} \to \widehat{\mathbf{R}})$ is the corresponding PEP of choosing $\widehat{\mathbf{R}}$ given that $\mathbf{R}$ was transmitted and $e(\mathbf{R}, \widehat{\mathbf{R}})$ is the number of bit errors for the corresponding PEP. According to the received signal vector in (4.10) and the corresponding ML detection, the conditional PEP is formulated as:

$$P(\mathbf{R} \to \widehat{\mathbf{R}} | \mathbf{H}) = P\left(\left\| \boldsymbol{y} - \sqrt{\frac{\rho}{2}} \mathbf{RH} \right\|_F^2 > \left\| \boldsymbol{y} - \sqrt{\frac{\rho}{2}} \widehat{\mathbf{R}} \mathbf{H} \right\|_F^2 \right). \quad (4\text{-}13)$$

By carrying out the closed-form approximation of [59] for $Q(\cdot)$ the Q-function, the unconditional PEP is written as:

$$P(\mathbf{R} \to \widehat{\mathbf{R}}) = Q\left(\sqrt{\frac{\rho}{16} \left\| \mathbf{H}(\mathbf{R} - \widehat{\mathbf{R}}) \right\|_F^2} \right). \quad (4\text{-}14)$$

The PEP of the system is validated by employing the trapezoidal approximation of the Q-function over a total of n iterations. The PEP can then be determined by applying a similar technique to [60] using the MGF to derive:

$$P(\mathbf{R} \to \widehat{\mathbf{R}}) = \frac{1}{2n} \left[\frac{1}{2} \mathrm{M}\left(\frac{1}{2}\right) + \sum_{l=1}^{n-1} \mathrm{M}\left(\frac{1}{2\sin^2\left(\frac{l\pi}{2n}\right)} \right) \right], \quad (4\text{-}15)$$

where M(·) depicts the MGF function expressed as:

$$\mathrm{M}(w) = \frac{1}{\pi}\left(\frac{1}{1+2\sigma_{\propto 1}^{2}w}\right)^{\mathrm{N}_{RX}}, \tag{4-16}$$

where $\sigma_{\propto 1}^{2} = \frac{\rho}{16}g$ and $g = \left\|\mathbf{R} - \widehat{\mathbf{R}}\right\|_{F}^{2}$.

4.6 Simulated Results of the BER of the Space-Time Quadrature Spatial Modulation System

In this section, we present the Monte Carlo simulations and analytical results for the ST-QSM scheme against existing literature. The union bound approach is employed in deriving the analytical results for the ST-QSM system. The average BER was plotted against the average SNR per symbol for varying spectral efficiencies. The number of transmit antennas considered for the results are 4, 6 and 8 antennas. The BER performance is compared with various MIMO configurations, i.e., QSM scheme.

It is important to note that Gray mapping was applied to symbol constellations and N_{RX} is considered equal to two and four in all cases presented for the ST-QSM schemes whilst keeping generalization straightforward.

Furthermore, it is assumed that the channel information is perfectly known at the receiver. The notation used to denote the configuration of the ST-QSM and QSM schemes are $(\mathrm{N}_{TX}, \mathrm{N}_{RX}, M)$. The notation $\mathrm{N}_{TX} \times \mathrm{N}_{RX}$ denotes the number of transmit antennas and the number of receive antennas, respectively.

As seen in Figure 4-2, the system presents the ST-QSM scheme's simulation results with transmit antenna ranging between 4, 6 and 8. It also comprises of receive antennas ranging between 2 and 4. When employing 4-QAM, it presents a 4×4, 6×4 and 8×2 system, while when employing 8-QAM, it presents a 6×2 system. Also, when employing 16-QAM, it presents a 6×2 system. There was a noticeable improvement in the BER performances as the SNR increased.

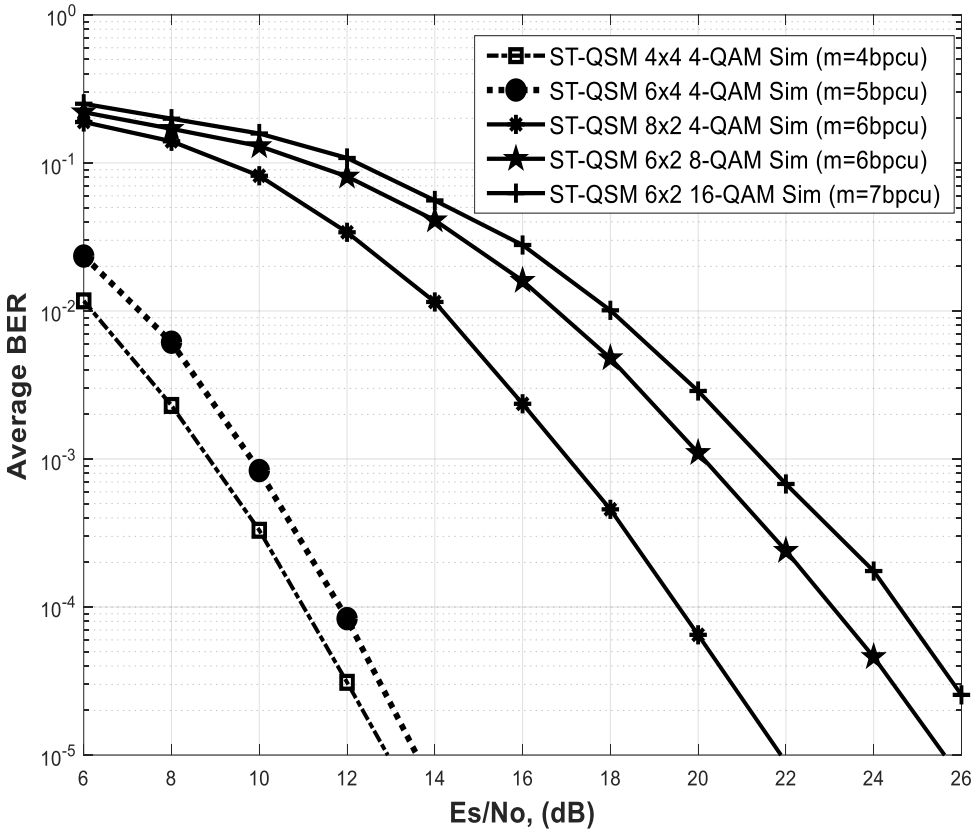

Figure 4-2. Comparing the 4-QAM 4 × 4, 6 × 4, 8 × 2, 8-QAM 6 × 2 and the 16-QAM 6 × 2 ST-QSM Monte Carlo simulation results.

As seen in Figure 4-3, the system presents theoretical ST-QSM results of transmit antenna ranging between 4, 6 and 8 compared with their respective simulated results. It also has receive antennas ranging between 2 and 4. When employing 4-QAM, it presents a 4 × 4, 6 × 4 and 8 × 2 system, while when employing 8-QAM, it presents a 6 × 2 system. There was a noticeable improvement in the BER performances as the SNR increased.

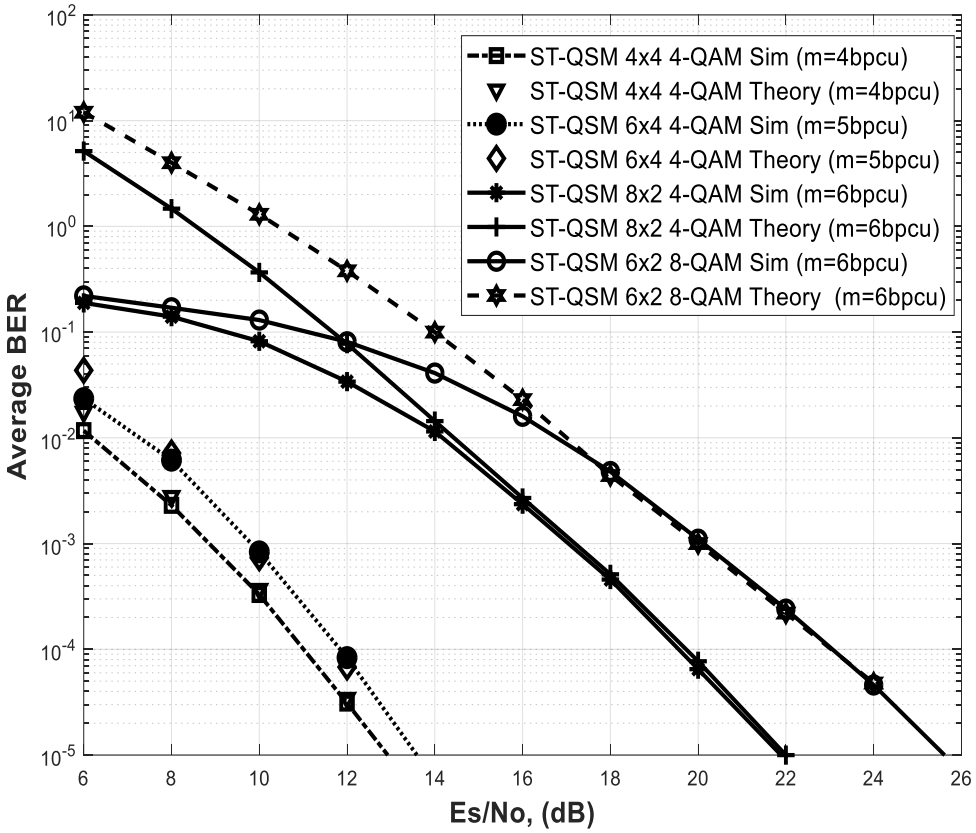

Figure 4-3. Validation of the 8-QAM 6 × 2 ST-QSM, 4-QAM 4 × 4, 6 × 4 and 8 × 2 ST-QSM theoretical analysis with their Monte Carlo simulation result.

Figure 4-4 consists of four system configurations for both the ST-QSM and QSM scheme, i.e., the 4 × 4, 6 × 4 4-QAM ST-QSM, the 2 × 4 4-QAM QSM and lastly, the 2 × 4 8-QAM QSM system. As seen in Figure 4-4, the 4 × 4 4-QAM ST-QSM and 2 × 4 4-QAM QSM with spectral efficiency of 4 and 5 b/s/Hz respectively are compared with each other, while the 6 × 4 4-QAM ST-QSM and 2 × 4 8-QAM QSM with spectral efficiency of 4 and 5 b/s/Hz respectively are compared with each other. It is noticed that the ST-QSM scheme performs better on both occasions as the gain of ST-QSM over QSM for a spectral efficiency of 4 b/s/Hz is 3.9 dB, while the gain of ST-QSM over QSM for a spectral efficiency of 5 b/s/Hz is 7.2 dB.

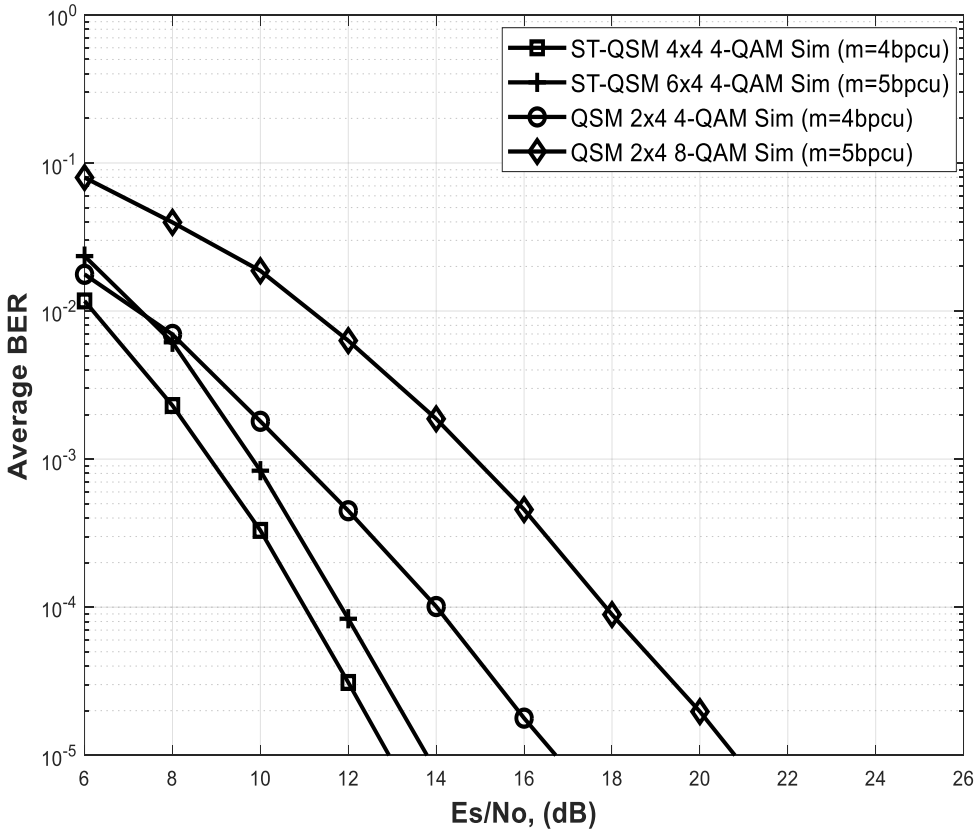

Figure 4-4. BER comparison of 4 × 4, 6 × 4 4-QAM ST-QSM, 2 × 4 4-QAM QSM and 2 × 4 8-QAM QSM for spectral efficiency of 4 and 5 b/s/Hz, respectively.

Figure 4-5 consists of four system configurations for both the ST-QSM and QSM scheme, i.e., the 6 × 2 8-QAM ST-QSM scheme, 4 × 2 4-QAM ST-QSM, the 6 × 2 16-QAM ST-QSM and lastly, the 4 × 2 8-QAM QSM system. As seen in Figure 4-4, the 6 × 2 8-QAM ST-QSM and 4 × 2 4-QAM ST-QSM are compared with each other while also the 6 × 2 16-QAM ST-QSM and 4 × 2 8-QAM QSM compared with each other. It is noticed that the ST-QSM scheme performs better on both occasions as the gain of ST-QSM over QSM for a spectral efficiency of b/s/Hz is 6 dB, while the gain of ST-QSM over QSM for a spectral efficiency of 7 b/s/Hz is 8.4 dB. As it is a well-known fact that the lower the spectral efficiency, the better the error performance, so it is proven that the ST-QSM scheme has a higher diversity gain over the QSM scheme according to the results presented.

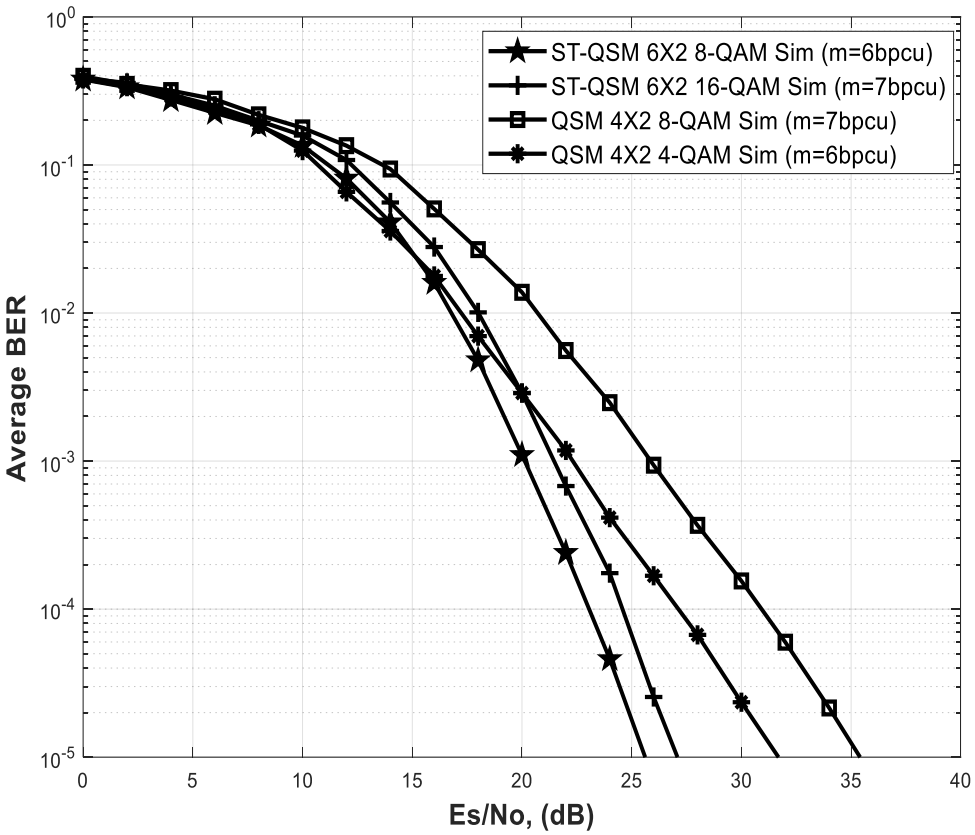

Figure 4-5. BER comparison of 6 × 2 8-QAM ST-QSM, 4 × 2 4-QAM ST-QSM, the 6 × 2 16-QAM ST-QSM and the 4 × 2 8-QAM QSM system with spectral efficiency of 6 and 7 b/s/Hz, respectively.

CHAPTER SUMMARY

An innovative MIMO transmission approach, called ST-QSM, was introduced in this chapter. The scheme integrates the working principle of QSM along with the STBCs to exploit the diversity gain. In this design framework, the antennas are split into two groups. The data is then conveyed independently by the antennas' indices in both groups alongside the two complex symbols. An optimal detector is utilized over an i.i.d. entry with zero mean, unit variance $CN(0,1)$, and the Rayleigh fading channel **H** to deduce the average BER performance for the M-QAM ST-QSM scheme.

Moreover, for various configurations of MIMO, the Monte Carlo simulations and analytical results were obtained and compared. At the same spectral efficiency, extensive computer simulations have also proven that the ST-QSM scheme yields greater error performance than the QSM schemes. Figures 4-2, 4-3, and 4-4 shows the diversity obtained when in the simulated BER between the QSM and ST-QSM.

Chapter 5

A Reduced Complexity Near-ML Detector for Space-Time Block Coded Spatial Modulation using Orthogonal Projection

5 Introduction

The telecommunication industry faces various challenges which range from improving radio coverage, improving the speed of data transmission and several others; therefore research has been done and still ongoing by telecommunication engineers to ensure that next-generation communication systems are better than the already existing systems.

Employing multiple transmit and the receive antennas has proven to be an efficient approach to increase performance and efficiency over the traditional single antenna wireless systems [61]. MIMO is fundamental to the advancement of present-day and future wireless communication systems. Numerous researchers have extensively studied MIMO transmission techniques over the past decade and it has been proven that the MIMO technique improves spectral efficiency, improves link reliability and data throughput [62, 63].

Tarokh *et al.* in [64] introduced space-time codes (STCs) which is a MIMO technique that carries trellis encoded message bits employing N_{TX} transmit antennas over multiple time slots. This technique exploits the transmit diversity of a MIMO configuration system, thereby achieving the needed diversity order. Although the STC was shown to have high-performance gains, it, however, had an increased receiver complexity.

In an attempt to reduce the receiver complexity, Alamouti *et al.* introduced a new scheme (STBC) in [57]. The STBC scheme is a two-branched transmit diversity scheme for MIMO systems in which two symbols are transmitted with two transmit antennas over two-time slots [57]. However, in relation to MRC performance, it was deduced that there was a 3 dB loss in performance in the STBC scheme a as a result of simultaneous data transmission, and this less to less power generation. Even with this drawback, researchers still prefer STBC as it has proven to provide transmit diversity gains in comparison to the STC scheme and other diversity MIMO schemes as it possesses a low decoding complexity and the implementation of this scheme is relatively simple [64]. In the last decade, several high rate STBC schemes have been introduced [49, 65-67] but the high rate of their ML decoding complexity relative to their constellation size makes the implementation complicated and exorbitant for future work.

Mesleh *et al*. in [17, 49] introduced the SM scheme. The SM scheme's working principle is based on an extension of two-dimensional signal constellations to a third dimension, i.e., the spatial (antenna) dimension. However, the information is not only conveyed by the APM techniques, but

also by the antenna indices. Employing an optimal ML decoder for the SM scheme to search thoroughly over the three-dimensional space was shown in [19]. It was also proven in [19] that with the use of the optimal detector under conventional channel assumptions, the SM scheme's error performance could be significantly improved by approximately 4 dB [49] which then results in the SM scheme producing a greater error performance than MRC and V-BLAST.

Both the SM and SSK modulation systems were introduced to exploit the multiplexing gain of multiple transmit antennas; however, both modulation systems failed to exploit the potential for transmit diversity of MIMO systems. This led to the introduction of the STBC-SM, which was designed to take advantage of both SM and STBC.

The STBC-SM combines the primary benefits of both schemes whilst avoiding their major challenges. The STBC-SM scheme utilizes the unique pattern with which the SM scheme conveys message bits and transmits the message bits by employing both the Alamouti STBC symbol and the index of the chosen antenna pair. The STBC-SM scheme employs the special information conveying mode of SM and transmits information by using both selected antenna pair index, ℓ as well as the Alamouti STBC codeword $\boldsymbol{X}$. Thus the STBC-SM's spectral efficiency is formulated as $\eta_{STBC-SM} = \frac{1}{2}\log_2 c + \log_2 M$, where c is the number of antenna pair combinations and M is the symbol constellation size. Consequently, STBC-SM exploits the benefits of both the SM and Alamouti STBC.

The success of multimedia services depends on high data rate transmission. However, for STBC-SM and other MIMO schemes, the level of CC at the receiver, especially for high data rate transmission represents a significant challenge to its practicality. Example, in [16] an ML detection scheme for STBC-SM was presented and in terms of metric calculations requires cM^2 such operations. This represents a high CC. Motivated by this, Basar *et al*. [16] also presented a simplified ML detector which reduces the number of metric calculations to $2cM$; however, the complexity is still relatively high, especially as the size of the symbol constellation. In the remainder of this chapter, we refer to the simplified ML detector [16] as STBC-SM-ML.

Over time it has been evident that for a data service to be considered efficient, it must effectively exhibit specific characteristics such as a wide range of data coverage, high rate of data transmission, e.t.c.

In an attempt to generate this high rate of data transmission, the high CC at the receiver became a stumbling block, and this problem seems to affect the hardware practicality of most STBC-SM and MIMO schemes. Therefore to overcome this challenge, Basar *et al.* in [16], proposed the STBC-SM-ML scheme; but, it was discovered the CC increased as the size of the symbol constellation also increased. In a bid to fix the problem of the high CC, several detectors have been employed but compared to the ML detector, they all generated poor error performance

results. As a result, it was critical to develop a scheme that would generate an error performance near to the ML detection while maintaining a significantly lower CC than the current detectors.

The signal orthogonal projection (OP) was employed by the authors of [69] as a technique to lower the CC of a MIMO system. Also, the reduction of the CC of STBC-SM with labelling diversity was accomplished by utilizing OP in [70]. The results achieved in the two cases showed an error performance in close proximity to ML and a reduced CC relative to that of the ML detectors.

The OP based detector for spatially multiplexed MIMO firstly rearranges the received layers in descending order of the SNR. Then by considering the largest SNR channel gain vector and corresponding data symbol, a projection matrix which propagates a signal orthogonal to the subspace of the remaining channel gain vectors is employed. The candidates of the data symbol are then searched for the most likely data symbol by taking advantage of the orthogonal nature of the projection matrix.

The scenario of OP for spatially multiplexed MIMO transmission corresponds very closely to the dual antenna transmission of the STBC symbol and antenna bits in STBC-SM. This motivated us to investigate OP for STBC-SM to reduce the CC at the receiver, and it is further explained in the subsections that follow.

5.1 System Model & Background

5.1.1 System Model for STBC-SM

Given N_{TX} transmit antennas, the STBC-SM scheme assumes $c = \left\lfloor \binom{\mathrm{N}_{TX}}{2} \right\rfloor_{2^p}$ possible antenna pair combinations, where N_{TX} denotes the amount of transmit antennas available and p is a positive integer. The first $\log_2 c$ symbol bits are mapped to the ℓ^{th} antenna pair combination, where $0 \leq \ell \leq c-1$. Example, for $\mathrm{N}_{TX} = 4$, $c = 4$, the c antenna pair combinations of the form $\{\ell_1, \ell_2\}$ are given as $\{1,2\}, \{3,4\}, \{2,3\}$ and $\{4,1\}$. Applying the Alamouti STBC symbol defined as $\boldsymbol{X} = \begin{pmatrix} x_1 & x_2 \\ -x_2^* & x_1^* \end{pmatrix}$ [57], the transmission matrix, $\boldsymbol{X}_\chi$ can be expressed as:

$$\boldsymbol{X}_\chi = [\boldsymbol{x}_{\chi,1} \quad \boldsymbol{x}_{\chi,2}] = \begin{bmatrix} 0 & \cdots & x_{q_1} e^{j\theta_\ell} & \cdots \cdots & x_{q_2} e^{j\theta_\ell} & \cdots & 0 \\ 0 & \cdots & -\left(x_{q_2} e^{j\theta_\ell}\right)^* & \cdots \cdots & \left(x_{q_1} e^{j\theta_\ell}\right)^* & \cdots & 0 \end{bmatrix}^T, \qquad (5\text{-}1)$$

where $\boldsymbol{x}_{\chi,1}$ and $\boldsymbol{x}_{\chi,2}$ are $\mathrm{N}_{TX} \times 1$ column vectors, the elements $x_{q_1} e^{j\theta_\ell}$ and $-\left(x_{q_2} e^{j\theta_\ell}\right)^*$ are placed in the ℓ_1^{th} position and $x_{q_2} e^{j\theta_\ell}$, $\left(x_{q_1} e^{j\theta_\ell}\right)^*$ are placed in the ℓ_2^{th} position based on the selected antenna pair index ℓ of the form $\{\ell_1, \ell_2\}$ and corresponds to the only non-zero entries in the $\mathrm{N}_{TX} \times 2$ transmission matrix. x_{q_m}, $q_m \in [1{:}M]$, $m \in [1,2]$ represents the q_m^{th} symbol in the constellation. θ_ℓ represents the rotation angle based on the selected antenna pair index and when

optimized, it ensures maximum diversity and coding gain [16]. The computation of the optimized rotation angle is discussed further in [16], and the values are given for selected modulation formats. Example for 16-QAM, $N_{TX} = 4$, $c = 4$ and $0 \leq \ell \leq c-1$, $\theta_0 = 0$, $\theta_1 = 0$, $\theta_2 = 0.75$ and $\theta_3 = 0.75$.

Next, assume an $N_{TX} \times N_{RX}$ STBC-SM system which transmits $\boldsymbol{X}_\chi$ over two consecutive time slots. The received signal vector for the i^{th} time slot can be expressed as,

$$\boldsymbol{y}_i = \sqrt{\frac{\rho}{\mu}}\boldsymbol{H}\boldsymbol{x}_{\chi,i} + \boldsymbol{n}_i, \ i = 1,2, \tag{5-2}$$

where $\boldsymbol{y}_i$ represents the $N_{RX} \times 1$ received signal column vector for the i^{th} time slot. $\boldsymbol{H} = [\boldsymbol{h}_1 \quad \boldsymbol{h}_2 \quad \cdots \quad \boldsymbol{h}_{N_{TX}}]$ is the $N_{RX} \times N_{TX}$ channel gain matrix, where $\boldsymbol{h}_j, j \in [1: N_{TX}]$ represents a column vector of $\boldsymbol{H}$ and is defined as $\boldsymbol{h}_j = \left[h_{1j} \quad h_{2j} \quad \cdots \quad h_{N_{RX}j}\right]^T$, and $\boldsymbol{n}_i$ is the $N_{RX} \times 1$ noise matrix. The elements of both $\boldsymbol{H}$ and $\boldsymbol{n}_i$ are assumed to be i.i.d complex random variables distributed according to $CN(0,1)$. Furthermore, it is assumed that the channel gain matrix remains constant over the i time slots and is perfectly known at the receiver ρ represents the average SNR at each receive antenna and μ depicts the normalization factor since two transmit antennas are active per time slot.

Considering the overall $N_{RX} \times 2$ received signal matrix per two consecutive time slots, $\boldsymbol{y} = \sqrt{\frac{\rho}{\mu}}\boldsymbol{H}\boldsymbol{X}_\chi + \boldsymbol{N}$ the conventional ML detector metric was defined as ([16], Eq. (15)). However, Basar *et al*. presented a simplified ML detector which offers a reduced complexity relative to the conventional ML detector and is detailed in the subsequent subsection.

5.1.2 Simplified ML detector for STBC-SM

Based on the orthogonal nature of the scheme, the received signal vector can be equivalently formulated as [16],

$$\boldsymbol{y} = \sqrt{\frac{\rho}{\mu}}\boldsymbol{H}_\ell \begin{bmatrix} x_{q_1} \\ x_{q_2} \end{bmatrix} + \boldsymbol{n}, \tag{5-3}$$

where $\boldsymbol{y}$ and $\boldsymbol{n}$ represent the $2N_{RX} \times 1$ equivalent received signal and noise vectors, respectively, and $\boldsymbol{H}_\ell$ is a $2N_{RX} \times 2$ equivalent channel gain matrix.

The ℓ^{th} channel gain matrix is defined as,

$$\boldsymbol{H}_\ell = [\boldsymbol{h}_{\ell,1} \quad \boldsymbol{h}_{\ell,2}] = \begin{bmatrix} h_{1,\ell_1}\varphi & h_{1,\ell_2}\varphi \\ h^*_{1,\ell_2}\varphi^* & -h^*_{1,\ell_1}\varphi^* \\ \vdots & \vdots \\ h_{N_{RX},\ell_1}\varphi & h_{N_{RX},\ell_2}\varphi \\ h^*_{N_{RX},\ell_2}\varphi^* & -h^*_{N_{RX},\ell_1}\varphi^* \end{bmatrix}, \tag{5-4}$$

where $h_{a,b}$ is the channel fading coefficient between transmit antenna b and receive antenna a, $b \in [\ell_1, \ell_2]$, $a \in [1{:}\,\mathrm{N}_{RX}]$, $\varphi = e^{j\theta_\ell}$ and $\boldsymbol{h}_{\ell,m}$ is a $2\mathrm{N}_{RX} \times 1$ column vector of the channel matrix.

The detector then estimates the antenna pair combination as [16],

$$\hat{\ell} = \underset{\ell}{\operatorname{argmin}} \left\{ \min_{x_{q_1} \in \gamma} \left\| \boldsymbol{y} - \sqrt{\frac{\rho}{\mu}} \boldsymbol{h}_{\ell,1} x_{q_1} \right\|_F^2 + \min_{x_{q_2} \in \gamma} \left\| \boldsymbol{y} - \sqrt{\frac{\rho}{\mu}} \boldsymbol{h}_{\ell,2} x_{q_2} \right\|_F^2 \right\}, \tag{5-5}$$

and finally chooses the transmit symbol pair using,

$$\left(\hat{x}_{q_1}, \hat{x}_{q_2}\right) = \left(\underset{x_{q_1} \in \gamma}{\operatorname{argmin}} \left\| \boldsymbol{y} - \sqrt{\frac{\rho}{\mu}} \boldsymbol{h}_{\hat{\ell},1} x_{q_1} \right\|_F^2, \underset{x_{q_2} \in \gamma}{\operatorname{argmin}} \left\| \boldsymbol{y} - \sqrt{\frac{\rho}{\mu}} \boldsymbol{h}_{\hat{\ell},2} x_{q_2} \right\|_F^2 \right), \tag{5-6}$$

where γ denotes a complex *M*-QAM signal constellation.

5.1.3 ML approaching MIMO detection using OP

Consider a spatially multiplexed MIMO system with four different data streams each transmitted from one of four transmit antennas. Further to this, assume four antennas at the receiver so as to separate the data streams. Upon reception, the receiver rearranges the streams in descending order of SNR and the received signal vector can be formulated as,

$$\boldsymbol{y}_{OP} = \boldsymbol{H}_{OP} \boldsymbol{x}_{OP} + \boldsymbol{n}_{OP}, \tag{5-7}$$

where $\boldsymbol{x}_{OP} = [\boldsymbol{x}_{OP,1} \quad \boldsymbol{x}_{OP,2} \quad \boldsymbol{x}_{OP,3} \quad \boldsymbol{x}_{OP,4}]^T$ represents the $\mathrm{N}_{TX} \times 1$ rearranged input signal vector, $\boldsymbol{H}_{OP}$ and $\boldsymbol{n}_{OP}$ are respectively, the $\mathrm{N}_{RX} \times \mathrm{N}_{TX}$ rearranged channel gain matrix and the $\mathrm{N}_{RX} \times 1$ rearranged noise vector with i.i.d elements distributed according to $CN(0,1)$.

Also, (5-7) can be equivalently written as,

$$\boldsymbol{y}_{OP} - \boldsymbol{h}_{OP,1} x_{OP,1} = \boldsymbol{h}_{OP,2} x_{OP,2} + \boldsymbol{h}_{OP,3} x_{OP,3} + \boldsymbol{h}_{OP,4} x_{OP,4} + \boldsymbol{n}_{OP}. \tag{5-8}$$

Then suppose a projection matrix $\boldsymbol{P}_1$ which propagates a signal on the subspace orthogonal to $\boldsymbol{h}_{OP,2}$, $\boldsymbol{h}_{OP,3}$, $\boldsymbol{h}_{OP,4}$ and defined by,

$$\boldsymbol{P}_1 = \boldsymbol{I}_4 - \boldsymbol{H}_{OP,2:4} \left(\boldsymbol{H}_{OP,2:4}^{\dagger} \boldsymbol{H}_{OP,2:4} \right)^{-1} \boldsymbol{H}_{OP,2:4}^{\dagger}, \tag{5-9}$$

where $\boldsymbol{H}_{OP,2:4} = [\boldsymbol{h}_{OP,2} \quad \boldsymbol{h}_{OP,3} \quad \boldsymbol{h}_{OP,4}]$, is constructed.

Due to the orthogonality of the projected signal with $\boldsymbol{h}_{OP,2}$, $\boldsymbol{h}_{OP,3}$, $\boldsymbol{h}_{OP,4}$ when we compute $\boldsymbol{P}_1 \left(\boldsymbol{y}_{OP} - \boldsymbol{h}_{OP,1} x_q \right)$, $q \in [1{:}\,M]$, the result is $\boldsymbol{P}_1 \boldsymbol{n}_{OP}$ if $x_q = x_{OP,1}$. When $x_q \neq x_{OP,1}$ the result yielded is $\boldsymbol{P}_1 \left(\boldsymbol{h}_{OP,1} x_{OP,1} - \boldsymbol{h}_{OP,1} x_q + \boldsymbol{n}_{OP} \right)$. One could then deduce with a high probability that $\| \boldsymbol{P}_1 \boldsymbol{n}_{OP} \|_F < \left\| \boldsymbol{P}_1 \left(\boldsymbol{h}_{OP,1} x_{OP,1} - \boldsymbol{h}_{OP,1} x_q + \boldsymbol{n}_{OP} \right) \right\|_F$ especially as the SNR becomes larger for a fixed transmit signal power, and the proof is included in [69].

Hence in the first step to determine candidates for $x_{OP,1}$ the algorithm computes $\boldsymbol{P}_1(\boldsymbol{y}_{OP} - \boldsymbol{h}_{OP,1}x_q)$, calculates the norm for every $q \in [1{:}\,M]$ and chooses $\widetilde{M}$ symbols based on the $\widetilde{M}$ smallest projection norms from $\arg\min_{x_q} \left\|\boldsymbol{P}_1(\boldsymbol{y}_{OP} - \boldsymbol{h}_{OP,1}x_q)\right\|_F$. These $\widetilde{M}$ symbols then form the candidate set for $x_{OP,1}$. Similarly, the candidate sets are formed for $(x_{OP,1}, x_{OP,2})$, $(x_{OP,1}, x_{OP,2}, x_{OP,3})$ and $(x_{OP,1}, x_{OP,2}, x_{OP,3}, x_{OP,4})$ in a layered fashion [69]. Finally, an ML search is performed only over the $\widetilde{M}$ candidate sequences for $(x_{OP,1}, x_{OP,2}, x_{OP,3}, x_{OP,4})$ to evaluate the transmitted symbol streams. Thus unlike the optimal ML detector where an exhaustive search is required, only a partial search is needed, hence, bringing about a reduction of the CC at the receiver. The detailed algorithm is presented in [69].

Motivated by the reduced CC and ML approaching error performance, in (5.2), we implement the concept of OP to STBC-SM to lower the receiver CC and to obtain a near-ML error performance.

5.2 Reduced Complexity Detection for STBC-SM

In the STBC-SM scheme the special information conveying mode of SM is utilized, thus the antenna pair index, ℓ of the form $\{\ell_1, \ell_2\}$ carries information in addition to the transmission of the Alamouti symbol by the ℓ_1^{th} and ℓ_2^{th} antenna elements over two consecutive time slots [16]. For the Alamouti scheme, detection at the receiver is relatively straightforward [57]; however, for STBC-SM there exists c antenna pairs and at the receiver the ℓ^{th} antenna pair employed for transmission is not known; thus the detector needs to estimate the Alamouti symbol for every possible antenna pair index from which the most likely combination of antenna pair index and Alamouti symbol can be chosen. The proposed algorithm is based on this principle and applies the concept of OP and is subsequently detailed.

Consider the c antenna pair combinations. For the ℓ^{th} antenna pair of the form $\{\ell_1, \ell_2\}$, we construct the projection matrix $\boldsymbol{P}_{\ell_{12}} = \boldsymbol{I}_{\mathrm{N}_{RX}} - \boldsymbol{H}_{\ell_{12}}\left(\boldsymbol{H}_{\ell_{12}}^{\dagger}\boldsymbol{H}_{\ell_{12}}\right)^{-1}\boldsymbol{H}_{\ell_{12}}^{\dagger}$, where the $\mathrm{N}_{RX} \times 2$ matrix $\boldsymbol{H}_{\ell_{12}} = [\boldsymbol{h}_{\ell_1} \quad \boldsymbol{h}_{\ell_2}]$, which projects a signal on the subspace orthogonal to the subspace composed of $\boldsymbol{h}_{\ell_1}$ and $\boldsymbol{h}_{\ell_2}$. Then as a result of the induced orthogonality, using (5-2), the computation of $\boldsymbol{P}_{\ell_{12}}\boldsymbol{y}_1$ and $\boldsymbol{P}_{\ell_{12}}\boldsymbol{y}_2$ yield $\boldsymbol{P}_{\ell_{12}}\boldsymbol{n}_1$ and $\boldsymbol{P}_{\ell_{12}}\boldsymbol{n}_2$, respectively, when the projection matrix is constructed orthogonal to the correct channel gain vectors. Consider the following example for the first time slot:

Suppose $\mathrm{N}_{TX} = 4$, $c = 4$ and the antenna pair combinations are {1, 2}, {3, 4}, {2, 3}, {4, 1}. Next consider that the antenna pair {2, 3} is being tested against the received signal vector $\boldsymbol{y}_1 = \sqrt{\frac{\rho}{\mu}}\boldsymbol{H}\boldsymbol{x}_{\chi,1} + \boldsymbol{n}_1$ then for $\boldsymbol{x}_{\chi,1} = \begin{bmatrix} 0 & x_{q_1}e^{j\theta_\ell} & x_{q_2}e^{j\theta_\ell} & 0 \end{bmatrix}^T$, $\boldsymbol{P}_{\ell_{12}}\boldsymbol{y}_1 =$

$\sqrt{\frac{\rho}{\mu}}\boldsymbol{P}_{\ell_{12}}[\boldsymbol{h}_1 \quad \boldsymbol{h}_2 \quad \boldsymbol{h}_3 \quad \boldsymbol{h}_4]\begin{bmatrix}0 & x_{q_1}e^{j\theta_\ell} & x_{q_2}e^{j\theta_\ell} & 0\end{bmatrix}^T + \boldsymbol{P}_{\ell_{12}}\boldsymbol{n}_1 = \boldsymbol{P}_{\ell_{12}}\boldsymbol{n}_1$ due to the induced orthogonality. However, if instead $\boldsymbol{x}_{\chi,1} = \begin{bmatrix}x_{q_2}e^{j\theta_\ell} & 0 & 0 & x_{q_1}e^{j\theta_\ell}\end{bmatrix}^T$ was transmitted then the product of the projection matrix and received signal yields the result $\boldsymbol{P}_{\ell_{12}}\boldsymbol{y}_1 = \sqrt{\frac{\rho}{\mu}}\boldsymbol{P}_{\ell_{12}}[\boldsymbol{h}_1 \quad \boldsymbol{h}_2 \quad \boldsymbol{h}_3 \quad \boldsymbol{h}_4]\begin{bmatrix}x_{q_2}e^{j\theta_\ell} & 0 & 0 & x_{q_1}e^{j\theta_\ell}\end{bmatrix}^T + \boldsymbol{P}_{\ell_{12}}\boldsymbol{n}_1 = \sqrt{\frac{\rho}{\mu}}\boldsymbol{P}_{\ell_{12}}\boldsymbol{h}_1 x_{q_2}e^{j\theta_\ell} + \sqrt{\frac{\rho}{\mu}}\boldsymbol{P}_{\ell_{12}}\boldsymbol{h}_4 x_{q_1}e^{j\theta_\ell} + \boldsymbol{P}_{\ell_{12}}\boldsymbol{n}_1$ since the projected signal is not orthogonal to the channel gain vectors $\boldsymbol{h}_1$ and $\boldsymbol{h}_4$. Thus if the symbol positions (antenna pair combination) of the received signal vector in the first time slot do not match the antenna pair combination being tested, we can expect the norm of the result to be larger than $\left\|\boldsymbol{P}_{\ell_{12}}\boldsymbol{n}_1\right\|_F$. The same reasoning applies to the second time slot. Thus by testing each of the antenna pair combinations against the received signal, the concept of OP can be employed to determine the most likely transmit antenna pair. The method to determine the transmit symbols is straightforward. Consider the case that the most likely transmit antenna pair was estimated to be {2, 3}, which we assume is correct. We can then write $r_1 = \boldsymbol{h}_2^\dagger\boldsymbol{y}_1 + \boldsymbol{y}_2^\dagger\boldsymbol{h}_3 = \sqrt{\frac{\rho}{\mu}}x_{q_1}e^{j\theta_\ell}(\|\boldsymbol{h}_2\|_F^2 + \|\boldsymbol{h}_3\|_F^2) + \boldsymbol{h}_2^\dagger\boldsymbol{n}_1 + \boldsymbol{n}_2^\dagger\boldsymbol{h}_3$, assuming the received signal vectors have correct symbol positions. The estimate of the transmit symbol x_{q_1} can then be demodulated using $\mathcal{D}\left(\frac{r_1}{(\|\boldsymbol{h}_2\|_F^2+\|\boldsymbol{h}_3\|_F^2)}e^{-j\theta_\ell}\right)$. A similar method can be used to evaluate the transmit symbol x_{q_2}. Based on the above reasoning, the detection algorithm for STBC-SM proceeds as follows:

Step 1: Construct the $\mathrm{N}_{RX} \times 2$ matrix $\boldsymbol{H}_{\ell_{12}} = [\boldsymbol{h}_{\ell_1} \quad \boldsymbol{h}_{\ell_2}]$ for the ℓ^{th} antenna pair combination of the form $\{\ell_1, \ell_2\}$.

Step 2: Compute the projection matrix for the ℓ^{th} antenna pair combination such that the projected signal is orthogonal to the subspace containing $\boldsymbol{h}_{\ell_1}$ and $\boldsymbol{h}_{\ell_2}$,

$$\boldsymbol{P}_\ell = \boldsymbol{I}_{N_R} - \boldsymbol{H}_{\boldsymbol{\ell}_{12}}\left(\boldsymbol{H}_{\ell_{12}}^\dagger\boldsymbol{H}_{\ell_{12}}\right)^{-1}\boldsymbol{H}_{\ell_{12}}^\dagger,\ 0 \le \ell \le c-1. \tag{5-10}$$

Step 3: Compute the norm for the ℓ^{th} antenna pair combination and i^{th} time slot,

$$\alpha_{\ell,i} = \|\boldsymbol{P}_\ell\boldsymbol{y}_i\|_F^2,\ 0 \le \ell \le c-1,\ i \in [1{:}\,2]. \tag{5-11}$$

Step 4: Sort the results from Step 3 in ascending order and construct the vector for the i^{th} time slot,

$$\boldsymbol{\alpha}_i = [\alpha_{l_1^i,i} \quad \cdots \quad \alpha_{l_c^i,i}],\ i \in [1{:}\,2], \tag{5-12}$$

where $\alpha_{l_c^i,i} \geq \cdots \geq \alpha_{l_1^i,i}$ and $l_1^i, \cdots, l_c^i$ represent the rearranged values of ℓ for the i^{th} time slot. Assume the indices of the sorted elements are $\beta_{l_1^i,i}, \cdots, \beta_{l_c^i,i}$.

Step 5: Determine if the first L_1 indices, where $L_1 \in \mathbb{Z}^p$ and $L_1 \leq c$, of (5-12) are equal for both $\boldsymbol{\alpha}_1$ and $\boldsymbol{\alpha}_2$, i.e. check if $\beta_{l_1^1,1} = \beta_{l_1^2,2}, \cdots, \beta_{l_{L_1}^1,1} = \beta_{l_{L_1}^2,2}$. If the condition is true then set $L = L_1$ and store the indices $\beta_{l_1^1,1}, \cdots, \beta_{l_L^1,1}$. Otherwise, go to Step 6.

(Note if $L = L_1$ then in the final search only the antenna pairs corresponding to the L_1 smallest indices of $\boldsymbol{\alpha}_i$ are considered. The choice of L in this step is further discussed in (5.4)).

Step 6: Sort $\alpha_{\ell,1} + \alpha_{\ell,2}$ (from Step 3) in ascending order for $0 \leq \ell \leq c-1$ to yield the vector,

$$\boldsymbol{\alpha}_{12} = [\bar{\alpha}_{l_1^{12},12} \quad \cdots \quad \bar{\alpha}_{l_c^{12},12}], \tag{5-13}$$

with indices $\beta_{l_1^{12},12}, \cdots, \beta_{l_c^{12},12}$, and set $L = L_2$, where $L_2 \in \mathbb{Z}^p$ and $L_2 \leq c$. Note $\bar{\alpha}_{l_c^{12},12} \geq \cdots \geq \bar{\alpha}_{l_1^{12},12}$ and $l_1^{12}, \cdots, l_c^{12}$ represent the rearranged values of ℓ. Store the indices $\beta_{l_1^{12},12}, \cdots, \beta_{l_L^{12},12}$.

(Note in the final search only the antenna pairs corresponding to the L_2 smallest indices of $\boldsymbol{\alpha}_{12}$ are considered if Step 6 was executed. The choice of L in this step is further discussed in (5.4)).

Step 7: Demodulate the $2L$ possible symbols using,

$$\begin{aligned} r_{1,k} &= \boldsymbol{h}_{k_1}^{\dagger}\boldsymbol{y}_1 + \boldsymbol{y}_2^{\dagger}\boldsymbol{h}_{k_2}, \ k \in [1{:}L], \\ r_{2,k} &= \boldsymbol{h}_{k_2}^{\dagger}\boldsymbol{y}_1 - \boldsymbol{y}_2^{\dagger}\boldsymbol{h}_{k_1}, \ k \in [1{:}L], \end{aligned} \tag{5-14}$$

$$\begin{aligned} s_{1,k} &= \mathcal{D}\left(\frac{r_{1,k}}{\left(\|\boldsymbol{h}_{k_1}\|_F^2 + \|\boldsymbol{h}_{k_2}\|_F^2\right)} e^{-j\theta_k}\right), \\ s_{2,k} &= \mathcal{D}\left(\frac{r_{2,k}}{\left(\|\boldsymbol{h}_{k_1}\|_F^2 + \|\boldsymbol{h}_{k_2}\|_F^2\right)} e^{-j\theta_k}\right), \end{aligned} \tag{5-15}$$

where $\{k_1, k_2\}$ represents the form of the k^{th} antenna pair ordered according to the indices stored in Step 5 ($\beta_{l_1^1,1}, \cdots, \beta_{l_L^1,1}$) or Step 6 ($\beta_{l_1^{12},12}, \cdots, \beta_{l_L^{12},12}$).

Step 8: Detect the antenna combination pair index estimate, $\hat{\ell}$ and transmit symbol estimates, $\hat{x}_{q_1}$ and $\hat{x}_{q_2}$ using a reduced ML search defined by,

$$\widehat{\boldsymbol{X}}_{\chi} = \underset{k}{\operatorname{argmin}} \left\{ \|\boldsymbol{y}_1 - \boldsymbol{H}\boldsymbol{x}_{s_k,1}\|_F^2 + \|\boldsymbol{y}_2 - \boldsymbol{H}\boldsymbol{x}_{s_k,2}\|_F^2 \right\}, \tag{5-16}$$

where $\boldsymbol{x}_{s_k,1} = \left[0 \ \cdots \ s_{1,k}e^{j\theta_k} \ \cdots \ s_{2,k}e^{j\theta_k} \ 0\right]^T$ and $\boldsymbol{x}_{s_k,2} = \left[\left[0 \ \cdots \ -\left(s_{2,k}e^{j\theta_k}\right)^* \cdots \left(s_{1,k}e^{j\theta_k}\right)^* \ 0\right]^T\right]$, with the position of the symbols (non-zero entries) corresponding to the k^{th} antenna pair.

5.3 Computational Complexity

In this section, the receiver CC analysis for the proposed STBC-SM-OP detector is formulated. For comparison purposes, the simplified ML detector's complexity analysis [16] is also evaluated. The CC is formulated in terms of the number of complex multiplications and additions, similar to [49].

5.3.1 Complexity analysis of the simplified ML detector

The CC at the receiver for the STBC-SM-ML scheme by inspection of (5-5) and (5-6) involves the computation of $\left\|\boldsymbol{y}-\sqrt{\frac{\rho}{\mu}}\boldsymbol{h}_{\ell,1}x_{q_1}\right\|_F^2$ and $\left\|\boldsymbol{y}-\sqrt{\frac{\rho}{\mu}}\boldsymbol{h}_{\ell,2}x_{q_2}\right\|_F^2$ since the result can be stored and used in the computation of (5-6). Furthermore, due to the decoupled nature of the detection, the complexity involves the computation of only one of the terms. We consider the first term. It can be verified that this term is equivalent to $\sqrt{\frac{\rho}{\mu}}\left\|\boldsymbol{g}_{\ell,1}\right\|_F^2-2\Re\left(\boldsymbol{y}^{\dagger}\boldsymbol{g}_{\ell,1}\right)$, where $\boldsymbol{g}_{\ell,1}=\boldsymbol{h}_{\ell,1}x_{q_1}$, and $\boldsymbol{y}$, $\boldsymbol{h}_{\ell,1}$ are $2\mathrm{N}_{RX}\times 1$ vectors. In addition, to reduce complexity, $\left\|\boldsymbol{g}_{\ell,1}\right\|_F^2$ can be simplified to $\left\|\boldsymbol{h}_{\ell,1}\right\|_F^2\left|x_{q_1}\right|^2$.

It can then be verified that computation of $\left\|\boldsymbol{h}_{\ell,1}\right\|_F^2\left|x_{q_1}\right|^2$ requires $(2\mathrm{N}_{RX}c+M)$ complex multiplications for $0\leq\ell\leq c-1$ and $q_1\in[1{:}M]$. The computation of the second term $\boldsymbol{y}^{\dagger}\boldsymbol{h}_{\ell,1}x_{q_1}$ requires a total of $c(4\mathrm{N}_{RX}-1+M)$ complex multiplications and additions. Thus, the total CC at the receiver for STBC-SM-ML is formulated as $\delta_{STBC-SM-ML}=c(6\mathrm{N}_{RX}+M-1)+M$.

5.3.2 Complexity analysis of the proposed STBC-SM-OP detector

In the STBC-SM-OP scheme, only Steps 2, 3, 7 and 8 contribute to the CC at the receiver. The CC is formulated as follows.

Step 2 involves the computation of the projection matrix $\boldsymbol{P}_{\ell}$ for each value of ℓ. Computation of $\boldsymbol{H}_{\ell_{12}}\left(\boldsymbol{H}_{\ell_{12}}^{\dagger}\boldsymbol{H}_{\ell_{12}}\right)^{-1}\boldsymbol{H}_{\ell_{12}}^{\dagger}$ involves $4\mathrm{N}_{RX}+2\mathrm{N}_{RX}^2$ complex multiplications and zero complex additions for one antenna pair. Thus for c antenna pairs, the complexity of Step 2 is given as $\delta_{STBC-SM-OP_{Step2}}=c(4\mathrm{N}_{RX}+2\mathrm{N}_{RX}^2)$.

Step 3 involves the computation of $\|\boldsymbol{P}_{\ell}\boldsymbol{y}_i\|_F^2$. $\boldsymbol{P}_{\ell}$ is a $\mathrm{N}_{RX}\times\mathrm{N}_{RX}$ matrix and $\boldsymbol{y}_i$ is a $\mathrm{N}_{RX}\times 1$ matrix. Therefore for one pair, this amounts to $2\mathrm{N}_{RX}^2-\mathrm{N}_{RX}$ complex multiplications and additions. A single norm operation incurs N_{RX} complex multiplications. Thus for all antenna pairs and over two consecutive time slots the complexity of Step 3 is defined as $\delta_{STBC-SM-OP_{Step3}}=4c\mathrm{N}_{RX}^2$.

Step 7 involves the computation of $r_{1,k}$, $r_{2,k}$, $s_{1,k}$ and $s_{2,k}$ for $k \in [1:L]$. It can be verified that computation of $r_{1,k}$ involves $L(4\mathrm{N}_{RX}-1)$ complex multiplications and additions. Similarly $r_{2,k}$ incurs $L(4\mathrm{N}_{RX}-1)$ complex multiplications and additions. In the computation of $s_{1,k}$ and $s_{2,k}$ the denominator is common; thus the result can be stored and used in the computation of $s_{2,k}$. Therefore $s_{1,k}$ involves $L(2\mathrm{N}_{RX}+1)$ complex multiplications and $s_{2,k}$ involves only L complex multiplications. Hence the overall complexity for Step 7 is defined as $\delta_{STBC-SM-OP_{Step7}} = 10L\mathrm{N}_{RX}$.

Step 8 involves searching for the most likely combination of antenna pair index and Alamouti symbol. The computation of $\left\|\boldsymbol{y}_1 - \boldsymbol{H}\boldsymbol{x}_{s_k,1}\right\|_F^2$ for $k=1$ involves $\mathrm{N}_{RX} + 2\mathrm{N}_{TX}\mathrm{N}_{RX}$ complex multiplications and additions. Construction of $\boldsymbol{x}_{s_k,1}$ and $\boldsymbol{x}_{s_k,2}$ includes 2 complex multiplications. Therefore for $k \in [1:L]$ the complexity of Step 8 is defined as $\delta_{STBC-SM-OP_{Step8}} = 2L + 2L(\mathrm{N}_{RX} + 2\mathrm{N}_{TX}\mathrm{N}_{RX})$. Therefore the overall CC at the receiver for STBC-SM-OP is $\delta_{STBC-SM-OP} = 4c\mathrm{N}_{RX} + 6c\mathrm{N}_{RX}^2 + 12L\mathrm{N}_{RX} + 2L + 4L\mathrm{N}_{TX}\mathrm{N}_{RX}$.

Firstly, it is evident that the CC of STBC-SM-OP is not a function of the symbol constellation size compared to STBC-SM-ML thus the complexity will remain the same even if higher data rates (large constellation size) are demanded when keeping the other parameters constant. In (5.4) we evaluate $\delta_{STBC-SM-ML}$ and $\delta_{STBC-SM-OP}$ and compare to demonstrate the significance of the proposed detector. Note that the value of L can take on values of either L_1 or L_2 (Step 5, 6). Suitable values for L_1 and L_2 are investigated in Section (5.4) and we further compare the complexity for STBC-SM-ML and STBC-SM-OP for these values yielding a worst-case and best-case CC for STBC-SM-OP.

5.4 Comparison of error performance for STBC-SM-ML and STBC-SM-OP

In this section, we present Monte Carlo simulation results to compare the error performance of STBC-SM-ML and STBC-SM-OP. The theoretical lower bound for STBC-SM for square *M*-QAM is implemented and included for comparison. In each of the models, we consider *M*-QAM modulation with Gray mapping. We assume a quasi-static Rayleigh flat fading channel similar to [49], [19]. For $\mathrm{N}_{TX} = 4$ antennas the antenna pairs considered are {1, 2}, {3, 4}, {2, 3} and {4, 1}, and $\theta_{\ell=0:1} = 0$ and $\theta_{\ell=2:3} = 0.75$. For $\mathrm{N}_{TX} = 6$ the antenna pairs are {1, 2}, {3, 4}, {5, 6}, {2, 3}, {4, 5}, {6, 1}, {1, 3} and {2, 4}, and $\theta_{\ell=0:2} = 0$, $\theta_{\ell=3:5} = \frac{\pi}{6}$ and $\theta_{\ell=6:7} = \frac{\pi}{3}$. Note, rotation angles have been attained from [16].

In the first investigation, we compare the error performance of STBC-SM for the optimal ML detector to the proposed OP detector for 16-QAM and $\mathrm{N}_{TX} = \mathrm{N}_{RX} = 4$. The results are presented

in Figure 5-1 and Figure 5-2. Due to the curves been obscured, we have presented the results in two separate figures.

Figure 5-1 presents the results for STBC-SM-ML and STBC-SM-OP. In the graph legend, we use the notation STBC-SM-OP - (L_1, L_2) for the proposed detection scheme, where L_1 and L_2 are the possible values L can take on and is set in the simulation (refer to (5.2)). The STBC-SM-OP curves for different combinations of L_1 and L_2 have been presented. It can be seen that the OP results for $(1,1)$, $(2,1)$ and $(3,1)$ are identical but does not match the STBC-SM-ML result at any SNR from 0 to 18 dB. STBC-SM-OP - $(1,3)$ and STBC-SM-OP - $(1,2)$ match the STBC-SM-ML result down to a BER of approximately 9×10^{-2} and an SNR of 5 dB. The result then diverges and STBC-SM-OP - $(1,3)$ exhibits a slightly better error performance at higher SNRs compared to STBC-SM-OP - (1,2). STBC-SM-OP - $(3,2)$ matches the STBC-SM-ML result down to a BER of approximately 3×10^{-3} and SNR of 10.2 dB; however, at a BER of 10^{-5} is approximately 1.8 dB worse. STBC-SM-OP - $(2,3)$ and STBC-SM-OP - $(3,3)$ match the STBC-SM-ML result down to a BER of approximately 1.5×10^{-4} and diverges by 0.7 and 0.3 dB, respectively, at a BER of 10^{-6}. Thus STBC-SM-OP - $(2,3)$ and STBC-SM-OP - $(3,3)$ represent suitable alternatives for low-complexity near-ML detection of STBC-SM compared to STBC-SM-ML.

In the second part of this section, we further quantify the CC at the receiver for STBC-SM-OP - $(2,3)$ and STBC-SM-OP - $(3,3)$ using the analysis presented in (5.3).

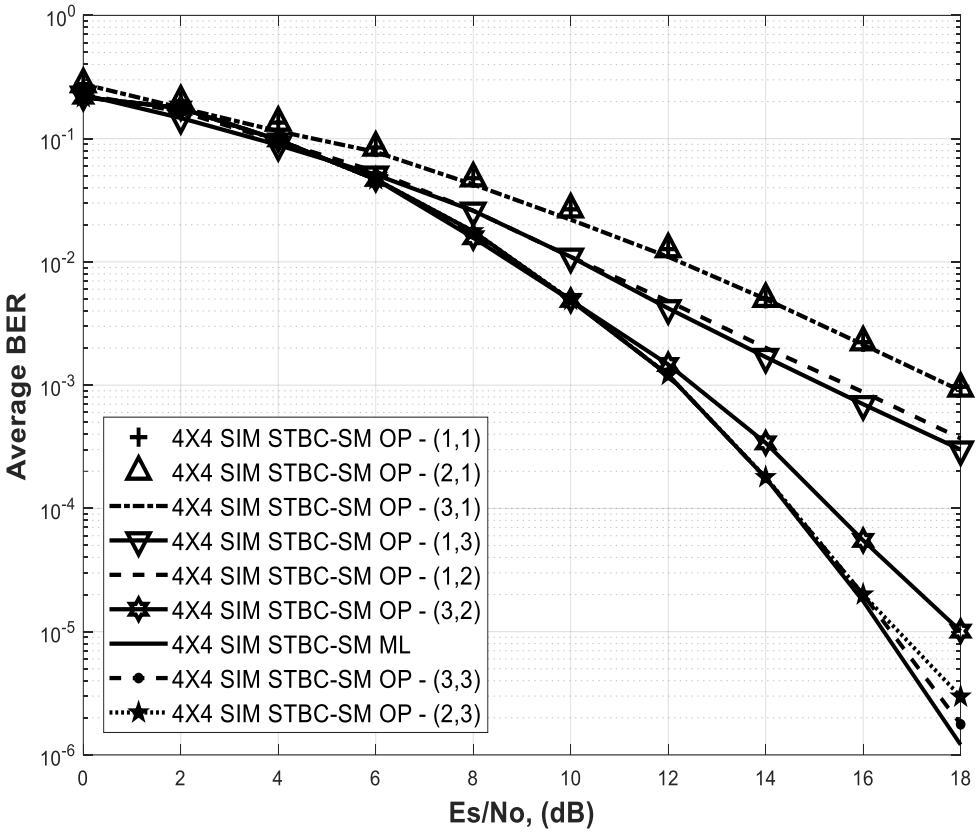

Figure 5-1. STBC-SM-ML, including bound versus STBC-SM-OP - (2, 4),

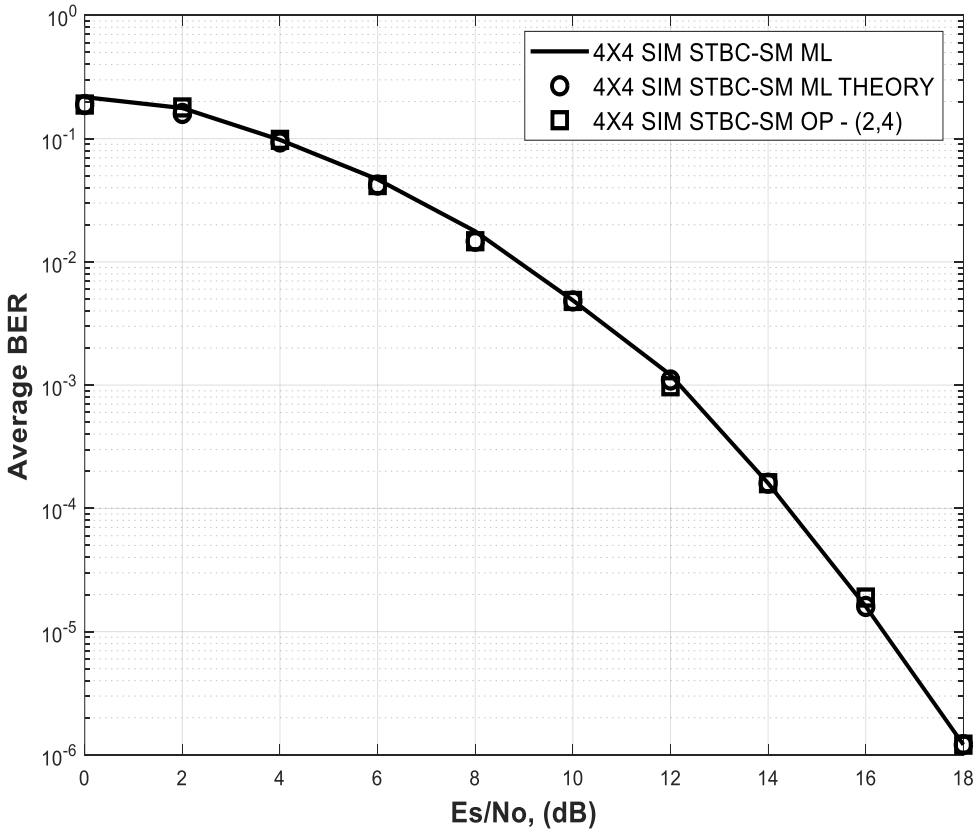

Figure 5-2. Comparison of error performance for STBC-SM-ML and STBC-SM-OP for 16-QAM and $N_{TX} = N_{RX} = 4$.

Figure 5-2 then presents the curve for the theoretical lower bound for the 4×4 configuration. It is evident that the result matches the STBC-SM-ML result very closely and becomes very tight at high SNR. The result for STBC-SM-OP - (2,4) is also included and matches the STBC-SM-ML result very closely right down to a BER of 10^{-6} and even outperforms STBC-SM-OP - (3,3). In part b) of this section we further quantify the CC at the receiver for STBC-SM-OP - (2,4).

Figure 5-3 then presents the curves for the 6×4 antenna configuration. Once again, the theoretical result has been evaluated and the results for STBC-SM-ML and STBC-SM-OP have been included. It is evident from the curves that for the 6×4 antenna configuration, the theoretical result represents a good fit to the optimal detector error performance. STBC-SM-OP was then evaluated for $(L_1 = 2, L_2 = 7)$, $(L_1 = 3, L_2 = 5)$ and $(L_1 = 3, L_2 = 6)$. It can be seen that at a BER of 10^{-5} STBC-SM-ML outperforms STBC-SM-OP - (2,7) by approximately 1.2 dB. At the same BER STBC-SM-ML outperforms STBC-SM-OP - (3,5) by approximately 0.8 dB. STBC-SM-OP - (3,6) on the other hand matches the ML result very closely at 10^{-5} and at a BER of 10^{-6} diverges by approximately 0.2 dB from the ML result. STBC-SM-OP for other values of L_1 and L_2 that match the results in Figure 5-3 or perform more poorly have been omitted

for the 6×4 antenna configuration. From simulation results, we can conclude that STBC-SM-OP represents a good alternative for low-complexity near-ML detection of STBC-SM.

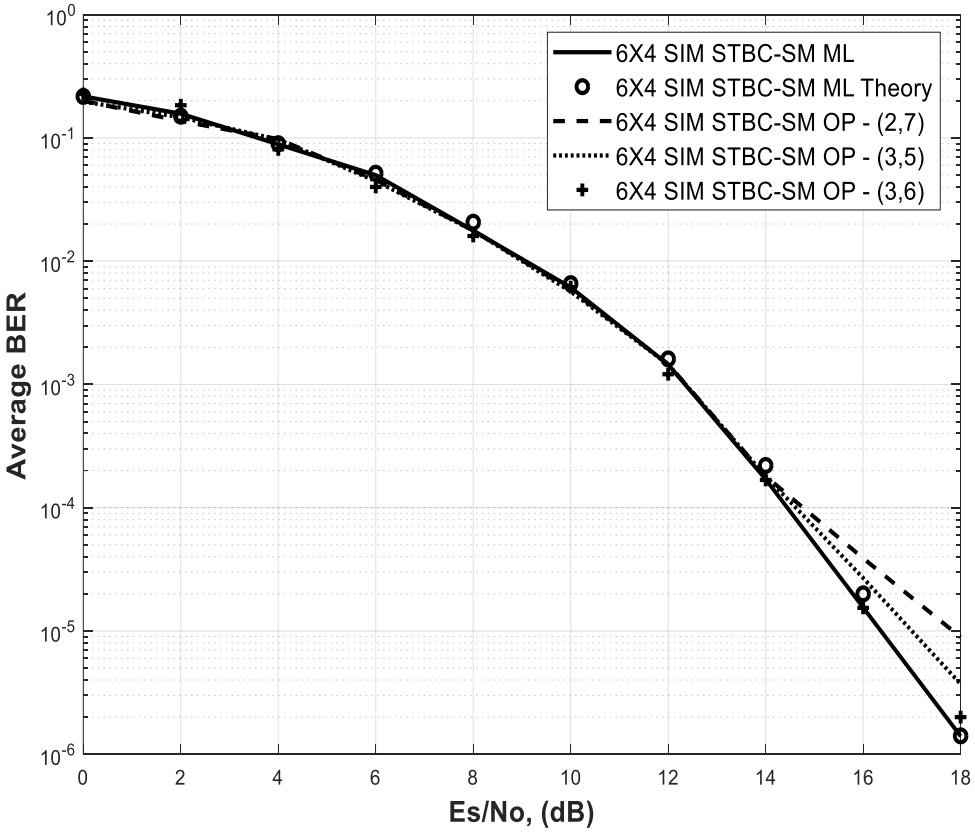

Figure 5-3. Comparison of error performance for STBC-SM-ML, STBC-SM-OP, including bound for 16-QAM and $N_{TX} = 6$, $N_{RX} = 4$.

5.5 Comparison of computational complexity for STBC-SM-ML and STBC-SM-OP

Table 5-1 tabulates the results for the CC for STBC-SM-ML and STBC-SM-OP. The expressions $\delta_{STBC-SM-ML}$ and $\delta_{STBC-SM-OP}$ as derived in (5.3) have been evaluated for various settings.

Table 5-1: CC for STBC-SM-ML and STBC-SM-OP

	STBC-SM-ML Configuration	**STBC-SM-ML**	**STBC-SM-OP Configuration**	**STBC-SM-OP**	
				Best case	**Worst Case**
1.	$N_{TX} = N_{RX} = 4,$ $M = 256$	1,372	$\mathrm{N}_{TX} = \mathrm{N}_{RX} = 4,$ $M = 256, L_1 = 2, L_2 = 3$	676	790
			$\mathrm{N}_{TX} = \mathrm{N}_{RX} = 4,$ $M = 256, L_1 = 3, L_2 = 3$	790	790
			$\mathrm{N}_{TX} = \mathrm{N}_{RX} = 4,$ $M = 256, L_1 = 2, L_2 = 4$	676	904
2.	$N_{TX} = 6, N_{RX} = 4,$ $M = 256$	2,488	$\mathrm{N}_{TX} = 6, \mathrm{N}_{RX} = 4,$ $M = 256, L_1 = 2, L_2 = 7$	1,188	1,918
			$\mathrm{N}_{TX} = 6, \mathrm{N}_{RX} = 4,$ $M = 256, L_1 = 3, L_2 = 5$	1,334	1,626
			$\mathrm{N}_{TX} = 6, \mathrm{N}_{RX} = 4,$ $M = 256, L_1 = 3, L_2 = 6$	1,334	1,772

The results in Table 5-1 have been evaluated for 256-QAM to demonstrate the significance of the proposed STBC-SM-OP. Since L can take on two values, L_1 or L_2 the best case and worst case results for STBC-SM-OP have been shown. The results show that the CC of STBC-SM-OP is much lower than STBC-SM-ML. Example for $\mathrm{N}_{TX} = \mathrm{N}_{RX} = 4$, $M = 256$, $L_1 = 2$, $L_2 = 4$ for the worst case there is a reduction of approximately 34% and for $\mathrm{N}_{TX} = 6$, $\mathrm{N}_{RX} = 4$, $M = 64$, $L_1 = 3$, $L_2 = 6$ for the worst case there is a reduction of approximately 29%. For the best case for the same settings, the percentage drops are 51% and 46%, respectively. Thus the significance of STBC-SM-OP is demonstrated.

CHAPTER SUMMARY

In this chapter, we have presented a reduced complexity detector for STBC-SM based on the concept of OP. The receiver CC analysis was presented for the proposed STBC-SM-OP scheme and demonstrated the significance of the detector in comparison to the STBC-SM-ML detector especially for high-order symbol constellation size, which is required in high data rate applications. The theoretical result for STBC-SM-ML for square *M*-QAM was presented and matched the simulation results very closely. From the numerical results, it was evident that the proposed STBC-SM-OP scheme's error performance can match that of STBC-SM-ML very closely down to low BER.

CHAPTER 6

CONCLUSION

6 Concluding Remarks

In Chapter 1, the summary of the introduction to MIMO systems was presented. The advantages of implementing the MIMO system, its shortcomings and how they were mitigated were discussed. Chapter 1 also contained a brief overview of some of the MIMO schemes which contributed to the literature presented in this dissertation.

In Chapter 2, SM as a major technique under the MIMO system was discussed at length. The SM scheme was able to fix the shortcomings associated with the conventional MIMO systems, i.e., IAS and ICI. Also, in Chapter 2, the SM scheme's performance analysis validated by its simulated results was presented.

In Chapter 3, the QSM scheme was presented. This Chapter was set to determine how the QSM scheme proves to have better error performance than the SM scheme. The lower bound approach was employed to derive the average BER of the M-QAM in a Rayleigh fading channel. The Monte Carlo simulation results validated the analytical lower bound approach. Table 6-1 shows the comparison between the QSM and SM error performance gains

Table 6-1: Summary of QSM and SM's error performance gains at a BER of 10^{-5}

SM			**QSM**			**SPECTRAL EFFICIENCY**	**SNR GAINS AT BER OF 10^{-5}(dB)**
M	N_{TX}	N_{RX}	M	N_{TX}	N_{RX}		
4	2	2	4	2	2	4	1.7
16	2	2	4	4	2	6	2.0
64	4	2	16	4	2	8	1.2
4	2	4	4	2	4	4	2.0
16	2	4	4	4	4	6	3.0
64	4	4	16	4	4	8	2.0

In Chapter 4, the ST-QSM scheme was presented. A comparison was drawn between the error performance of STQSM and QSM for matching spectral efficiencies of 4, 5, 6 and 7 b/s/Hz. This Chapter was set to determine how the ST-QSM scheme proves to have better error performance than the QSM scheme. Table 6-2 shows the comparison between the ST-QSM and QSM error performance gains.

Table 6-2: Summary of ST-QSM and QSM's error performance gains at a BER of 10^{-5}

QSM			ST-QSM			SPECTRAL EFFICIENCY	SNR GAINS AT BER OF 10^{-5} (dB)
M	N_{TX}	N_{RX}	M	N_{TX}	N_{RX}		
4	2	4	4	4	4	4	3.9
8	2	4	4	6	4	5	7.2
4	4	2	8	6	2	6	6.0
8	4	2	16	6	2	7	8.2

In Chapter 5, a scheme was introduced to fix the high computational complexity (CC) that affects MIMO systems transmitting at high data rates. Signal orthogonal projection (OP) was employed to decrease the CC of the space-time block coded spatial modulation (STBC-SM). The proposed scheme is called STBC-SM-OP and its results were investigated by comparing it with the STBC-SM with maximum likelihood (STBC-SM-ML). The proposed STBC-SM-OP scheme's error performance matched that of STBC-SM-ML tightly down to low BER whilst maintaining a low CC. It is proven that the CC of STBC-SM-OP does not depend on the constellation size as compared to the STBC-SM-ML detector; therefore, the CC at the receiver will remain constant even at an increased data rate whilst keeping the other parameters constant.

The results generated proves that the CC of STBC-SM-OP is much lower than STBC-SM-ML.

Table 6-3: Summary of the CC between the STBC-SM-OP and STBC-SM-ML

	STBC-SM-ML Configuration	STBC-SM-OP Configuration	Percentage drop in CC	
			Best case	Worse case
1.	$N_{TX} = N_{RX} = 4$, $M = 256$	$N_{TX} = N_{RX} = 4$, $M = 256, L_1 = 2, L_2 = 4$	51%	34%
2.	$N_{TX} = 6, N_{RX} = 4$, $M = 64$	$N_{TX} = 6, N_{RX} = 4$, $M = 64, L_1 = 3, L_2 = 6$	46%	29%

REFERENCES

[1] V. Ziegler, T. Wild, M. Uusitalo, H. Flinck, V. Räisänen, and K. Hätönen, "Stratification of 5G Evolution and Beyond 5G," in *Proceedings of the 2nd 5G World Forum (5GWF)*, pp. 329-334, Sep./Oct. 2019.

[2] T. Huang, W. Yang, J. Wu, J. Ma, X. Zhang, and D. Zhang, "A Survey on Green 6G Network: Architecture and Technologies," *IEEE Access*, vol. 7, pp. 175758-175768, Dec. 2019.

[3] A. Goldsmith, *Wireless Communications*: Cambridge University Press, 2005.

[4] D. Gesbert, M. Shafi, D. Shiu, P. J. Smith, and A. Naguib, "From Theory to Practice: An Overview of MIMO Space-Time Coded Wireless Systems," *IEEE Journal on Selected Areas in Communications*, vol. 21, no. 3, pp. 281-302, Apr. 2003.

[5] S. Moghe and R. Upadhyay, "Comparison of SISO and MIMO Techniques in 802.11n Wireless Local Area Network," in *Proceedings of the International Conference on Emerging Trends in Electronic and Photonic Devices & Systems*, pp. 245-246, Dec. 2009.

[6] X. Wang, J. Geng, X. Zhang, and D. Yang, "Spatial Multiplexing with Opportunistic Multiuser Scheduling in Ad Hoc Networks," in *Proceedings of the IEEE Vehicular Technology Conference (VTC Fall)*, pp. 1-5, Sep. 2012.

[7] M. K. Simon and M. S. Alouini, *Digital Communication over Fading Channels*: John Wiley & Sons, 2005.

[8] B. Vucetic and J. Yuan, *Space-Time Coding*: John Wiley & Sons, 2003.

[9] N. R. Naidoo, H. Xu, and T. Quazi, "Spatial Modulation: Optimal Detector Asymptotic Performance and Multiple-Stage Detection," *IET Communications*, vol. 5, no. 10, pp. 1368-1376, Jul. 2011.

[10] N. R. Naidoo, "Performance Analysis and Enhancement Schemes for Spatial Modulation," MSc Thesis, School of Electrical, Electronics and Computer Engineering, University of KwaZulu-Natal, Dec. 2010.

[11] Cisco, "Multi-path and Diversity," available at http://www.cisco.com/c/en/us/support /docs/wireless-mobility/wireless-lan-wlan/27147-multipath.html, Jun. 2016.

[12] N. A. Tran, V. V. Mai, T. C. Thang, and A. T. Pham, "Impact of Reflections and ISI on the Throughput of TCP over VLC Networks with ARQ-SR Protocol," in *Proceedings of the 4th IEEE International Conference on Photonics (ICP)*, pp. 172-174, Oct. 2013.

[13] P. W. Wolniansky, G. J. Foschini, G. D. Golden, and R. A. Valenzuela, "V-BLAST: An Architecture for Realizing Very High Data Rates over the Rich-Scattering Wireless Channel," in *Proceedings of the URSI International Symposium on Signals, Systems, and Electronics. (Cat. No. 98EX167)*, pp. 295-300, Oct. 1998.

[14] G. J. Foschini, "Layered Space-Time Architecture for Wireless Communication in a Fading Environment when Using Multi-Element Antennas," *Bell Labs Technical Journal*, vol. 1, no. 2, pp. 41-59, Sep. 1996.

[15] T. Liu, "Analysis of the Alamouti STBC MIMO System with Spatial Division Multiplexing over the Rayleigh Fading Channel," *IEEE Transactions on Wireless Communications*, vol. 14, no. 9, pp. 5156-5170, Sep. 2015.

[16] E. Basar, U. Aygolu, E. Panayirci, and H. V. Poor, "Space-Time Block Coded Spatial Modulation," *IEEE Transactions on Communications*, vol. 59, no. 3, pp. 823-832, Mar. 2011.

[17] R. Y. Mesleh, H. Haas, S. Sinanovic, C. W. Ahn, and S. Yun, "Spatial Modulation," *IEEE Transactions on Vehicular Technology*, vol. 57, no. 4, pp. 2228-2241, Jul. 2008.

[18] Q. Tang, Y. Xiao, P. Yang, Q. Yu, and S. Li, "A New Low-Complexity Near-ML Detection Algorithm for Spatial Modulation," *IEEE Wireless Communications Letters*, vol. 2, no. 1, pp. 90-93, Feb. 2013.

[19] J. Jeganathan, A. Ghrayeb, and L. Szczecinski, "Spatial Modulation: Optimal Detection and Performance Analysis," *IEEE Communications Letters*, vol. 12, no. 8, pp. 545-547, Aug. 2008.

[20] A. Younis, R. Mesleh, H. Haas, and P. M. Grant, "Reduced Complexity Sphere Decoder for Spatial Modulation Detection Receivers," in *Proceedings of the IEEE Global Telecommunications Conference GLOBECOM*, pp. 1-5, Dec. 2010.

[21] A. Younis, M. Di Renzo, R. Mesleh, and H. Haas, "Sphere Decoding For Spatial Modulation," in *Proceedings of the IEEE International Conference on Communications (ICC)*, pp. 1-6, Jun. 2011.

[22] S. Hwang, S. Jeon, S. Lee, and J. Seo, "Soft-Output ML Detector for Spatial Modulation OFDM Systems," *IEICE Electronics Express*, vol. 6, no. 19, pp. 1426-1431, Oct. 2009.

[23] J. Wang, S. Jia, and J. Song, "Signal Vector-Based Detection Scheme for Spatial Modulation," *IEEE Communications Letters*, vol. 16, no. 1, pp. 19-21, Jan. 2012.

[24] N. Pillay and H. Xu, "Comments on" Signal Vector-Based Detection Scheme for Spatial Modulation," *IEEE Communications Letters*, vol. 17, no. 1, pp. 2-3, Jan. 2013.

[25] J. Zheng, "Signal Vector-Based List Detection for Spatial Modulation," *IEEE Wireless Communications Letters*, vol. 1, no. 4, pp. 265-267, Aug. 2012.

[26] S. Ganesan, R. Mesleh, H. Ho, C. W. Ahn, and S. Yun, "On the Performance of Spatial Modulation OFDM," in *Proceedings of the Fortieth Asilomar Conference on Signals, Systems and Computers*, pp. 1825-1829, Nov. 2006.

[27] R. Mesleh, S. Ganesan, and H. Haas, "Impact of Channel Imperfections on Spatial Modulation OFDM," in *Proceedings of the IEEE 18th International Symposium on Personal, Indoor, and Mobile Radio Communications*, pp. 1-5, Sep. 2007.

[28] N. Serafimovski, M. D. Renzo, S. Sinanovic, R. Mesleh, and H. Haas, "Fractional Bit Encoded Spatial Modulation (FBE-SM)," *IEEE Communications Letters*, vol. 14, no. 5, pp. 429-431, May. 2010.

[29] J. Jeganathan, A. Ghrayeb, L. Szczecinski, and A. Ceron, "Space Shift Keying Modulation for MIMO Channels," *IEEE Transactions on Wireless Communications*, vol. 8, no. 7, pp. 3692-3703, Jul. 2009.

[30] H. Liang, R. Y. Chang, W. Chung, H. Zhang, and S. Kuo, "Bi-Space Shift Keying Modulation for MIMO Systems," *IEEE Communications Letters*, vol. 16, no. 8, pp. 1161-1164, Aug. 2012.

[31] A. Younis, N. Serafimovski, R. Mesleh, and H. Haas, "Generalized Spatial Modulation," in *Proceedings of the Record of the Forty-Fourth Asilomar Conference on Signals, Systems and Computers*, pp. 1498-1502, Nov. 2010.

[32] J. Fu, C. Hou, W. Xiang, L. Yan, and Y. Hou, "Generalized Spatial Modulation with Multiple Active Transmit Antennas," in *Proceedings of the IEEE Globecom Workshops*, pp. 839-844, Dec. 2010.

[33] J. Wang, S. Jia, and J. Song, "Generalized Spatial Modulation System with Multiple Active Transmit Antennas and Low Complexity Detection Scheme," *IEEE Transactions on Wireless Communications*, vol. 11, no. 4, pp. 1605-1615, Apr. 2012.

[34] A. Younis, R. Mesleh, and H. Haas, "Quadrature Spatial Modulation Performance over Nakagami-m Fading Channels," *IEEE Transactions on Vehicular Technology*, vol. 65, no. 12, pp. 10227-10231, Dec. 2016.

[35] R. Mesleh and S. S. Ikki, "On the Impact of Imperfect Channel Knowledge on the Performance of Quadrature Spatial Modulation," in *Proceedings of the IEEE Wireless Communications and Networking Conference (WCNC)*, pp. 534-538, Mar. 2015.

[36] Z. Yigit and E. Basar, "Space-Time Quadrature Spatial Modulation," in *Proceedings of the IEEE International Black Sea Conference on Communications and Networking (BlackSeaCom)*, pp. 1-5, Jun. 2017.

[37] P. Yang, Y. Xiao, Y. Yu, and S. Li, "Adaptive Spatial Modulation for Wireless MIMO Transmission Systems," *IEEE Communications Letters,* vol. 15, no. 6, pp. 602-604, Jun. 2011.

[38] B. M. Mthethwa and H. Xu, "Adaptive M-ary Quadrature Amplitude Spatial Modulation," *IET Communications,* vol. 6, no. 18, pp. 3098-3108, Dec. 2012.

[39] P. Yang, Y. Xiao, L. Li, Q. Tang, Y. Yu, and S. Li, "Link Adaptation for Spatial Modulation with Limited Feedback," *IEEE Transactions on Vehicular Technology,* vol. 61, no. 8, pp. 3808-3813, Oct. 2012.

[40] R. Rajashekar, K. V. S. Hari, and L. Hanzo, "Antenna Selection in Spatial Modulation Systems," *IEEE Communications Letters,* vol. 17, no. 3, pp. 521-524, Mar. 2013.

[41] N. Pillay and H. Xu, "Comments on" Antenna Selection in Spatial Modulation Systems, " *IEEE Communications Letters,* vol. 17, no. 9, pp. 1681-1683, Sep. 2013.

[42] N. Wang, W. Liu, H. Men, M. Jin, and H. Xu, "Further Complexity Reduction using Rotational Symmetry for EDAS in Spatial Modulation," *IEEE Communications Letters,* vol. 18, no. 10, pp. 1835-1838, Oct. 2014.

[43] S. Thoen, L. Van der Perre, B. Gyselinckx, and M. Engels, "Performance Analysis of Combined Transmit-SC/Receive-MRC," *IEEE Transactions on Communications,* vol. 49, no. 1, pp. 5-8, Jan. 2001.

[44] Z. Chen, "Asymptotic Performance of Transmit Antenna Selection with Maximal-Ratio Combining for Generalized Selection Criterion," *IEEE Communications Letters,* vol. 8, no. 4, pp. 247-249, Apr. 2004.

[45] Z. Chen, J. Yuan, and B. Vucetic, "Analysis of Transmit Antenna Selection/Maximal-Ratio Combining in Rayleigh Fading Channels," *IEEE Transactions on Vehicular Technology,* vol. 54, no. 4, pp. 1312-1321, Jul. 2005.

[46] S. Sanayei and A. Nosratinia, "Antenna Selection in MIMO Systems," *IEEE Communications Magazine,* vol. 42, no. 10, pp. 68-73, Oct. 2004.

[47] S. Oladoyinbo, N. Pillay, and H. Xu, "Adaptive Quadrature Spatial Modulation," *IETE Technical Review,* pp. 1-12, Oct. 2019.

[48] S. Naidu, N. Pillay, and H. Xu, "A Study of Quadrature Spatial Modulation," in *Proceedings of the South African Telecommunications and Network Applications Conference*, Sept. 2015.

[49] R. Mesleh, H. Haas, C. W. Ahn, and S. Yun, "Spatial Modulation - A New Low Complexity Spectral Efficiency Enhancing Technique," in *Proceedings of the First International Conference on Communications and Networking in China*, pp. 1-5, Oct. 2006.

[50] Y. Yang and B. Jiao, "Information-Guided Channel-Hopping for High Data Rate Wireless Communication," *IEEE Communications Letters*, vol. 12, no. 4, pp. 225-227, Apr. 2008.

[51] R. Mesleh, S. Engelken, S. Sinanovic, and H. Haas, "Analytical SER Calculation of Spatial Modulation," in *Proceedings of the 10th International Symposium on Spread Spectrum Techniques and Applications*, pp. 272-276, Aug. 2008.

[52] H. Xu, "Symbol Error Probability for Generalized Selection Combining Reception of *M*-QAM," *SAIEE Africa Research Journal*, vol. 100, no. 3, pp. 68-71, Sep. 2009.

[53] R. Mesleh, S. S. Ikki, and H. M. Aggoune, "Quadrature Spatial Modulation," *IEEE Transactions on Vehicular Technology*, vol. 64, no. 6, pp. 2738-2742, Jun. 2015.

[54] R. Mesleh and S. S. Ikki, "A High Spectral Efficiency Spatial Modulation Technique," in *Proceedings of the IEEE 80th Vehicular Technology Conference (VTC2014-Fall)*, pp. 1-5, Sep. 2014.

[55] R. Mesleh, "Spatial Modulation: A Spatial Multiplexing Technique for Efficient Wireless Data Transmission," Ph.D. thesis Jacobs University, Bremen, Germany, Jun. 2007.

[56] Z. Yigit, and E. Basar. "Space-time Quadrature Spatial Modulation," in *proceedings of the IEEE International Black Sea Conference on Communications and Networking (BlackSeaCom)*, pp. 1-5, Jun. 2017.

[57] S. M. Alamouti, "A Simple Transmit Diversity Technique for Wireless Communications," *IEEE Journal on Selected Areas in Communications*, vol. 16, no. 8, pp. 1451-1458, Oct. 1998.

[58] O. Tirkkonen, A. Boariu and A. Hottinen, "Minimal Non-Orthogonality Rate 1 Space-time Block Code for 3+ Tx antennas," in *Proceedings of the IEEE Sixth International Symposium on Spread Spectrum Techniques and Applications (ISSTA)*, vol. 2, pp. 429-432, 2000.

[59] G. K. Karagiannidis and S. A. Lioumpas, "An improved approximation for the Gaussian Q-function," *IEEE Communications Letters*, vol. 11, no. 8, pp. 644-646, Aug. 2007.

[60] H. Xu, K. Govindasamy and N. Pillay, "Uncoded space-time labelling diversity," *IEEE Communications Letters*, vol. 20, no. 8, pp. 1511-1514, Jan. 2016.

[61] E. Telatar, "Capacity of Multi-Antenna Gaussian Channels," *European Transactions on Telecommunications*, vol. 10, no. 6, pp. 558-595, Nov./Dec. 1999.

[62] G.J. Foschini, M.J. Gans, "On Limits of Wireless Communications in a Fading Environment when Using Multiple Antennas," *Wireless Personal Communications,* vol. 6, pp. 311–335, Mar. 1998.

[63] R. Ran, J. Yang, D. Kim, "Multimode Pre-coder Design for STBC with Limited Feedback in MIMO Based Wireless Communication Systems," *IEICE Electronics Express*, vol. 6, no. 3, pp. 222–229, Feb. 2009.

[64] V. Tarokh, N. Seshadri and A. R. Calderbank. "Space-Time Codes for High Data Rate Wireless Communications: Performance Criteria and Code Construction," *IEEE Transactions on Information Theory*, vol. 44, no. 2, pp. 744-765, Mar. 1998.

[65] E. Biglieri, Y. Hong, and E. Viterbo, "On Fast-Decodable Space-Time Block Codes,*"* *IEEE Transactions on Information Theory*, vol. 55, no. 2, pp. 524-530, Feb. 2009.

[66] E. Basar and U. Aygolu, "High-Rate Full-Diversity Space-Time Block Codes for Three and Four Transmit Antennas," *IET Communications,* vol. 3, no. 8, pp.1371-1378, Aug. 2009.

[67] E. Basar U. Aygolu, "Full - Rate Full-Diversity Space-Time Block Codes for Three and Four Transmit Antennas," *Electronic Letters,* vol. 44, no. 18, pp. 1076-1077, Aug. 2008.

[68] J. Jeganathan, A. Ghrayeb, and L. Szczecinski, "Generalized Space Shift Keying Modulation for MIMO Channels," *in Proceedings of the 19th IEEE International Symposium on Personal, Indoor and Mobile Radio Communications, (PIMRC),* Cannes, France, pp. 1-5, Sep. 2008.

[69] S. Bahng, S. Shin, and Y. O. Park, "ML Approaching MIMO Detection Based on Orthogonal Projections, " *IEEE Communication Letters,* vol. 11, no. 6, pp. 474–476, Jun. 2007.

[70] K. Govindasamy, H. Xu, and N. Pillay, "Space-Time Block Coded Spatial Modulation with Labeling Diversity, "*International Journal of Systems,* Sep. 2017.

[71] W. V. Etten, "Maximum likelihood receiver for multiple channel transmission systems," *IEEE Transaction Communications,* vol. 24, no. 2, pp. 276-283, Feb. 1976.

[72] L. Bai, J. Choi, "Low Complexity MIMO Detection, "*Springer*, 2012.

[73] W. Wang and W. Zhang, "Orthogonal Projection-Based Channel Estimation for Multi-Panel Millimeter Wave MIMO," in *IEEE Transactions on Communications*, vol. 68, no. 4, pp. 2173-2187, April 2020.

[74] Y. Yang, S. Xiao and X. Wang, "Radar Detection of Small Target in Sea Clutter Using Orthogonal Projection," in *IEEE Geoscience and Remote Sensing Letters*, vol. 16, no. 3, pp. 382-386, March 2019.